Prediction of Permanent Deformations in Asphalt Concrete using the Mechanistic-Empirical Pavement Design Guide

Erik Oscarsson

Department of Technology and Society
Lund University

Prediction of Permanent Deformations in Asphalt Concrete using the Mechanistic-Empirical Pavement Design Guide

Erik Oscarsson

Erik Oscarsson

Prediction of Permanent Deformations in Asphalt Concrete using the Mechanistic-Empirical Pavement Design Guide

2007

Abstract:

Permanent deformations, or rutting, are internationally considered to be one of the most serious distress mechanisms in asphalt pavements. Deterioration modeling is an important tool for performance prediction and diagnostics of pavements.

The Mechanistic-Empirical Pavement Design Guide (M-E PDG) model used for calculation of permanent deformation in asphalt layers was to be evaluated. It was accomplished by accelerated loading testing of two flexible pavements with the Heavy Vehicle Simulator (HVS), specimen production, laboratory testing of materials, and calculation of permanent deformations using the M-E PDG software v0.910. Field calibration factors were assessed in order to match the model's results with the HVS results.

It was also to be investigated whether the indirect tensile test (IDT) on cored pavement specimens can replace the compressive uniaxial test on gyratory compacted specimens for determination of dynamic moduli. This was carried out by comparing mastercurves from the uniaxial test on gyratory compacted specimens with those from the IDT on gyratory compacted specimens, which in turn were compared to mastercurves from the IDT using pavement cores.

Results from the uncalibrated M-E PDG model underestimated the total permanent deformation in the asphalt layers but matched when a specific set of field calibration factors were used. The calibration factors found in this work increased the model's temperature susceptibility and decreased its dependency on the number of passages. Regional field calibration factors can be assessed by employing a performance study of existing pavements. However, the model's permanent deformation contribution of each layer to total rut depth did not correlate with HVS results in this investigation, and should therefore be refined with further trench studies on existing pavements.

Contrary to expectation, mastercurves derived with the uniaxial test and the IDT using gyratory compacted specimens were not similar. Most importantly, they appeared to differ regarding dependency on frequency and temperature. The mastercurves from the IDT on gyratory compacted specimens and pavement cores were comparable.

ACKNOWLEDGEMENTS

Erik Oscarsson
Lund, May 2007

TABLE OF CONTENTS

SUMMARY

Background

Permanent deformation is internationally considered the most serious mechanism of distress in asphalt pavements along with fatigue and thermal cracking. It often occurs as longitudinal depressions in the wheel paths of the road, which are called ruts. Rutting has a negative effect on traffic safety, vehicle wear, and comfort, provided that the speed is unaffected. There are three types of permanent deformation: structural rutting located in the subgrade, flow rutting in the asphalt layers, and wear rutting on the pavement surface.

Flow rutting has been found to occur in three stages that have been observed both in the field and the laboratory. In the initial stage, the cause is primarily densification due to post compaction. After a short period of time, the second stage begins. Densification decreases while the main flow rutting mechanism, shear deformation, increases. The second stage is relatively predictable and is the most prevalent. In the third stage, the asphalt concrete volume begins to increase and flow rutting accelerates rapidly.

Modeling is an important tool for performance prediction and diagnostics of pavements. The Mechanistic-Empirical Pavement Design Guide (M-E PDG), also called 2002 Design Guide, is an advanced modeling concept that addresses the most important pavement distress factors. Its clear division between mechanistic and empirical principles provides a sound basis for future model improvements. The current software version of M-E PDG is v0.910.

Objectives and scope

The first objective was to evaluate the flow rutting model used in the M-E PDG program. Further, the model should be calibrated to observed pavement performance.

The second objective was to compare dynamic moduli data from three test set-ups. Results from the uniaxial test were to be compared to the indirect tensile test (IDT) using only gyratory compacted specimens, as Kim et al. (2004) showed to be possible. Then the IDT was used to compare gyratory compacted specimens and pavement cores. If all three test set-ups show equal dynamic moduli, field cores can replace gyratory compacted specimens.

Method

In order to evaluate the flow rutting model used in the M-E PDG program, data from an accelerated loading test was used to compare permanent deformations. The data was derived by the Swedish National Road and Transport Research Institute (VTI) using a Heavy Vehicle Simulator (HVS) in a controlled environment at the temperature levels +10 °C, +20 °C and +30 °C. The HVS loading device simulated the half-axle super single tire impact of heavy vehicles. The two sections subjected to loading were a standard asphalt concrete (AC) structure constructed according to Swedish norms (ATB Väg, 2005) and a similar enhanced AC structure in which the binder layer bitumen was polymer modified to increase the asphalt mix resistance to permanent deformation. Both asphalt structures rested on equal structures of unbound materials. Permanent deformation data of each layer was collected using deformation gauges, surface measurement, and pavement coring.

In addition to climate and loading properties, the M-E PDG program requires comprehensive material input data for accurate predictions. Therefore, dynamic modulus data was determined for all asphalt mixes in both AC structures. In this situation, there was an opportunity to test whether the recommended uniaxial compressive test on gyratory compacted specimens can be replaced by the indirect tensile test on gyratory compacted or cored specimens. Therefore, specimens for uniaxial and indirect tensile testing were produced with the gyratory compactor. Additional IDT specimens were obtained by coring in the HVS test pavement. Dynamic modulus testing was then carried using the uniaxial test on gyratory compacted specimens, the IDT on gyratory compacted specimen and IDT on cored specimens. Mastercurves were constructed using data from dynamic modulus testing over a range of temperatures and frequencies. The three test set-ups were evaluated, as were the four asphalt mixes.

The modeling of permanent deformation in both AC structures was carried out using the M-E PDG v0.910 software at the highest recommended level of accuracy. In the first simulation, no field calibration factors were used. The model results were compared with the results from the HVS test and both total rut depth and the contribution of each layer were evaluated. In order to fit the model's total AC rut depth to the HVS total AC rut depth, a set of field calibration factors were assessed for each of the two AC structures.

Results

HVS testing showed that polymer modification of the binder layer reduced flow rutting in a conventional 220 mm asphalt concrete structure to approximately two thirds, as measured with EMU coils. The corresponding result from measurement on a single core was approximately one third. Further, the polymer modification also increased the load distribution capability, as shown with soil pressure cells. However, the permanent deformation of the unbound layers was not significantly affected in this investigation.

Specimens to be used in the uniaxial test and the IDT were gyratory compacted, cored, and cut to their proper dimensions. As it was difficult to reach the target density in some cases, it was necessary to increase the angle of gyration to 2.00°. In order to achieve proper mix viscosity, the compaction temperature of polymer modified mixes should be carefully evaluated before actual specimen production.

Dynamic modulus testing at the mean elastic strain interval 53 to 87 microstrains resulted in an average 4% decrease of dynamic modulus, although the test is considered nondestructive. However, specimens tested at high strain levels did not appear more damaged than those in which low strain levels were induced.

Mastercurves derived with the uniaxial test and the IDT using gyratory compacted specimens were not similar, contrary to expectation. Most importantly, they appeared to differ regarding dependency on frequency and temperature. However, it is likely that the discrepancy was due to problems with the gyratory compaction and dynamic modulus testing of the uniaxial specimens. The mastercurves from the IDT on gyratory compacted specimens and pavement cores were similar. However, in those cases where the air void content differed between groups, no conclusions could be drawn.

Mastercurves of the ABT, ABb, polymer modified ABbm, and AG mixes derived from IDT using pavement cores were compared. The general mix stiffness ranking, beginning with the stiffest, was ABbm, ABb, ABT, AG.

The M-E PDG model underestimated the flow rutting for both AC structures when no field calibration factors were used. However, the field calibrated model can describe the development of total AC rut depth well. The field calibration factors found in this work increased the temperature susceptibility of the model and decreased the dependency on the number of loadings.

The contribution of each layer to total rut depth was not correctly assessed by the field calibrated M-E PDG model. Most importantly, the permanent deformation of the AG asphalt base layer was seriously underestimated. The current distribution model is supported by a small-sized MnRoad trench study.

Conclusions and recommendations

HVS testing showed that polymer modification of the bitumen in the binder layer mix can significantly increase resistance to permanent deformation in AC layers. Laboratory testing of dynamic modulus using the IDT on cored specimens indicated that the modified binder mix was stiffer than the conventional mix.

Dynamic modulus results derived using the IDT and the uniaxial compressive test did not yield equal results. However, dynamic modulus results derived with the IDT using gyratory compacted specimens and cored specimens were similar. Dynamic modulus testing statistically reduced specimen stiffness by an average of 4%. No dependency was found between the stiffness reduction in a specimen and the strain levels to which it was subjected.

The M-E PDG model can be used for calculation of permanent deformation in asphalt layers. In order to increase accuracy of the model, regional field calibration factors should be assessed. For this purpose, extensive Long Term Pavement Performance data should be collected from existing pavements in the region. The data should include data describing the traffic, climate, structure and materials as well as surface measurements. The assessment of calibration factors can then be carried out by using the guidelines of NCHRP project 1-40B.

NCHRP should improve the M-E PDG model ability to determine the contribution of each asphalt concrete layer to the total AC rut depth. This should be accomplished with a large scale trench study on existing pavements within the Long-Term Pavement Performance database.

SAMMANFATTNING

Bakgrund

Permanenta deformationer betraktas internationellt som den allvarligaste nedbrytningsmekanismen i asfaltbeläggningar, tillsammans med sprickor till följd av utmattning och temperaturändringar. De permanenta deformationerna visar sig ofta som spårbildning, som är längsgående försänkningar i fordonens hjulspår. Spårbildning har en negativ inverkan på trafiksäkerhet, fordonsslitage och komfort förutsatt att hastigheten är opåverkad. Det finns tre typer av spårbildning: strukturella deformationer i vägöverbyggnad och undergrund, permanenta (plastiska) deformationer i asfaltbundna lager och nednötning av vägytan.

Permanenta deformationer sker i tre stadier: I det första stadiet är den främsta mekanismen förtätning, eller efterpackning, av asfaltbeläggningen. Efter en kort tid påbörjas det andra stadiet. Då minskar efterpackningen successivt och den huvudsakliga mekanismen, som är skjuvdeformation, ökar. Det andra stadiet är relativt förutsägbart. I det tredje stadiet börjar asfaltbeläggningens volym att öka på grund av upptryckning längs hjulspårens sidor och spårdjupet ökar kraftigt.

Modellering är ett viktigt verktyg för att förutsäga och diagnostisera nedbrytningen av vägar. Den amerikanska modellen "Mechanistic-Empirical Pavement Design Guide (M-E PDG)", även kallad "2002 Design Guide", är ett avancerat koncept som identifierar och modellerar de viktigaste nedbrytnings-mekanismerna. Konceptets klara distinkta uppdelning mellan mekanistiska och empiriska principer utgör en utomordentlig grund för ytterligare modellutveckling. Den nuvarande versionen av konceptets mjukvara är v0.910.

Syfte och omfattning

Det främsta syftet var att utvärdera M-E PDG:s modellera för permanenta deformationer i asfaltbeläggningar. Dessutom skulle modellen bli kalibrerad för att överensstämma med studiens observationer.

Det andra syftet var att jämföra dynamisk styvhetsmoduldata från tre olika försöksuppställningar. Resultat från det enaxiella tryckförsöket skulle jämföras med resultat från press-dragprovet på gyratoriskt packade provkroppar som Kim et al. (2004) visade var möjligt. Sedan användes press-dragprovet för att jämföra gyratoriskt packade provkroppar med uppborrade provkroppar. Om alla tre testuppställningarna resulterade i samma dynamiska styvhetsmoduler, skulle pressdragprov på uppborrade provkroppar kunna ersätta det enaxiella tryckförsöket på gyratoriskt packade provkroppar.

Metod

Data från accelererad nedbrytning av två vägsektioner jämfördes med motsvarande simulationsresultat från M-E PDG:s mjukvara för att utvärdera dess modell för permanenta deformationer i asfaltbetong. Den accelererade provningen utfördes av VTI (Statens väg-och transportforskningsinstitut) med en HVS (Heavy Vehicle Simulator) i en klimatstyrd hall vid temperaturerna +10 °C, +20 °C och +30 °C. Under HVS-försöket simulerades effekten av tunga fordon genom att lastanordningen försågs med ett supersingeldäck. De två vägsektionerna som utsattes för belastning var en standardkonstruktion med slitlager, bindlager och bundet bärlager enligt ATB Väg (2005) samt en förstärkt variant i vilken bindlagret var polymermodifierat för ökad stabilitet och motståndskraft mot permanenta deformationer. De båda asfaltkonstruktionerna hade samma grundläggning av obundna material. Data för permanenta deformationer samlades in med hjälp av deformationsgivare, ytmätning och borrkärnor från beläggningarna.

Förutom klimatdata och lastdata behövs även omfattande materialdata för att erhålla resultat med hög noggrannhet enligt M-E PDG. Dynamiska moduler (styvhetsmoduler) bestämdes för samtliga asfaltmaterial som ingick i de båda asfaltkonstruktionerna. I detta läge fanns möjlighet att testa huruvida det rekommenderade enaxiella tryckförsöket på gyratoriskt packade provkroppar kunde ersättas med press-dragprovet på gyratoriskt packade provkroppar eller borrkärnor från vägen. Därför tillverkades provkroppar för det enaxiella tryckförsöket och press-dragprovet genom gyratorisk packning. Ytterligare press-dragprovkroppar borrades upp från HVS-konstruktionerna. De dynamiska modulerna bestämdes sedan med det enaxiella tryckförsöket på gyratoriskt packade provkroppar, press-dragprovet på gyratoriskt packade provkroppar och press-dragprovet på uppborrade provkroppar. Masterkurvor skapades utifrån materialens dynamiska modul vid olika temperaturer och frekvenser. Totalt utvärderades tre försöksuppställningar och fyra beläggningar.

Modellering av permanent deformation i de båda asfaltkonstruktionerna utfördes i mjukvaran M-E PDG v0.910 vid de högsta nu rekommenderade precisionsnivå. I den första simulationen användes inga fältkalibrerings-faktorer. Modellens resultat jämfördes med resultat från HVS-testet och både totalt spårdjup i alla asfaltlager och bidraget från varje lager utvärderades. För varje av de två asfaltkonstruktionerna bestämdes en uppsättning med fältkalibrerings-faktorer som gjorde att modellens totala asfaltdeformation överensstämde med den observerade asfaltdeformationen från HVS-testet.

Resultat

Data från HVS-testet, uppmätt med EMU-spolar, visade att polymermodifiering av bindlagret minskade den asfaltrelaterade permanenta deformationen till cirka två tredjedelar i en konventionell 220 mm tjock asfaltkonstruktion. Motsvarande värde, bestämt med en enda borrkärna, var cirka en tredjedel. Polymermodifieringen ökade även beläggningens lastspridningsförmåga, vilket visades med tryckmätare. Trots det påverkades inte den permanenta deformationen i obundna lager i denna studie.

Provkroppar för användning i det enaxiella trycktestet och press-dragprovet tillverkades genom gyratorisk packning, borrning och sågning. Eftersom det var svårt att nå rätt densitet i vissa fall, blev det nödvändigt att öka gyrationsvinkeln till 2.00°. För att uppnå rätt viskositet på asfaltmassan bör packningstemperaturen utvärderas noga innan de riktiga provkropparna packas.

Testning av dynamisk modul vid det elastiska medeltöjningsintervallet 53 till 87 mikrostrain resulterade i en genomsnittlig minskning av dynamisk modul även om testet anses vara oförstörande. Trots det verkade inte provkroppar som utsattes för höga töjningsnivåer vara mer skadade än de som testades vid låga töjningsnivåer.

Masterkurvor som var framtagna med det enaxiella trycktestet och press-dragprovet var inte lika, vilket var oväntat. Framförallt verkade de ha olika beroende av belastningsfrekvens och temperatur. Det är troligt att skillnaden i resultat beror på de problem som erfors under den gyratoriska packningen och det enaxiella trycktestet. Masterkurvorna från press-dragprovet på gyratoriskt packade provkroppar och borrkärnor var lika. I de fallen där det var en tydlig skillnad i hålrumshalt mellan provkroppsgrupperna kunde inga slutsatser dras.

Masterkurvor från de olika massorna ABT, ABb, polymermodifierad ABbm och AG jämfördes. Den generella rangordningen utifrån styvhet var ABbm, ABb, ABT, AG.

M-E PDG:s modell underskattade den asfaltrelaterade permanenta deformationen i båda konstruktionerna när inga fältkalibreringsfaktorer användes. Däremot kan den fältkalibrerade modellen beskriva framväxten av total asfaltrelaterat spårdjup väl. De fältkalibreringsfaktorer som togs fram i denna studie ökade modellens temperaturkänslighet och minskade dess beroende av antal överfarter.

Tillskottet av permanent deformation som varje asfaltlager gav i förhållande till totalt asfaltrelaterat spårdjup kunde inte modelleras korrekt i M-E PDG:s modell. Framförallt underskattades den permanenta deformationen i konstruktionernas understa lager, AG-lagret. Den nuvarande föredelningen baseras på en mindre studie av uppgrävda asfaltbalkar.

Slutsatser och rekommendationer

HVS-testning visade att polymermodifiering av bindlagermassan kan väsentligt öka konstruktionens motstånd mot permanenta deformationer i asfaltbundna lager. Laboratorietestning med press-dragprovet på borrkärnor tydde även på att den polymermodifierade bindlagermassan var styvare än den konventionella bindlagermassan.

Dynamisk modulresultat från press-dragprovet och det enaxiella trycktestet gav inte samma resultat. Däremot överensstämde resultaten från press-dragprovet på gyratoriskt packade provkroppar och borrkärnor. Testning av dynamisk modul minskade styvheten med 4% i genomsnitt. Minskningen i styvhet verkade inte bero på hur stor töjning provkropparna utsattes för.

M-E PDG kan användas för modellering av permanenta deformationer i en vägs asfaltlager. Regionala fältkalibreringsfaktorer bör bestämmas för att öka modellens noggrannhet. För att göra detta behövs omfattande data från långtidsuppföljningar av vägar inom regionen eller landet. Trafik, klimat, väggeometri och material behöver beskrivas och även framväxten av spårdjup. Fältkalibreringsfaktorerna kan sedan bestämmas med hjälp av de riktlinjer som utvecklas inom NCHRP-projektet 1-40B.

NCHRP bör utveckla M-E PDG:s modell för permanenta deformation så att den kan bestämma bidraget av permanent deformation från varje asfaltlager. Detta kan åstadkommas genom att genomföra en storskalig studie där asfaltbalkar från vägar inom LTPP-databasen grävs upp och utvärderas.

1 INTRODUCTION

Along with fatigue and thermal cracking, permanent deformations are internationally considered the most serious mechanism of distress in asphalt pavements. They often occur as longitudinal depressions in the wheel paths of the road, which are called ruts.

The longitudinal ruts affect vehicle-handling characteristics, thus creating grave hazards for traffic. Furthermore, if the surface is impervious, ruts will trap water and, occasionally, ice and snow. This causes hydroplaning and also makes snow-clearance difficult. Deep ruts result in both increasingly difficult steering, which adds to the safety concern, and in abnormal vehicle wear. Deep ruts are also often accompanied by longitudinal cracks that make the ruts permeable to free water. Rut geometry suggests that a considerable part of the free water on the road is drained in this way (Sousa et al., 1991).

Permanent deformation in asphalt concrete typically develops as a result of one or more factors. They can be divided into traffic properties, material properties and climate.

The rut-inducing traffic properties include the number of heavy vehicles, axle loads, tire pressure, and the portion of track-bound traffic. The effects of traffic load gradually increase every year due to a number of factors. The average European traffic growth is approximately 3% per year. Both axle loading and total heavy-vehicle weight are increasing. Furthermore, tire pressures are increasing, and the use of high-pressure super single tires is expected to increase (EAPA, 1995). It is widely recognized that super single tires damage the flexible pavement more than dual tires (Sebaaly, 2003; Verstraeten, 1995 and EAPA, 1995). This development of ever-increasing loading effects is expected to continue. Pavement design must take this into account in order to produce long-lasting pavements (EAPA, 1995). Material properties deal with mix design and the qualities of the materials included. New materials are constantly evolving in order to withstand the increasing traffic impact. The main climate factor is high temperature, under which flow rutting accelerates seriously. The climate is fairly predictable for a single location, even though heavy vehicles can create visible ruts during a few days of excessive summer heat.

Historically, the occurrence of flow rutting is a relatively new problem. Before 1960, few formal investigations were made, even though the presence of ruts had been noticed earlier. In the early 60s, Shell Oil Company presented the first pavement-design approach that took rutting as well as fatigue into account. These two distress mechanisms were controlled by limiting the vertical compressive strain at the top of the subgrade by using thick asphalt layers with high binder content. This approach was successfully used in the

following years, until the gradual increases in allowable axle load limits, tire pressures, and truck volumes resulted in flow rutting.

In 1972, modeling made another leap forward, and several test tracks were constructed to confirm the analysis (Sousa et al., 1991). By 1975, many European countries considered rutting a major problem, while the US and Canada still experienced only limited rutting in asphalt layers (Verstraeten, 1995). In 1977, a number of additional design methods were described. These were statistical techniques based on observation, elastic analysis in combination with creep test data and linear viscoelastic analyses.

Around 1980, interest in flow rutting was on the decline again, only to be renewed after 1982. The occurrence and prediction of rutting in flexible pavements were discussed in several papers after 1982. Other missing pieces of knowledge regarding wheel-load and tire-pressure effects on stress and strain within the pavement layers were also collected (Sousa et al., 1991).

In 1987, the US initiated the Strategic Highway Research Program (SHRP), in which comprehensive transportation research was carried out. Methods for both material characterization and mix design were dealt with. The mix design part was carried out within the Superior Performing Asphalt Pavements (SUPERPAVE) concept. New HMA field-performance testing equipment and performance-graded binder specifications and tests were developed.

The National Cooperative Highway Research Program (NCHRP) launched Project 1-37 approximately at the same time as SUPERPAVE was initiated. It focused on implementing mechanistic principles into the 1993 AASHTO Guide for the Design of Pavement Structures. It was followed by NCHRP 1-37A, in which the Mechanistic-Empirical Pavement Design Guide (M-E PDG) was developed. The M-E PDG software takes the principal distress modes into account and is today considered the most comprehensive overall pavement-design tool. This approach is based on mechanistic considerations and empirically correlated to existing pavements.

As the SUPERPAVE and M-E PDG were initiated in the US, the Directorate for Transport of the European Commission initiated the COST 333 (Development of New Bituminous Pavement Design Method) project to increase pavement knowledge. It reviewed current pavement-design methods, including performance models and assessed traffic, material and climatic properties, in order to pave the way for a new European pavement-design method. COST 333 was continued by AMADEUS (Advanced Models for Analytical Design of European pavement Structures) in 1998. The purpose of AMADEUS was to evaluate existing design models for use in a future mechanistic design method (AMADEUS, 2000). Sustainable and Advanced Materials for Road Infrastructure (SAMARIS WP5) was another European

project initiated by the Competitive and Sustainable Growth (GROWTH) Program in 2002 and finished in 2006. It focused on permanent deformation in flexible pavements. The purpose was to facilitate the use of performance-based specifications for asphalt materials as well as unbound materials (SAMARIS, 2004).

The concept of Long Life Pavements or Perpetual Bituminous Pavements has been discussed during the last few years. The idea is to increase the service life of pavements from the standard 20 years to 50 years or more. This can be achieved with thick asphalt concrete structures that are known to perform beyond their design lives. Many of these only require periodic surface restoration, which means low overall costs for construction, rehabilitation and user delay (Newcomb et al., 2001).

2 OBJECTIVES AND SCOPE

The first objective was to evaluate the model for permanent deformation in flexible pavement asphalt concrete layers that is used in the Mechanistic-Empirical Pavement Design Guide (M-E PDG), which was earlier called the 2002 Design Guide. This guide was developed to be applicable to a wide range of loading conditions, materials and environments within the US. This study is aimed at evaluating how well it can model the flow rutting of two different asphalt concrete structures during a Heavy Vehicle Simulation.

The second objective was to investigate if dynamic moduli can be determined by using the indirect tensile test in lieu of the uniaxial test. In order to do this, mastercurves derived from three different types of laboratory test set-ups were determined and compared. These are: uniaxial test using gyratory compacted specimens, indirect tensile test using gyratory compacted specimens and indirect tensile test on specimens cored from the pavement. If the three test arrangements yield similar results using the same asphalt mix, it can be suggested that neither compaction type nor test type affects the results. In that case, it can be proposed that the uniaxial test using gyratory compacted specimens can be replaced by the indirect test using pavement cores.

In theory, mastercurves derived from the uniaxial and indirect tensile tests using the same material should be equal, as shown by Kim et al. (2004). Mastercurves from the uniaxial test using gyratory compacted specimens should therefore equal those derived from the indirect tensile test using gyratory compacted specimens. The connection between mastercurves from the indirect tensile test using gyratory compacted specimens and the indirect tensile test on specimens cored from the actual pavement could be more challenging.

It will be of great importance if a credible connection can be established between the uniaxial test on gyratory compacted specimen and the indirect tensile test on cored specimen. The uniaxial test on 150 mm high gyratory compacted specimen has been used extensively, and the M-E PDG relies on it. The gyratory compaction has, however, received criticism for not being representative of existing pavements. It is therefore desirable to use field cores instead, but unfortunately layers with a height exceeding 150 mm are rare. Indirect tensile test specimens can be very thin. However, they should not be thinner than approximately twice the maximum aggregate size in order to retain the continuous material phase.

3 LITERATURE REVIEW

3.1 Flow rutting mechanisms

Permanent deformation in asphalt pavements often occurs as longitudinal ruts in the wheel paths, which can be accompanied by small upheavals to the sides. These depressions are caused by repeated loadings and develop gradually as the number of load applications accumulates. There are three types of permanent deformation that causes rutting:

- Wear rutting, which is caused by wear of studded tires on the road surface during winter. With no abrasion, polishing will reduce the road surface friction.
- Flow rutting, or instability rutting, is permanent deformation in the asphalt layers due to its viscoplastic behavior. This type of rutting is often formed on ascending gradients, on junction approaches and in bends, i.e. where heavy vehicles have to reduce speed and tangential stresses in the tire-pavement contact area are high. Upheavals to the sides of the wheel track is commonly observed (Verstraeten, 1995).
- Structural rutting, which is permanent deformation in one or more layers, including the subgrade. This can be observed as wide ruts without humps on the sides, and is caused by load-induced structural deterioration.

Another related phenomenon is wave-formations, which have been observed in predominantly urban areas. They can be either symmetrical washboard corrugations or unsymmetrical push-waves in all directions (Christensen, 1978). The rutting mechanisms may act independently of each other or in combination, depending on the circumstances of the specific road, loading, climate etc. Since flow rutting is the object of this study, the other rutting mechanisms will not be addressed.

Initially, the main cause of rutting in an asphalt layer is densification due to post compaction. This appears to be concentrated to the top layers (Perret et al., 2004). After a short period of time, the pavement is compacted enough to withstand further densification. The other cause is shear deformation, which affects the pavement throughout its entire service life. Studies performed by the AASHO Road Test (1962) and Hofstra et al. (1972), reported by Sousa et al. (1991), suggested that shear deformation, rather than densification, is the primary rutting mechanism. Eisenmann and Hilmer (1987) reached similar conclusions in their research. They showed that most of the rutting is caused by flow deformation without volume change. Figure 3.1 illustrates how flow rutting accumulates under the influence of traffic loading. The study in this case focused on how the ruts and upheaval zones of the profile change, from which changes in volume can be calculated.
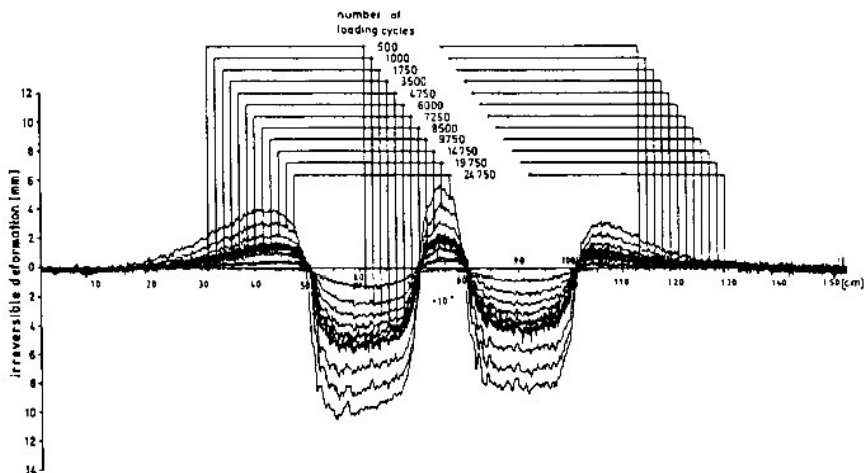
Figure 3.1. Effect of number of passes on transverse surface profile (Eisenmann and Hilmer, 1987).

In the initial phase of loading, the rut growth is distinctly greater than the volume increment in the upheaval zones. Consequently, densification is the predominant rutting mechanism in this phase. In the secondary phase, the volume decrease in the wheel path is approximately equal to the volume increase in the adjacent upheaval zones. This implies that the compaction mechanism has diminished and that further displacement will not change the total volume. This phase of constant volume deformation is regarded as the most common flow rutting mechanism. However, it was found that the volume increased at the end of the test runs, which implies that a third stage exists. The suggested cause was a lack of lateral drift that is not prevalent in most existing pavements (Eisenmann and Hilmer, 1987).

The distinct primary and secondary stages were found in the laboratory by using the repeated load permanent deformation test, as can be seen in Figure 3.2. The tertiary stage was also identified as the one in which permanent deformation accelerated.
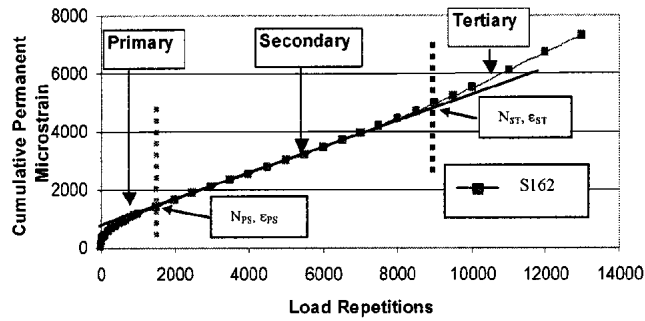
(a) In Linear Scale
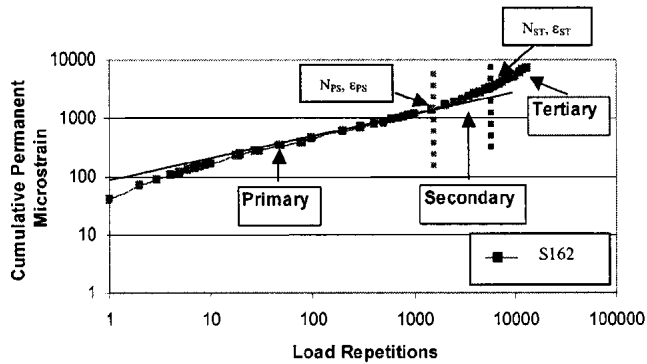
(b) In Log-Log Scale

Figure 3.2. Typical three-stage curve of accumulated permanent strain using the repeated load test (Zhou et al., 2004).

Data from an Accelerated Loading Facility simulation confirmed that the three stages of permanent deformation occurred in the field, as shown in Figure 3.3. This was confirmed when both wide-base single tires and conventional dual tires were used. However, it must be noted that it is difficult to find this pattern in field pavement performance data and in accelerated pavement test results. This is because most of them do not separate the flow rutting from permanent deformation in unbound layers. The permanent deformation rate is also dependent on temperature. A temperature increase can therefore be confused with the initiation of the secondary or tertiary stages (Zhou et al., 2004).
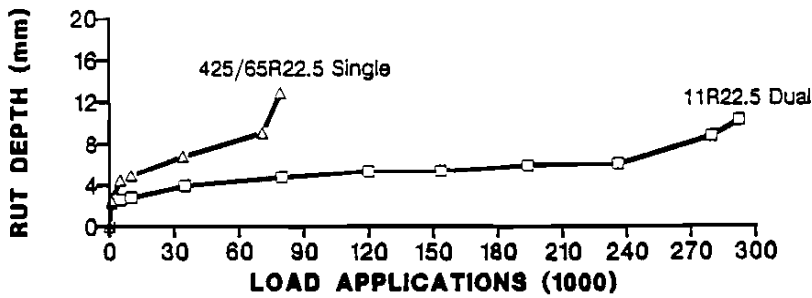
Figure 3.3. Rut depth growth on an 89 mm asphalt concrete pavement using both single and dual tires (Bonaquist, 1992) after (Zhou et al., 2004).

Several studies have been carried out in order to specify the depth at which permanent deformations mainly occur. Uge and van de Loo (1974) suggested that permanent deformation in asphalt concrete increased with increasing layer thickness up to 130 mm, but not beyond this threshold. The AASHO Road Test (1962) cited by Sousa et al. (1991) reported similar findings, but found the limit value to be approximately 250 mm. These results suggest that the mechanism of flow rutting is strongest at the pavement surface, only to diminish with increasing depth. Eisenmann and Hilmer (1987) partly agreed, but their elastic multi-layer simulation also showed that the shear deformation is initiated mainly in the base layer rather than in the surface. The maximum strain in their asphalt structure was located approximately 50 mm below the surface, as discussed in Chapter 3.4. Eisenmann and Hilmer (1987) also reported that flow rutting occurred to a depth of approximately 140 mm under heavy loading conditions. This flow rutting limit was reduced under gentle loading conditions.

3.2 Effect of material properties

The material characteristics and their proportions in the asphalt mix are crucial factors for pavement performance. The most important properties for obtaining high flow rutting resistance are stiffness and the relation between elastic and viscous strain. High mix stiffness leads to low strain levels, and a high degree of elasticity means that most of the strain that has arisen will recover.

Fatigue, the other major distress factor, is also affected by mix properties, even though it is partly a structural problem. The requirements for high resistance to both flow rutting and fatigue cracking are conflicting in some respects. An asphalt mix with high binder content made of soft bitumen and rounded aggregate will have excellent fatigue properties but poor resistance to flow rutting. This type of mix is smooth and workable, thus making it easy to lay. On the other hand, a stiff mix made of hard asphalt with relatively low binder content and crushed aggregate is expected to resist flow rutting but will suffer from fatigue instead. Since the pavement must have adequate resistance to both of these partly contradictory mechanisms, a compromise has to be found. Depending on the role of the layer in the road structure, the relation between durability and stability can be modified (Verstraeten, 1995). The effect of different material properties on Hot Mix Asphalt (HMA) is summed up in Table 3.1.

Table 3.1. Summary of impact of material characteristics on flow rutting resistance in conventional HMA (Sousa et al., 1991).

	Factor	Change in Factor	Effect of Change in Factor on Rutting Resistance
Aggregate	Maximum size	Increase in maximum size	Increase
	Gradation	Gap to continuous	Increase
	Shape	Rounded to angular	Increase
	Surface texture	Smooth to rough	Increase
Binder	Stiffness[a]	Increase	Increase
Mix	Binder content	Increase	Decrease
	Air-void content[b]	Increase	Decrease
	Voids in Mineral Aggregate (VMA)	Increase	Decrease[c]
	Method of compaction	_[d]	_[d]
Test field conditions	Temperature	Increase	Decrease
	State of stress/strain	Increase in tire contact pressure	Decrease
	Load repetitious	Increase	Decrease
	Water	Dry to wet	Decrease if mix is water sensitive
a) Refers to stiffness at temperature at which rutting propensity is being determined. Modifiers may be utilized to increase stiffness at critical temperatures, thereby reducing rutting potential.			
b) When air-void contents are less than about 3 percent, the rutting potential of mixes increases.			
c) It is argued that very low VMA (e.g. less than 10 percent) should be avoided.			
d) The method of compaction, either laboratory or field, may influence the structure of the system and therefore the propensity for rutting.			

3.2.1   Mineral aggregate

The asphalt mix consists of 90-95 % aggregate that greatly affects the mix properties. The main aggregate characteristics of importance for permanent deformation are maximum aggregate size, gradation, particle shape and texture.

Maximum aggregate size

A large maximum aggregate size can be beneficial to permanent deformation resistance on pavements subjected to high tire pressures. The large particles form a stiff internal skeleton structure that carries the load. However, the nominal maximum size must not exceed 2/3 of the layer thickness (Davis, 1988). Similar conclusions were drawn by Williams (2003), who also showed that mixes with larger aggregates are typically more resistant to rutting than finer mixes. Typical maximum aggregate sizes are: 25 mm for asphalt base layer mixes, 13-19 mm for binder layer mixes and less than 13 mm for wear layer mixes (Asphalt Institute, 1989). Typical Swedish maximum aggregate sizes are: 16-32 mm for asphalt base layer mixes, 11-22 mm for binder layer mixes and 8-16 for wear layer mixes (ATB Väg, 2004).

Gradation

The aggregate gradation effect on permanent deformation of HMA is great and widely acknowledged. In fact, changes in gradation have been found to have a greater impact on permanent deformation resistance than changes in the grade or amount of binder (Williams, 2003). Resistance to permanent deformation is achieved by using a gradation that is continuous rather than gap-graded. The continuous gradation fills unnecessary voids and increases the number of contact points, which creates a strong mineral aggregate skeleton (Sousa et al., 1991).

Permanent deformation was, however, observed in extremely dense asphalt mixes with high amounts of natural sands and, especially, with gradation humps of fine sands. The concept of "The Restricted Zone" was therefore created to describe an area on the gradation chart along the theoretical maximum density line. Superpave Mix Design recommended local agencies to avoid gradations that passed the Restricted Zone in order to avoid premature rutting. This recommendation was often adopted as an absolute criterion. Later studies have shown that The Restricted Zone concept is redundant if all other Superpave mix design criteria are fulfilled (Kandhal and Cooley, 2001). Zhang et al. (2004) have also shown that HMA gradations through The Restricted Zone can perform as well as, or even better than, gradations above or below it. The typical Swedish AG base mix with 100% crushed aggregate also runs through The Restricted Zone, as shown in Figure 3.4, but it is nonetheless considered rut resistant. Modern mix design should therefore not take The Restricted Zone concept into account.
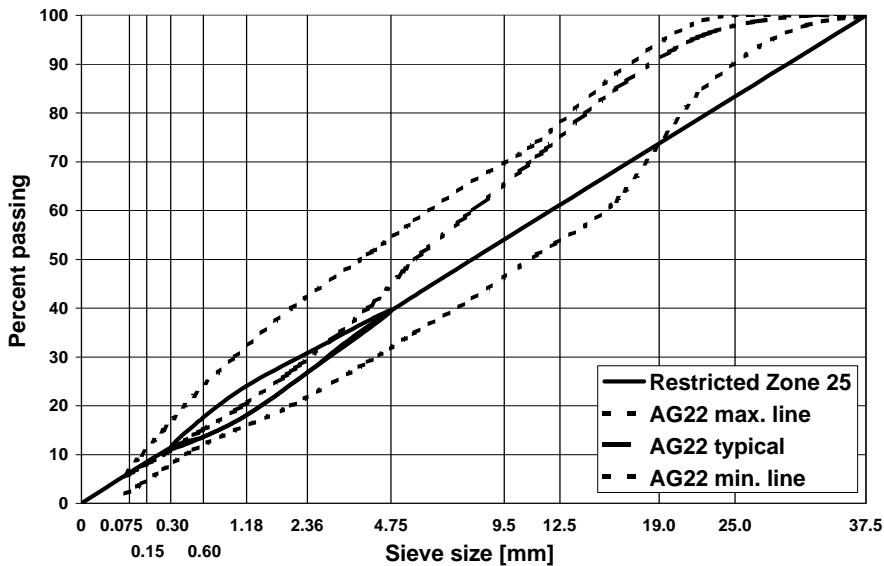
Figure 3.4. A typical Swedish AG22 base mix that violates The Restricted Zone.

Stone Mastic Asphalt (SMA), which is used for wear layers, relies on a different mix design concept than HMA. Since it consists mainly of stone, filler and bitumen, it is gap-graded in contrast to the continuous-graded HMA. Its resistance to permanent deformation is entirely dependent on the interlocking mechanism of the larger aggregate particles, and not on the support of a continuous gradation. A large stone SMA has also been tested for binder layers in Sweden due to its resistance to permanent deformation (EAPA, 1998).

Shape
The shape or angularity of the aggregates is well known for its impact on permanent deformation. The more irregular the form of the aggregates, the higher the interlocking capability and the stiffer the mix. The shape is dependent on the portion of crushed aggregate as opposed to natural gravel. Adding natural sands, which are rounded, to the mix therefore increases rutting susceptibility (Kandhal and Cooley, 2001). This is very important for fine mixes, while coarse mixes do not necessarily display the same behavior. Guler et al. (2000) suggested that it was due to a reduced number of contact points between the aggregates in course mixes.

Surface texture
Surface texture, or roughness, is closely related to shape on a finer scale. A rough aggregate surface texture provides higher rut resistance than a smooth one. This is due to a higher interlocking capability of the aggregate particles, which stiffens the asphalt mix (Sousa et al., 1991). The effect of roughness on

permanent deformation resistance is especially evident in the fine parts of the gradation (Kandhal and Cooley, 2001). Only crushed mineral aggregate should therefore be used for asphalt mix.

3.2.2 Asphalt binder

Even though bitumen is a minor asphalt mix constituent, the properties of the mix are governed by the bitumen properties to a great extent. The main bitumen performance criteria can be summed up as the following four properties: Rheology, cohesion, adhesion to mineral aggregate and durability (The Shell Bitumen Handbook, 2003).

Bitumen is composed of a wide spectrum of molecules that can be divided into saturates, aromatics, resins and asphaltenes. The molecular weights and polarity properties of the constituents are very different, which makes a strict binder definition impracticable (The Shell Bitumen Handbook, 2003). Instead, paving grade bitumens are categorized by means of functional laboratory tests. The European Committee for Standardization specifies bitumen in terms of penetration, softening point, resistance to hardening, flash point, and solubility test results. The Superpave binder specification is called Performance Grading. The Performance Grading bitumen classes are named according to the temperature span in which they should be used. They are classified by means of laboratory tests to determine minimum flash point, viscosity, dynamic shear, mass loss during heating, low temperature creep stiffness and low temperature direct tension (The Shell Bitumen Handbook, 2003).

Bitumen is viscoelastic, and its stiffness is heavily dependent on temperature and load frequency. The bituminous binder is stiff at low temperatures and/or high load frequency. Loadings that the asphalt concrete is subjected to will be carried by the binder matrix. The asphalt concrete will therefore adopt the bitumen properties to a high extent. Hence asphalt concrete is considered viscoelastic under these conditions. However, high temperature and/or low load frequency weakens the bitumen matrix. Under these conditions, the mix properties are therefore determined by the aggregate to a greater extent (Chowdhury et al., 2001). The asphalt concrete will therefore exhibit additional plastic behavior.

Another issue is the workability of the asphalt mix. Gudimettla and Cooley (2003) showed that workability is substantially decreased as a consequence of increased bitumen viscosity. Stiff and harsh asphalt mixes can be harder to compact to the desired density than other mixes.

Polymers

The addition of polymer modifiers to the asphalt mix increases steadily when new flexible pavements are constructed. Adding polymers to the binder improves pavement service life considerably. One of the most important advantages is that it increases resistance to permanent deformations. This can be achieved in two ways. The first approach is to displace the balance between the elastic and the viscous strain response components. This means that the elastic part is increased, while the viscous part is reduced. The second approach is to increase overall bitumen stiffness, thereby stiffening the asphalt mix. An increase in stiffness means less strain for a given load.

There are many types of polymers that all have their special qualities. For the purpose of mitigating permanent deformation, thermoplastic elastomers and thermoplastic polymer are the essential subgroups. The first group, thermoplastic elastomers, forms a three-dimensional network on the molecular scale. This elastomer network increases the bitumen elasticity. As the elastomer is thermoplastic, the structure weakens or dissociates at laying temperatures. The second group, i.e. thermoplastic polymers, is also temperature dependent, as the polymer associates only below a certain temperature. The effect is primarily not an increase in elasticity, but rather an increase in the overall stiffness of the bitumen (The Shell Bitumen Handbook, 2003). The ideal polymer-modified bitumen has an adequate viscosity with minimal temperature dependence at normal pavement service temperatures. The viscosity should, however, be low at laying temperatures. An example of the ideal modified bitumen can be seen in Figure 3.5 (Brûlé, 1996).
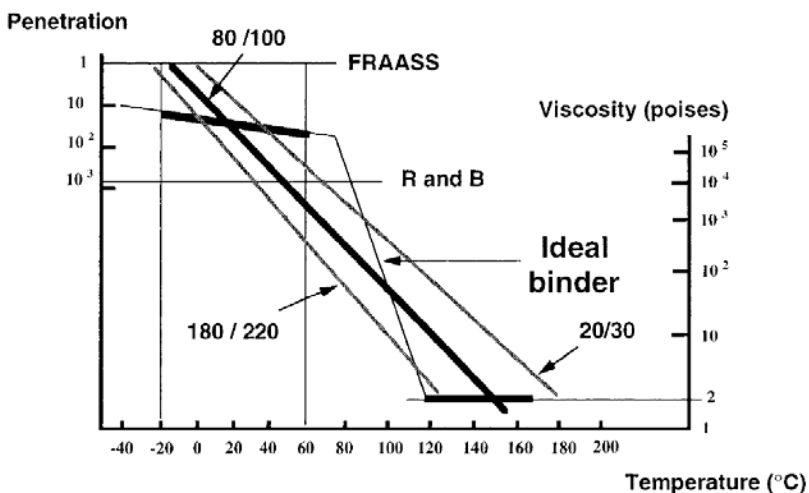
Figure 3.5. Temperature susceptibility of an ideal thermoplastic bitumen (Brûlé, 1996).

Ageing of bitumen

"Ageing" is a generic term for a number of chemical and physical reactions that cause bitumen to harden. Hardening means that the bitumen becomes stiffer as the viscosity increases. The main factors can be divided into oxidation, evaporation, exudation, and physical hardening.

Oxidation is the chemical reaction in which bitumen reacts with oxygen. This results in molecules with higher polarity. Polar molecules are attracted to one another and form a complex and strong micelle structure within the bitumen. The higher the content of polar molecules, the greater the viscosity of the bitumen. The process of oxidation is highly dependent on temperature, but also on bitumen film thickness and time. Oxidation is considered to be the main mechanism that causes ageing in bitumen.

Evaporation is the loss of volatiles that can be observed at high temperatures in particular. As the light-weight non-polar molecules disappear, the viscosity increases. Exudation, or exudative hardening, occurs when oily components flow from the aggregate surface into its pores. The remaining bitumen compound shows higher stiffness than before. Physical hardening, which is also called steric hardening, occurs when the bitumen is at rest and at ambient temperatures. This mechanism is usually attributed to a reorientation of the bitumen molecules and a crystallization of waxes. The process is reversed upon reheating (The Shell Bitumen Handbook, 2003).

The total ageing process can be divided into short-term ageing and long-term ageing. Short-term ageing occurs during mixing and laying, when the asphalt mix is subjected to excessive temperature and oxygen. This is the major source of the total ageing. Once the asphalt mix has been laid, ultraviolet radiation, high temperature and oxygen cause long-term ageing. Pavements that experience premature long-term ageing often have an air-void content that is too high (The Shell Bitumen Handbook, 2003).

Aging propensity can be determined by comparing penetration or viscosity of the bitumen before and after artificial ageing. The artificial laboratory aging is divided into short-term and long-term aging. The Short-term aging can be simulated with the Rolling Thin Film Oven Test (RTFOT), in which the bitumen sample is subjected to excessive heat and air for a short period of time. Long-term aging is simulated by using the Pressure Ageing Vessel (PAV), which subjects the bitumen sample to high pressure and moderate temperature for a relatively long period of time.

Ageing can be described with reference to an ageing index, which is defined as the ratio of viscosity of the aged bitumen to the viscosity of the virgin bitumen. Said (2005) has shown that the increase in the ageing index is greater during the first service year than during the second to fourth years. Viscosity is closely linked to several important distress modes, such as

permanent deformation, fatigue and thermal cracking. The asphalt concrete pavement is an ever-changing material that will respond to different distress mechanisms according to its present state. Permanent deformations will therefore tend to develop at an early stage after laying.

3.2.3   Mix composition

The quality and proportions of aggregates, bitumen and additives determine the properties of the asphalt mix. The mix of each asphalt layer should be designed for optimal performance in withstanding the different deterioration mechanisms.

High mix stiffness is a key factor of resistance to permanent deformation. The Shell Bitumen Handbook compared two HMA mixes with bitumen contents of 5 % and 11 %, respectively. By means of creep tests, the mix stiffness was determined as a function of bitumen stiffness. The results strongly support the idea that the 11 % mix displayed a considerably lower stiffness as compared to the 5 % mix. This was especially evident at low bitumen stiffness (The Shell Bitumen Handbook, 2003). Perret et al. (2004) investigated the rut susceptibility of different mixes with the LCPC rutting test. They found that high mastic content could reduce rutting resistance considerably. These test results imply that the bitumen content should be kept low in order to increase rutting resistance. However, low bitumen content can reduce the resistance against fatigue and cracking, which underlines that mix design is a matter of compromise in order to achieve resistance to all distress mechanisms.

Air-void content is also known to have strong impact on HMA properties. It should be sufficiently low to obtain mix stiffness, thereby avoiding permanent deformation. Tayebali et al. (1994) compared the stiffness of specimens with an air-void content of 4 % and 8 %. The stiffness was measured with both the uniaxial and the indirect tensile tests under a wide range of temperatures. The results strongly suggest that an air-void content of 4 % provides higher stiffness than 8 % for that particular asphalt mix, as shown in Figure 3.6 (Tayebali et al., 1994).
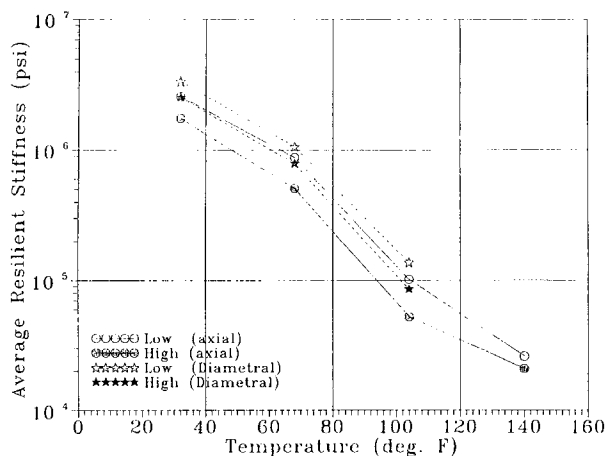
Figure 3.6. Effect of high and low air-void content on average resilient stiffness (Tayebali et al., 1994).

Roberts (1980), as reported by Martinez et al. (1991), also studied how HMA material properties are dependent on air void content. He found that a relatively low air void content improves resistance to permanent deformation. It was recommended that the air void content should normally be between 3% and 8% to obtain optimum performance, as shown in Figure 3.7.
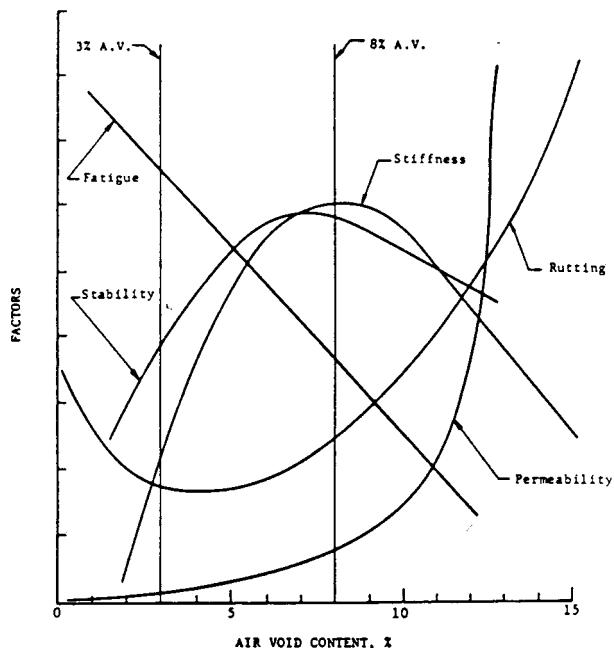
Figure 3.7. Relationship between mixture properties and air void content (Roberts 1980) after Martinez et al. (1991).

18

The concepts of "Voids in Mineral Aggregate" (VMA) and "Voids Filled with Asphalt" (VFA) are closely related to bitumen content and air-void content. They are often used as a performance criterion for asphalt pavements. VMA is defined as the percentage of void space between the aggregate particles in a compacted mix as shown in Figure 3.8. The voids are filled with bituminous binder and air. VFA is defined as the portion of bitumen in the voids (Chadbourn et al., 2000).
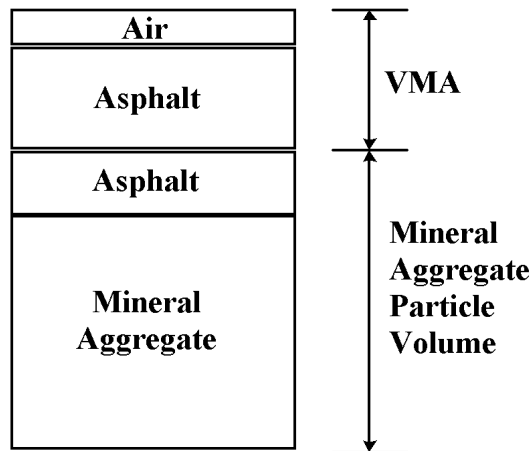
Figure 3.8. Illustration of VMA (Chadbourn et al., 2000).

The apparent binder film thickness is another concept that addresses the same issues as the VMA. Asphalt film that is too thin or VMA that is too low can lead to reduced durability and moisture susceptibility. The Asphalt Institute has therefore used a minimum VMA criterion for many years (Chadbourn et al., 2000). Some criticism has been directed against the Superpave minimum VMA criterion because it does not consider the effect of different gradations. It was suggested that the apparent binder film thickness is a better criterion, since it represents a more direct approach. This point is illustrated by the fact that a coarse and a fine mix with the same VMA will have very different apparent binder film thickness (Kandhal et al., 1998).

3.3   Compaction principles and their effect on flow rutting

Asphalt concrete specimens for material testing can be produced in many different ways. The procedure of choice in order to produce realistic replicate specimens is pavement coring. However, it is not possible to obtain specimens higher than the layer thickness. Cylindrical specimens of 150 mm in height must therefore often be laboratory compacted. There is also a need to test new asphalt mixes before employment, which makes laboratory compaction a necessity.

Besides, laboratory compaction offers a number of additional benefits. It is considered less complicated, and it provides high precision in terms of temperature, compaction force and material quantity (Airey et al., 2006). Nevertheless, laboratory compaction studies have shown that it can be difficult to imitate pavement cores in terms of air-void content, particle orientation and mechanical properties (Airey et al., 2006; Button et al., 1994).

The most common laboratory compactors can be divided into plate compactors, vibratory compactors and gyratory compactors. The plate compactor produces asphalt concrete slabs from which test specimens can be cut and cored. The vibratory compactor uses a vibration hammer to compact the asphalt mix in the mould. Slabs can also be used directly in a wheel-tracking device. The gyratory compactor produces gyratory plugs that are cut and cored to the desired specimen dimensions. It can also be used for mix design by measuring resistance of compaction for classification.

The heated asphalt mix is placed in a metal mould before gyratory compaction. A low static pressure is applied at the top and at the bottom. Gyratory compaction is accomplished through the low static pressure and the circular movement of the mould top. This subjects the specimen to a shearing action that results in a kneading type of compaction, as shown in Figure 3.9.
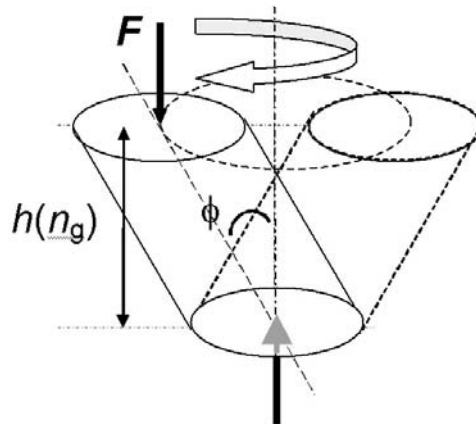
Figure 3.9. Principal drawing of gyratory compactor motion (SS-EN 12697-31, 2005).

Although the settings of the gyratory compactor can be adjusted, standard procedures are often used for specimen fabrication. Two common protocols have been identified: the American Association of State Highway and Transportation Officials (AASHTO) T312-04 standard (AASHTO, 2006) and the European Committee for Standardization (CEN) EN 12697-31 standard. They are essentially equal, except for the angle of gyration, which is 1.25 ° for the AASHTO method and 1.00 ° for the CEN method. The gyration angle has a great impact on the kneading ability and, consequently, on the degree of compaction. Both AASHTO and CEN prescribe a vertical static pressure of approximately 600 kPa and a speed of approximately 30 revolutions per minute (SS-EN 12697-31, 2005; AASHTO, 2006).

The simplicity of the method and the modest mix quantity required provide gyratory compaction with substantial advantages as compared to pavement coring and plate compaction. There has, however, been some criticism directed against it. The gyratory compactor is a standard tool manufactured according to certain specifications, but different brands of Superpave gyratory compactors can yield significantly different specimen heights. The problem appears to be dependent on mix type and is greater for course graded mixes than for fine graded ones. Hinrichsen (2001) suggested that specimen height differences are due to differences in the initial loading and setting of the angle. Another research group also reported significant differences in calculated air voids. The air void difference between specimens from two Superpave gyratory compactors was occasionally close to 2 % (Buchanan and Brown, 2001).

It has been reported that the air voids in gyratory compacted specimens are unevenly distributed. Many researchers have produced specimens, cut them into pieces and evaluated their composition. The center of the specimen tends to reach higher density than the eccentric parts (Raaberg, 1999; Viman, 1998; Masad et al., 1999). Other researchers report that specimens compacted according to the Superpave protocol displayed mechanical properties that were significantly different from field cores produced with the same material and compacted to the same air void content (Peterson et al., 2004). However, Button et al. (1994) found that gyratory compactors were at least as good as any other compaction method. The gyratory compactor is a standard method for test specimen fabrication within the AASHTO Provisional Standards (AASHTO, 2006).

As mentioned before, gyratory compaction can be utilized as a mix design tool. The air void content as a function of the number of gyrations is often used to describe asphalt mix stability. An unstable mix tends to lose stability at a very low air void content. The ratio between the work needed to attain a 2 % and 5 % air void content should be at least 4 when the Superpave gyratory compactor is used. The mix can be considered stabile if this criterion is met (Mallick, 1999).

3.4 Analysis of the traffic loading effect on flow rutting

Traffic load is the direct cause of most deterioration mechanisms, including rutting. The loading is dynamic, which means that it varies over time. It is particularly important to recognize this due to the time-dependent properties of asphalt concrete. The traffic loading effects are classified in terms of vehicle speed, axle load, tire pressure, axle configuration and lateral wander.

3.4.1 Vehicle speed

The loading effect of passing vehicles induces stresses and strains in the pavement directly beneath the tire. Low vehicle speed implies high loading time, which equals low loading frequency. The stiffness of a viscoelastic material like asphalt concrete will decrease under these conditions. The low speed loading will therefore result in high flow rutting (White et al., 2002). This effect can be observed at traffic lights, bus stops, traffic circles and at steep uphill slopes, especially in the southern direction.

3.4.2 Axle load and tire pressure

Eisenmann and Hilmer (1987) conducted elastic multi-layer simulations to investigate how various conditions of load and tire pressure affect strain at different depths. The assumptions included a single tire and typical summer temperature. Different tire pressures were simulated, while the load was constant in the first simulation. It was concluded that an increased tire pressure and constant axle load predominantly increased strain close to the surface but had a very small impact at high depth, as shown in Figure 3.10. The second approach involved different axle loads, while the tire pressure was kept constant. Under these circumstances the strain shifted mainly at high depths but not near the surface, as presented in Figure 3.11.
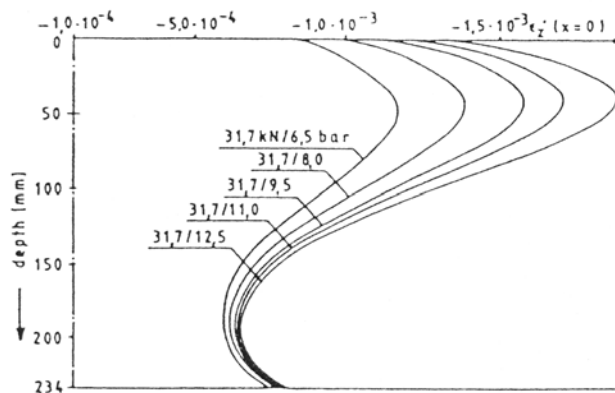
Figure 3.10. Vertical strain as a function of depth for a constant single tire load of 31.7 kN and variable inflation pressure (Eisenmann and Hilmer, 1987).
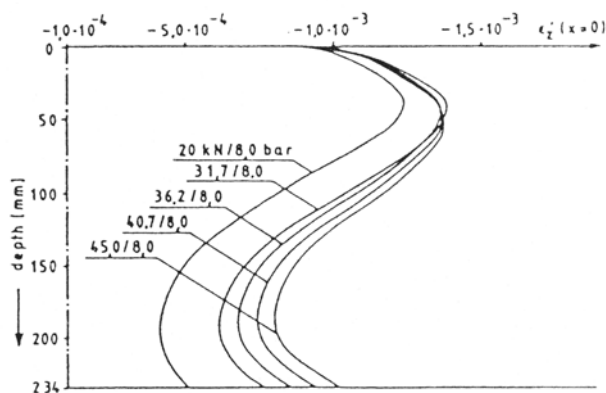
Figure 3.11. Vertical strain as a function of depth for a constant inflation pressure of 8 bars and variable single tire load (Eisenmann and Hilmer, 1987).

The tire-pavement contact stress distribution is non-uniform, and it is significantly different at the tire edge and tire center. Permanent deformation near the surface is considered to increase when contact stresses at the tire edge are high (Blab, 1999). Still, many road deterioration models use uniform pressure distributions for reasons of simplicity. It is assumed that the contact pressure is equal to the inflation pressure. Load and inflation pressure define the contact area, which is assumed to be circular.

Several studies have been carried out to investigate the differences between uniform and non-uniform tire pressures, using conventional and wide-base tires. Siddharthan et al. (2002) compared strain response from uniform and non-uniform tire pressure distributions using a finite-layer analytical model. Surprisingly, the responses computed using the non-uniform stress distribution were significantly lower than using the uniform stress distribution. The difference varied within the interval of 6% and 30% and was dependent on such factors as tire inflation pressure, tire type and thickness of the pavement structure. Luo and Prozzi (2005) supported this conclusion using the multi-layer linear-elastic computer program CIRCLY. The uniform model showed a significant additional strain of up to 23 % as compared to the more realistic non-linear model. In conclusion, the uniform contact pressure approach generally results in higher strain levels than does the non-uniform approach.

It can be argued that uniform contact pressure is acceptable, as it results in higher strain levels that are on the safe side. However, an overestimation of strain leads to unbalance in field-calibrated models. A mechanistic understanding will not be possible if one error corrects another. This is therefore an important research area that needs further investigation.

3.4.3 Axle configuration

Heavy vehicles have traditionally used conventional dual tires, but the use of singled-out dual tires and super-single tires is increasing steadily. This is due to such benefits as lower vehicle weight and lower rolling resistance. Sebaaly (2003) summarized a great number of Accelerated Pavement Testing studies comparing single tires to conventional dual tires. The tests were carried out on representative pavements subjected to typical loads. The most prevalent finding is that super-single tires cause more damage than dual tires. The permanent deformation ratio was approximately 1.25-1.50 for thick asphalt concrete structures and somewhat greater for thin asphalt concrete structures (Sebaaly, 2003). This conclusion is illustrated by Bonaquist's accelerated pavement testing results, as shown in Figure 3.12 and Figure 3.13. The rut depth growth occurred much faster with super-single tires than with conventional dual tires on both thick and thin asphalt concrete structures.
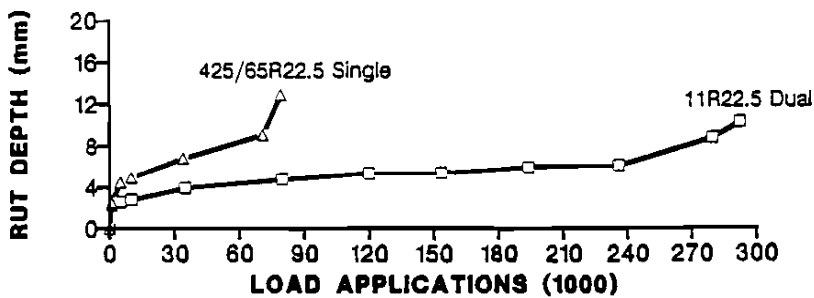
Figure 3.12. Rut depth propagation of an 89 mm thick AC structure using super single and dual tires (Bonaquist, 1992) after (Sebaaly, 2003).
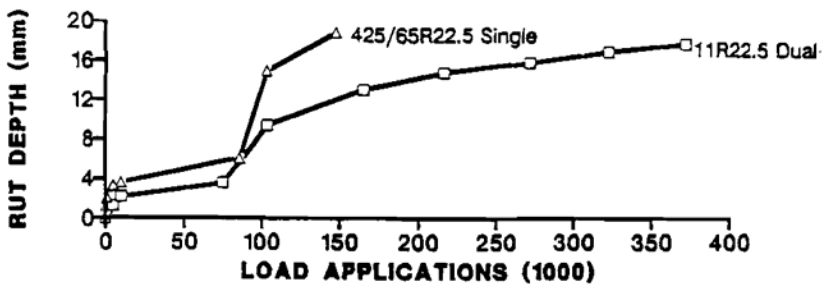
Figure 3.13. Rut depth propagation of a 178 mm thick AC structure using super single and dual tires (Bonaquist, 1992) after (Sebaaly, 2003).

3.4.4   Lateral wander

"Lateral wander" is the phenomenon of wheels not following the same wheel paths. Wander will affect road deterioration and can be described by a statistical distribution. The amount of wander is typically dependent on vehicle-type distribution, road width and the amount of previous rutting. White et al. (1999) conducted Accelerated Pavement Testing and found that lateral wander mitigated flow rutting on both high and low density AC structures, as shown in Figure 3.14 and Figure 3.15. They suggested two explanations, namely that lateral wander reduces the loading time of any possible wheel path and that loadings applied on typical heave areas will compact the asphalt concrete, thereby increasing rutting resistance.
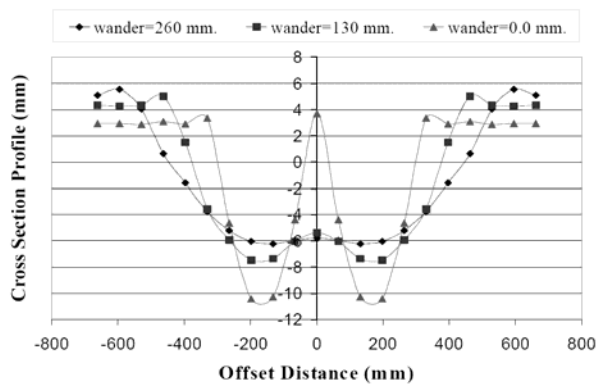
Figure 3.14. Low-density cross-sections subjected to 5000 passes with various amounts of wander (White et al., 1999).
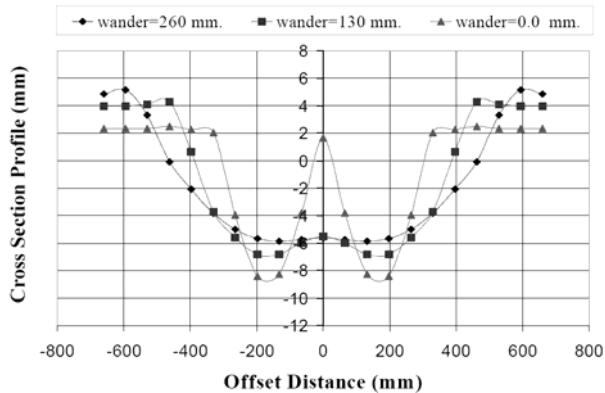
Figure 3.15. High-density cross-sections subjected to 5000 passes with various amounts of wander (White et al., 1999).

Epps et al. (2001) also conducted Accelerated Pavement Testing at WesTrack, which confirmed that lateral wander mitigates flow rutting in AC structures.

LITERATURE REVIEW

3.5   Pavement temperature

As explained in Chapter 3.2, the mechanical properties of asphalt concrete are heavily dependent on temperature. Asphalt concrete is stiff and elastic at low temperatures but softens and shows additional plastic behavior at high temperatures. This is manifested as an increased rutting propensity at high temperatures (Sousa, 1991). The maximum pavement surface temperature is approximately 50 to 60 °C in Europe and the US (Verstraeten, 1995).

Prediction of temperature profiles is important for the purpose of pavement deterioration modeling. This is normally carried out by means of a climate model that provides a temperature profile throughout the pavement. The most important factors to consider are conduction, convection, shortwave and longwave radiation, surface icing, infiltration, evaporation and condensation (Hermansson, 2004).

The Integrated Climate Model (ICM) was developed by the American Federal Highway Administration in 1989. It continuously simulates the pavement temperature profile throughout the one-dimensional pavement structure on the basis of pavement structure properties and climate data. The properties of the pavement structure are its geometry, heat conductivity, heat capacity, latent heat of fusion, surface absorptivity and surface emissivity. The climatic factors are solar shortwave radiation, incoming longwave radiation, conduction and convection. The effect of infiltration, transpiration, condensation, evaporation and sublimation is not accounted for within the original ICM model (Lytton et al., 1993A).

The improved ICM, the so-called Enhanced Integrated Climate Model (EICM), is being continuously developed. It is an integrated part of the Mechanistic-Empirical Pavement Design Guide (M-E PDG) software. Zaghloul et al. (2006) however found that the M-E PDG results were overly sensitive to climate changes. Liang et al. (2006) evaluated EICM v3.02 using measured and predicted pavement temperatures in asphalt pavements for nearly two years. They found that one of the main deficiencies was that the pavement surface temperature was over-estimated during all seasons. The discrepancy was up to 8 °C (15 °F) at the surface and slowly decreased with depth (Liang et al., 2006).

Åke Hermansson (2004) has also developed a pavement temperature simulation model that takes the most important factors into consideration. The model was validated using meteorological data and surface temperature data from nine sections in the US and Sweden. The results showed an average monthly error of less than 2 °C, which is considered very good. Hermansson's model was employed by Said et al. (2006) to predict temperature at different depths. It was concluded that sufficiently accurate results can be produced. However, the model has not yet been implemented in the Swedish standard concept ATB Väg (2005). Instead, ATB Väg

accounts for temperature effects in AC layers by dividing the country into five climate zones, as illustrated in Figure 3.16. Each climate zone has four or six subseasons, as shown in Table 3.2 and Table 3.3. Each combination of climate zone and subseason corresponds to a number of days at a specific temperature.
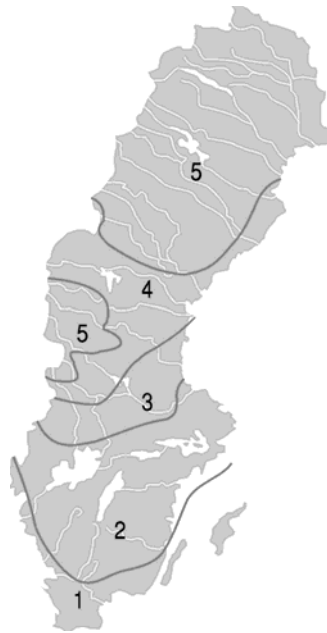
Figure 3.16. Climatic zones in Sweden (ATB Väg, 2005).

Table 3.2. Length of climatic period [days/year] (ATB Väg, 2005).

	Climatic zone				
	1	2	3	4	5
Winter	49	80	121	151	166
Thaw in winter	10	10			
Thaw period	15	31	45	61	91
Late spring	46	15			
Summer	153	153	123	77	47
Autumn	92	76	76	76	61

Table 3.3. Temperature in asphalt concrete [°C] (ATB Väg, 2005).

	Climatic zone				
	1	2	3	4	5
Winter	-1,9	-1,9	-3,6	-5,1	-7
Thaw in winter	1	1			
Thaw period	1	2,3	4,5	6,5	7,5
Late spring	4	3			
Summer	19,8	18,1	17,2	18,1	16,4
Autumn	6,9	3,8	3,8	3,8	3,2

3.6 Laboratory test principles and methods

Laboratory testing on asphalt concrete is carried out in order to describe material properties, which can subsequently be used for pavement deterioration modeling and mix design. A variety of tests have been developed to simulate realistic pavement conditions. The test must be valid, which means that there should be a strong relation between test results and permanent deformation in the field. A test for routine use should also be accurate, easy to perform, inexpensive and preferably widespread to facilitate comparison. Extensive testing has revealed that some primary factors should be represented. These are temperature, number of load applications, loading frequency, mix properties and the state of stress. (Sousa et al., 1991).

A selection of possible laboratory test methods that can be related to permanent deformation will be described. These are:

- Uniaxial and triaxial cylindrical tests
  - Static load creep test on cylindrical specimen
  - Repeated load creep test on cylindrical specimen
  - Dynamic modulus test on cylindrical specimen
- Indirect tensile dynamic modulus test on cylindrical specimen
- Shear tests
- Wheel-track tests

3.6.1 Uniaxial and triaxial cylindrical tests

The cylindrical test can be either uniaxial or triaxial, i.e. unconfined and confined, respectively. Both test types have their advantages and disadvantages. The uniaxial test is purely one-dimensional and therefore theoretically very simple. There are large quantities of old creep test data to compare with due to the wide distribution of the required equipment and expertise. The uniaxial tests have therefore been a well-established measure of mix characteristics for a variety of predictive methods since the 1970s (Sousa et al., 1991).

The confinement of the triaxial test is a uniform pressure that is applied laterally along the specimen. Triaxial tests allow simulation of a wide range of stress states that are encountered within pavements. They are therefore valuable for research purposes although they are considered overly advanced for routine testing (Sousa et al., 1991).

The test specimen is cylindrical with flat and parallel ends as shown in Figure 3.17. The specimen is placed between two stiff steel plates, and its ends are well lubricated to prevent lateral constraint of the specimen. LVDTs (Linear Variable Displacement Transducers) are attached. Triaxial testing also involves the application of a lateral pressure around the specimen circumference by means of a membrane and pressurized air. Before testing, temperature is allowed to stabilize at the prescribed level. The load program is then applied while the deformation of the specimen is measured as a function of time (Sousa et al., 1991).
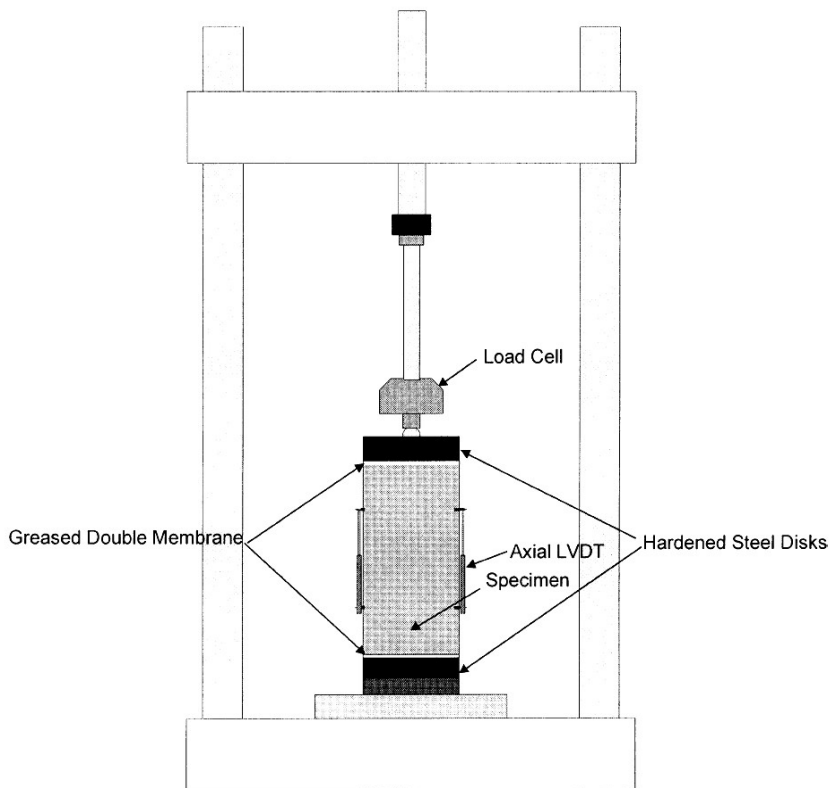
Figure 3.17. Schematic diagram of uniaxial cylindrical test device (Kaloush and Witczak, 2002).

Static load creep test on cylindrical specimen

The static creep test is a simple destructive test that has been used extensively for many years to determine the asphalt concrete propensity for permanent deformation. The simplicity and validity of this method have made it widespread, and most asphalt laboratories have the equipment and expertise required to perform it (Sousa et al., 1991).

Brown and Foo (1994) found that the unconfined creep test resulted in premature specimen failure when a realistic stress level and temperature, 55.2 kPa and 60 °C, were used. However, the confined creep test specimen endured 828 kPa when exposed to a confining pressure of 138 kPa at 60 °C, which is considered realistic pavement conditions. They therefore concluded that it was only the confined creep test that could reproduce pavement conditions, although loading times are very different. It is, however, possible to predict rutting behavior using unconfined creep test data at low stress levels and temperatures. Linearity of the viscoplastic strain over the range of load applications must be assumed. The asphalt concrete mastercurve can then be used to translate laboratory results into pavement conditions (Brown and Foo, 1994).

Another difference between the unconfined and the confined creep test is the change in air void content. Test specimens with air voids >2% tended to dilate, while specimens <2% were compressed during unconfined testing. This is contrary to known pavement behavior. On the other hand, the confined test specimens with air voids >1% were compressed while specimens <1% were dilated during confined testing. It can therefore be concluded that compression/dilatation behavior is more realistic with confined than with unconfined creep testing (Brown and Foo, 1994).

Materials are often characterized by their stiffness modulus, which is defined as the relation of stress and the corresponding strain. Since viscoelastoplastic materials have several strain components, the reciprocal to stiffness modulus is more useful. The term is called compliance and is defined as (Kaloush and Witczak, 2002):

$$D(t) = E(t)^{-1} = \frac{\varepsilon(t)}{\sigma_d} \qquad (3.1)$$

where

D(t)   Compliance [m²/N]
E(t)   Modulus [N/m²]
$\varepsilon(t)$ Strain [-]
σ_d Deviator stress [N/m²]

The concept of compliance allows the separation into elastic, plastic, viscoelastic and viscoplastic components at a constant stress level (Kaloush and Witczak, 2002):

$$\boldsymbol{\varepsilon}(t) = \boldsymbol{\sigma}_d D(t) = \boldsymbol{\sigma}_d \left(D_e + D_p + D_{ve}(t) + D_{vp}(t) \right) \tag{3.2}$$

where

$\varepsilon(t)$ Total strain [-]
σ_d Deviator stress [N/m^2]
D_e Instantaneous recoverable elastic compliance [m^2/N]
D_p Instanstaneous non-recoverable plastic compliance [m^2/N]
D_{ve} Time dependent viscoelastic (recoverable) compliance [m^2/N]
D_{vp} Time dependent viscoplastic (non-recoverable) compliance [m^2/N]

The deviator stress is dependent on whether the test is unconfined or confined (Kaloush and Witczak, 2002):

$$\boldsymbol{\sigma}_d = \boldsymbol{\sigma}_1 \qquad \text{for the unconfined condition} \tag{3.3}$$

$$\boldsymbol{\sigma}_d = \boldsymbol{\sigma}_1 - \boldsymbol{\sigma}_3 \qquad \text{for the confined condition} \tag{3.4}$$

where

σ_d Deviator stress [N/m^2]
σ_1 Vertical stress [N/m^2]
σ_3 Confining pressure [N/m^2]

The typical creep test exhibits a three-phase deformation behavior, as shown in Figure 3.18. The initial portion of the deformation is the primary zone, in which the strain rate is temporarily high but decreases with loading time. In the secondary zone, the strain rate is constant with loading time. In the final portion, the tertiary flow zone, the strain rate increases with loading time.

The time value of the tertiary stage starting point is of special interest due to its significance as a parameter in evaluating rutting resistance in HMA mixes. This point is called the "flow time", F_T, and is defined as the time at which the deformation occurs under constant volume. The volume subsequently increases. A simplified Superpave mix design procedure based on the flow time concept was developed in 1997 (Kaloush and Witczak, 2002).
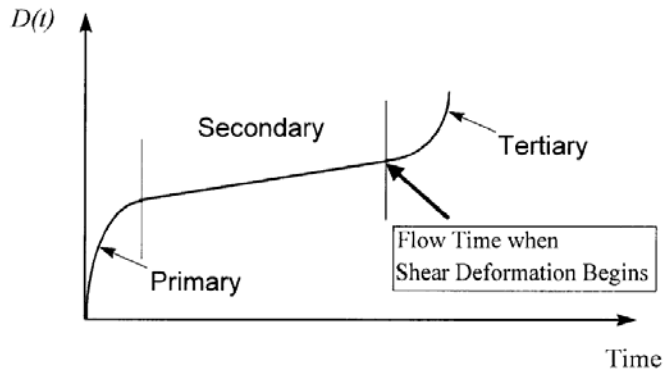
Figure 3.18. Typical test results between compliance and loading time (Kaloush and Witczak, 2002).

Generally, regression analysis is carried out for the second phase, which is approximately linear, as Figure 3.19 shows.
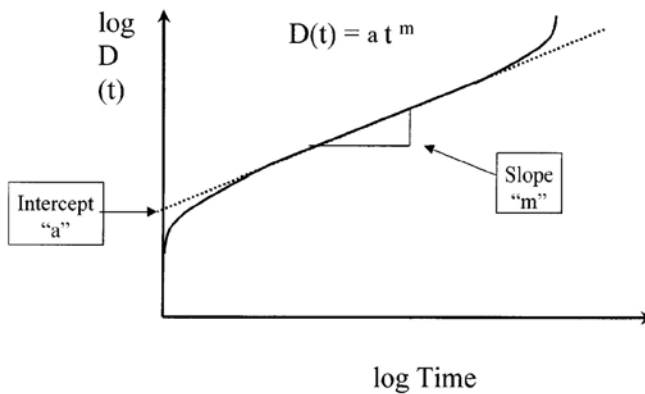
Figure 3.19. The regression constants "a" and "m" obtained from the secondary zone of the log compliance – log time plot (Witczak et al., 2002).

The viscoelastic compliance is expressed as:

$$D' = D(t) - D_0 = a \cdot t^m \qquad\qquad (3.5)$$

where

D'   Viscoelastic compliance component at any time [m²/N]
D(t)   Total creep compliance at any time [m²/N]
D_0 Instantaneous compliance (elastic and plastic) [m²/N]
t   Loading time [s]
a, m   Material regression coefficients

Repeated load creep test on cylindrical specimen
The repeated load creep test is a destructive test that can be used to measure the propensity for permanent deformation. The repeated loadings make the test more realistic, as it simulates the pounding effect of the traffic load. Several researchers have suggested that the repeated load test is more sensitive to variability of asphalt mix properties than the static load creep test (Brown et al., 2001; Sousa et al., 1991).

The repeated load can be either unconfined or confined, the latter being more realistic. Confinement also makes it possible to use the stress levels and temperatures prevalent in pavements (Brown et al., 2001). The equipment used for the repeated load test is basically static load creep test equipment, as described in Figure 3.17, but with variable loading ability. The more sophisticated types of this equipment can apply repeated axial and lateral stress pulses of any desired shape, in phase with each other (Sousa et al., 1991).

The cylindrical specimen is prepared in the same way as for the static creep test. The load pulse is normally haversine or rectangular. The load is applied for a split second, to be followed by a rest period that allows the viscoelastic specimen to regain its original shape. This procedure is typically repeated for several thousands of cycles. The accumulated strain is presented in a graph as a function of the number of cycles in Figure 3.20. The accumulated strain curves from the repeated load test and the static creep test are very similar, apart from the fact that the former is a function of the number of load cycles while the latter is a function of time. The strain curve of the repeated load creep test can consequently be divided into three stages: primary, secondary and tertiary. The flow number F_N is defined as the load cycle where the tertiary stage begins (Witczak et al., 2002).
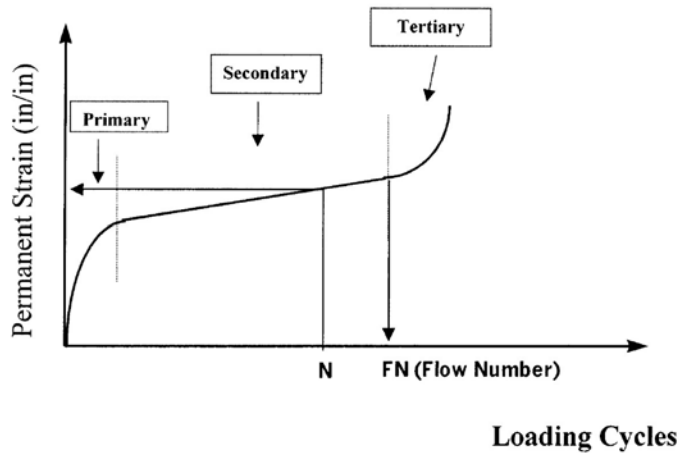
Figure 3.20. Typical relationship between total cumulative plastic strain and loading (Witczak et al., 2002).

The three-stage curve is further explained in Figure 3.21, which shows how the strain derivate develops.
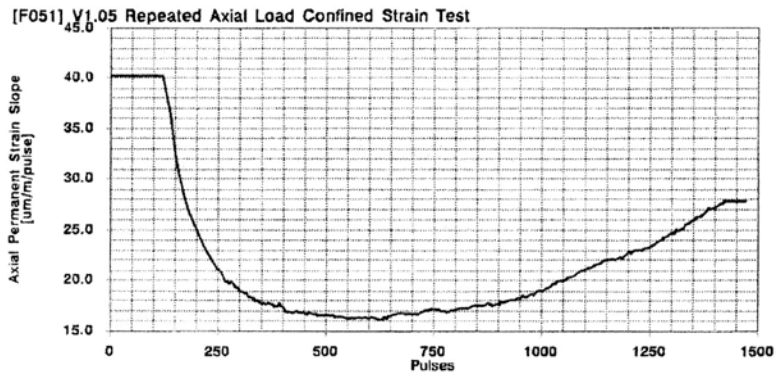
Figure 3.21. Typical plot of the rate of change in permanent strain versus loading cycles for a repeated load test (Witczak et al., 2002).

Regression analysis can be applied to the secondary stage in order to model its permanent deformation. The result is approximately linear, as shown in Figure 3.22.
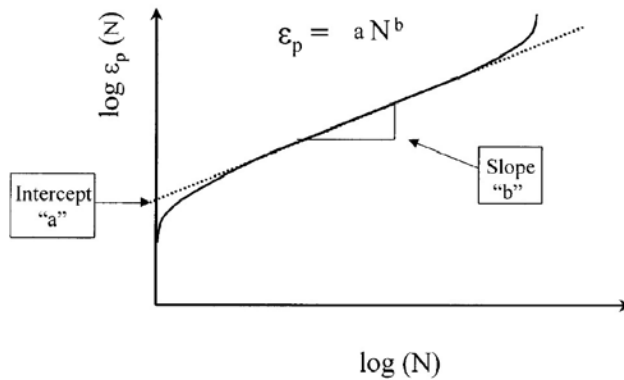
Figure 3.22. Regression constants "a" and "b" when plotted on a log – log scale (Witczak et al., 2002).

The plastic strain can be expressed as:

$$\boldsymbol{e}_p = aN^b \tag{3.6}$$

where

ε_p Permanent strain [-]
N   Number of load cycles [-]
a, b   Materials regression coefficients

In addition to providing data for the regression analysis, it is also possible to correlate several other material parameters to permanent deformation. These are resilient modulus (E_R), plastic strain (ε_p) per load cycle, and strain ratio ($\varepsilon_p/\varepsilon_r$) where the resilient strain, ε_r, is the recoverable axial strain during the rest period of the load cycle (Sousa et al., 1991).

In Sweden, routine testing is performed according to the standard FAS Metod 468 (2000). A cylindrical specimen with the dimensions H60xD148 mm is produced in a laboratory or cored from the pavement. It is treated to decrease end friction and placed on a steady foundation, and a stiff 100 mm diameter plate is mounted on top. The testing is carried out by applying rectangular load-unload pulses to the top plate and collecting deformation data. The frequency is 0.5 Hz, and the stress applied is 100 kPa at 40 °C (FAS Metod 468, 2000). No lateral pressure is applied to the specimen. However, the fact that the top plate has a smaller diameter than the specimen provides some lateral support by the circumferential specimen parts.

The new standard SS-EN 12697-25 (2005) describes a repeated load test that is essentially equal to FAS Metod 468. It also contains several methods and settings for triaxial repeated load testing. The test setup is illustrated in Figure

3.23. The axial stress can be sinusoidal or rectangular, and the confining pressure can be static or dynamic. However, the dynamic confining pressure will not be used in type testing. Specimens produced in a laboratory or cored from the pavement can be used. The specimen can be of different sizes, but it must be recognized that the mechanical properties depend on specimen dimensions. The minimum specimen dimensions are H50xD50 mm if the maximum aggregate size is less than, or equal to, 16 mm, or H75xD75 if it is more than 16 mm. Before testing, the specimen is greased and placed between two stiff plates larger than the specimen, in order to allow radial deformation without risking uneven stress distribution. Typical sinusoidal axial stress amplitudes range from 100 kPa to 300 kPa with confining pressure amplitudes of 50 kPa to 200 kPa applied with frequencies of 1 Hz to 5 Hz. Ordinary rectangular pulse loading stress ranges from 100 kPa up to 700 kPa, and the load-unload cycle is typically applied with 0.5 Hz. Test temperatures between 30 °C and 50 °C is recommended (SS-EN 12697-25, 2005).

Key

1	Actuator for dynamic pressure		4	Confining pressure
2	Pressure cell		5	Compressor
3	Specimen			
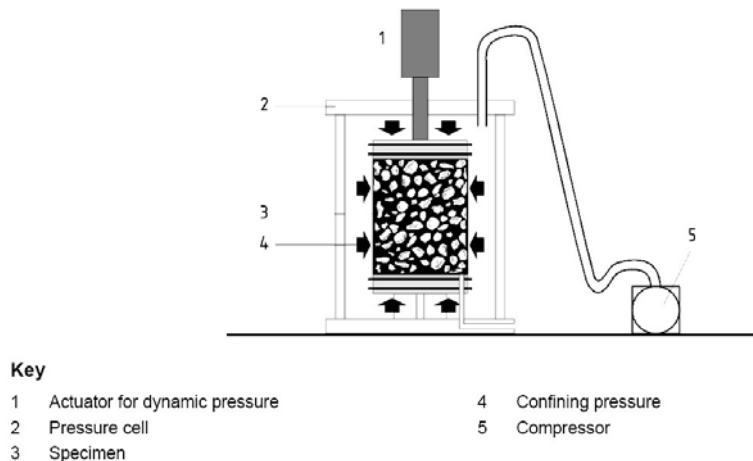
Figure 3.23. Schematic diagram of a triaxial cyclic compression test device with pressure cell (SS-EN 12697-25, 2005).

Several researchers have evaluated how well different fundamental and simulative test methods correlate. Said et al. (2000) verified the repeated load test by comparing its results with results obtained with the Road Simulator and the Wheel Tracking Machine. Both tests simulate accelerated traffic influence on asphalt layers under realistic conditions and several different mixes were used in the study. The results suggest that the repeated load test strongly correlates with both the Road Simulator and the Wheel Tracking Machine (Said et al., 2000). The repeated load test provides data for accurate rutting prediction if the two simulative test methods are considered realistic.

Dynamic modulus test on cylindrical specimen

The dynamic modulus test is a non-destructive test that can be performed on cylinder-shaped specimens by subjecting the specimen to axial sinusoidally varied stress that induces strain into the body. The dynamic modulus test can be either uniaxial or triaxial, i.e. either unconfined or confined. The confinement can be static or dynamic. The stress is applied using a range of frequencies, e.g. from 0.1 Hz to 25 Hz, beginning with the highest frequency. The frequency sweep is repeated at several temperatures, starting with the lowest temperature.

The strain must be kept low to remain linear and to avoid material damage, but sufficiently high to receive an acceptable noise to signal ratio. Nilsson (2001A) suggested that a reasonable linear behavior can be observed below approximately 50 microstrain based on uniaxial dynamic modulus testing. The limit was found to be higher at low temperatures and lower at high temperatures. However, Witczak et al. (2002), who performed similar tests, recommended 50 to 150 microstrains. AASHTO Provisional Standards (2006) also prescribed this interval in standard TP62-03. The uniaxial test stress and strain data are idealized into functions, as shown in Figure 3.24. The functions are expressed as (Kim et al., 2004):

$$\sigma(t) = a_\sigma + \sigma_0 * \cos(\omega * t + \theta_\sigma) + b_\sigma * t \tag{3.7}$$

where

σ	Stress [N/m²]
σ_0	Stress amplitude [N/m²]
ω_σ	Angular frequency [rad/s]
t	Time [s]
θ_σ	Phase shift constant [rad]
a_σ, b_σ	Constants

and

$$\varepsilon(t) = a_\varepsilon + \varepsilon_0 * \cos(\omega * t + \theta_\varepsilon) + b_\varepsilon * t \tag{3.8}$$

where

ε	Strain [N/m²]
ε_0	Strain amplitude [N/m²]
ω	Angular frequency [rad/s]
t	Time [s]
θ_ε	Phase shift constant [rad]
$a_\varepsilon, b_\varepsilon$	Constants
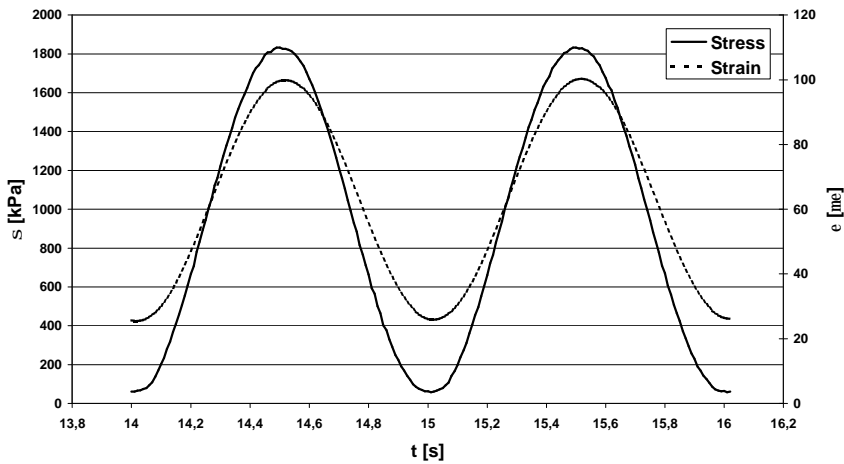
Figure 3.24. Schematic diagram of applied haversine stress the corresponding strain response using the dynamic modulus test.

The dynamic modulus is defined as the ratio of the stress and strain amplitudes (Nilsson, 2003):

$$|E*| = \frac{\boldsymbol{s}_0}{\boldsymbol{e}_0}$$

(3.9)

where

$|E*|$ Dynamic modulus [N/m²]
σ_0 Stress amplitude [N/m²]
ε_0 Strain amplitude [-]

The viscous part of a viscoelastic material causes a delay between the applied stress and the corresponding strain. This is represented by the phase angle, which is defined as (Kim et al., 2004):

$$\boldsymbol{f} = \boldsymbol{q}_s - \boldsymbol{q}_e$$

(3.10)

where

ϕ Phase angle [rad]
θ_σ Stress phase shift constant [rad]
θ_ε Stress phase shift constant [rad]

39

The phase angle is a measure of the balance between elasticity and viscosity. A purely elastic material is defined by α=0 ° and a purely viscous material by α=90 °.

The dynamic modulus is a function of frequency as well as of temperature, as shown in Figure 3.25.
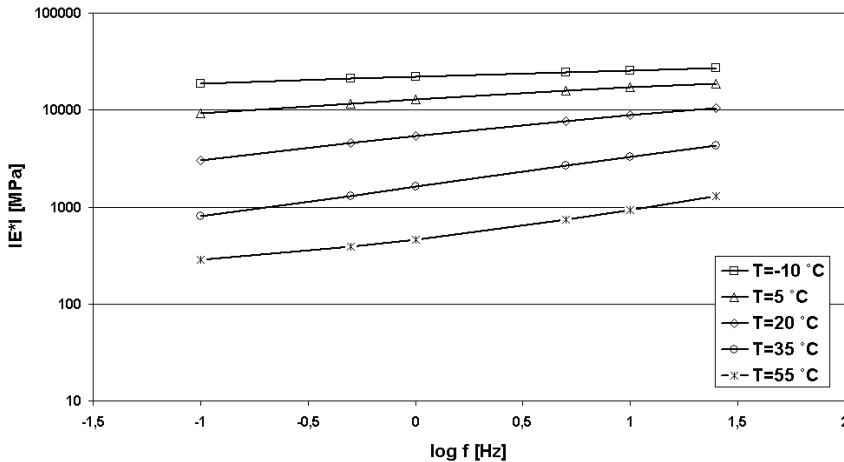
Figure 3.25. Schematic diagram of dynamic modulus as a function of frequency at different temperatures.

Asphalt concrete is considered a thermorheologically simple material, i.e. the time-temperature principle is valid. This means that the upper curves can be shifted to the right and the lower curves to the left in order to obtain one single curve, the mastercurve. The mastercurve is a function of reduced frequency, which is dependent on frequency and the shift factor. This relation can be expressed as follows (Nilsson, 2003):

$$\log(f_r) = \log(f) + \log(a(T)) \tag{3.11}$$

where

f_r Reduced frequency [Hz]
f Frequency [Hz]
$a(T)$ Time-temperature shift factor [-]

The time-temperature shift factor, in turn, is dependent on temperature. A reference temperature has to be selected in order to determine the shift factor function. No shifting will occur at the reference temperature, and the middle curve temperature is therefore most often used.

The well-known WLF equation defines the time-temperature shift factor:

$$\log(a(T)) = \frac{-C_1(T - T_{ref})}{C_2 + T - T_{ref}}$$

(3.12)

where

a(T)   Time-temperature shift factor [-]
T   Temperature [°C]
T_{ref} Reference temperature [°C]
C_1, C_2 Constants

The mastercurve in Figure 3.26 can be described with the sigmoidal function, which is an idealized equation that defines the mastercurve (NCHRP, 2004):

$$\log|E*| = d + \frac{a}{1 + e^{b - g \log(f_r)}}$$

(3.13)

where

|E*| Dynamic modulus [N/m²]
f_r Reduced frequency [Hz]
α, β, γ, δ   Constants
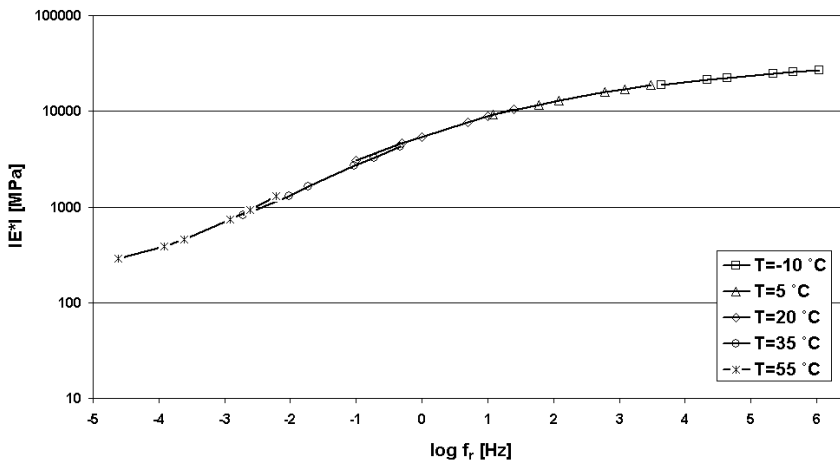
Figure 3.26. Schematic diagram of the mastercurve that shows the dynamic modulus as a function of reduced frequency.

Permanent deformation can be assessed by using a constitutive relation between plastic and elastic strain. The plastic/elastic strain ratio is typically dependent on temperature and the number of loadings. The elastic strain can be calculated by means of a multi-layer linear elastic program and dynamic modulus data from the mastercurve when loading frequency and temperature are known. One example of this procedure is the Mechanistic-Empirical Pavement Design Guide, which is further explained in Chapter 3.8.

3.6.2   Indirect tensile dynamic modulus test

The indirect tensile test (IDT), also called the diametral test, is carried out by applying a load on the circumference of a cylinder-shaped specimen. This induces tension stress along the vertical diameter in line with the load as shown in Figure 3.27. Only IDT for determining the dynamic modulus will be further discussed.

The diametral dynamic modulus test differs from the uniaxial dynamic modulus test in several ways. In contrast to the uniaxial case, a non-uniform compression-tension stress state is induced. The diametral test is also carried out in a direction perpendicular to the compaction direction, as opposed to the uniaxial test in which these directions are the same when utilizing gyratory compacted specimens. Any anisotropy that may be caused by gyratory compaction can increase this effect (Kim et al., 2004). In addition, the state of stress is highly dependent on specimen shape. Permanent deformation often occurs during testing, which changes the specimen geometry and affects the measurements (Brown et al., 2001).
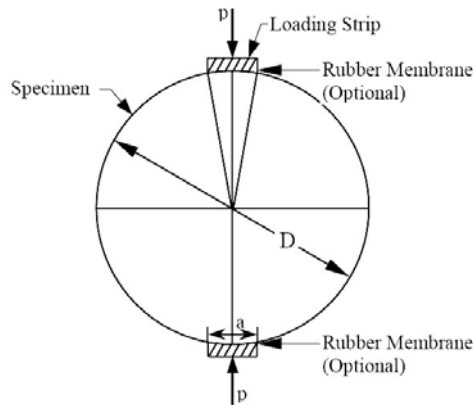
Figure 3.27. Schematic diagram of the indirect tensile test (Brown et al., 2001).

Kim et al. (2004) developed an analytical solution for the dynamic modulus in the IDT, using linear viscoelasticity and the plane stress assumption. The solution was confirmed by performing an IDT and a uniaxial test on a wide range of mixes. The comparison showed that the dynamic modulus mastercurves and the shift factors derived from the two methods are in good agreement. A complementing three-dimensional finite element analysis to calculate the center strain in the IDT specimen demonstrated that the error due to the plane stress assumption was negligible. It should therefore be possible to use the IDT for dynamic modulus determination instead of the uniaxial test (Kim et al., 2004).

Load data and vertical and horizontal displacement data at the specimen center are idealized into a function, which can be expressed as follows (Kim et al., 2004):

$$P(t) = a_P + P_0 * sin(w * t + q_P) + b_P * t \qquad (3.14)$$

where

P(t)	Load function [N]
P_0	Load amplitude [N]
ω	Angular frequency [rad/s]
t	Time [s]
$θ_P$	Phase shift constant [rad]
a_P, b_P	Constants

and

$$V(t) = a_V + V_0 * sin(w * t + q_V) + b_V * t \qquad (3.15)$$

$$H(t) = a_H + H_0 * sin(w * t + q_H) + b_H * t \qquad (3.16)$$

where

V(t), H(t)	Vertical and horizontal displacement functions [m]
V_0, U_0	Vertical and horizontal displacement amplitudes [m]
ω	Angular frequency [Hz]
t	Time [s]
$θ_P$	Phase shift constant [rad]
a_V, b_V, a_H, b_H	Constants

The final form of the dynamic modulus is based on the linear viscoelastic solution with a plane stress assumption. It can be simplified and expressed as (Kim et al., 2004):

$$\left|E^*\right| = 2\frac{P_0}{\pi s d}\frac{\beta_1\gamma_2 - \beta_2\gamma_1}{\gamma_2 V_0 - \beta_2 H_0} \tag{3.17}$$

where

$|E^*|$	Dynamic modulus [N/m²]
P_0	Load amplitude [N]
s	Loading strip width [m]
d	Specimen thickness [m]
V	Vertical displacement amplitude [m]
U_0	*Horizontal displacement amplitude [m]*
$\beta_1, \beta_2, \gamma_1, \gamma_2$	Geometry dependent coefficients listed in Table 3.4

The viscous part of a viscoelastic material causes a delay between the stress applied and the corresponding strain. This is represented by the vertical and horizontal phase angles, which are defined as (Kim et al., 2004):

$$\phi = \theta_s - \theta_e \tag{3.18}$$

where

ϕ	Phase angle [rad]
θ_σ	Stress phase shift constant [rad]
ϕ_ε	Strain phase shift constant [rad]

The expression for Poisson's ratio was simplified analogously (Kim et al., 2004):

$$\nu = \frac{\beta_1 U_0 - \gamma_1 V_0}{-\beta_2 U_0 + \gamma_2 V_0} \tag{3.19}$$

where

ν	Poisson's ratio [-]
V_0	Amplitude of vertical displacement [m]
U_0	Amplitude of horizontal displacement [m]
$\beta_1, \beta_2, \gamma_1, \gamma_2$	Geometry dependent coefficients listed in Table 3.4

The geometry dependent coefficients, listed in Table 3.4, were determined using linear viscoelasticity and the plane stress assumption.

Table 3.4. Coefficients for Poisson's Ratio and Dynamic Modulus (Kim et al., 2004).

Specimen diameter [mm]	Gauge length [mm]	b_1	b_2	g	g
101.6	25.4	-0.0098	-0.0031	0.0029	0.0091
101.6	38.1	-0.0153	-0.0047	0.0040	0.0128
101.6	50.8	-0.0215	-0.0062	0.0047	0.0157
152.4	25.4	-0.0065	-0.0021	0.0020	0.0062
152.4	38.1	-0.0099	-0.0032	0.0029	0.0091
152.4	50.8	-0.0134	-0.0042	0.0037	0.0116

The dynamic modulus data obtained in laboratory tests can also be fitted into a mastercurve and used to predict permanent deformation, as described in Chapter 3.6.1.

In Sweden, a similar routine test is used to assess the stiffness according to the standard FAS Metod 454 (1998). The specimens can be Marshall compacted or cored from the pavement. The minimum specimen dimensions are H40xD100 mm or H75xD150 mm for the maximum aggregate sizes 22 mm and 32 mm, respectively. Diametral testing is performed by applying a pulsating load on the mantle surface of the specimen, as shown in Figure 3.28. The testing load should not exceed 10 % of the fracture load. After a number of cycles, the elastic strain of each load cycle stabilizes and horizontal deformation data is collected. These data are subsequently used for calculating the stiffness. Testing can be carried out at -5 °C, 10 °C and 25 °C (FAS Metod 454, 1998).
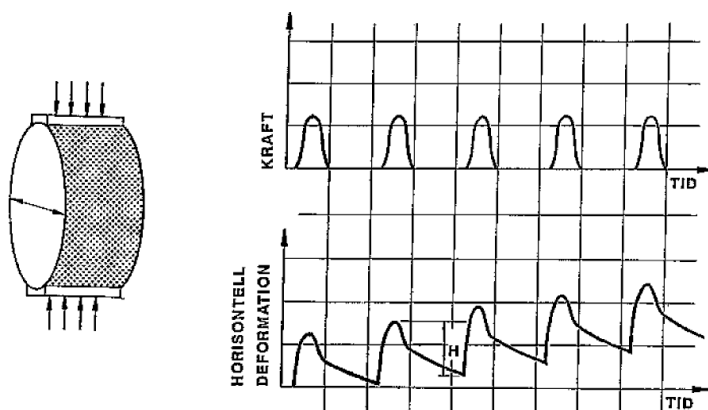
Figure 3.28. Schematic diagram of the cyclic diametral test (FAS Metod 454, 1998).

3.6.3   Shear tests

Shear deformation is considered the major cause of rutting, as described in Chapter 3.1. It is therefore logical to employ shear tests to determine the asphalt mix propensity for permanent deformation (Sousa et al., 1991). The shear test can be conducted either confined unconfined and can be destructive (static or repeated load test) or non-destructive (dynamic modulus test).

Different types of shear test arrangements have been used to characterize materials. Bonnot (1986) studied fatigue properties and suggested that shear tests can effectively account for the stress induced in thin surface courses and sublayers. Junker (1987) showed a shear test in which the load was induced with a metal rod inserted into the center of a uniaxial specimen. Subsequently, the Superpave concept adopted and developed shear testing that can be performed with the Superpave Shear Tester (SST). Examples of shear test types within the Superpave concept are the Simple Shear at Constant Height (SSCH) Test, the Repeated Shear at Constant Height (RSCH) Test and the Frequency Sweep at Constant Height (FSCH) Test. FSCH testing should not induce more than 100 microstrains to avoid material damage (Witczak et al., 2002).

Results derived from shear tests can be used in analytically based modeling for predicting permanent deformation, as Deacon et al. (2002) has shown using RSCH. In order to use dynamic modulus data derived with FSCH, they should be refined analogous to the procedure described in Chapter 3.6.1. The mastercurve can then be used as material input data in a multi-layer linear elastic program.

3.6.4   Wheel-track test

The Wheel-Track Test (WTT) is an empirical destructive test used to rank asphalt mixes according to their rutting propensity at a fixed temperature. The simulation does not determine any fundamental properties, and it cannot reproduce entirely realistic conditions. However, it provides a simple functional test to rank the rutting propensity of asphalt mixes. Wheel-track testing will not result in any structural rutting, as the specimen is placed on a stiff foundation. Wear rutting can also be disregarded, since the test wheel is non-studded and the number of passages is relatively low. The accumulated permanent deformation can therefore only be flow rutting.

There are various kinds of wheel-tracking devices that use the same principle. The most common ones are the Asphalt Pavement Analyzer (APA), the Hamburg Wheel-Tracking Device (HWTD), the French Pavement Rutting Tester (FPRT) and the Extra-Large Wheel-Tracking Test (ELWTT) device. The principal component of the test equipment is a suspended wheel that is able to roll back and forth while exerting pressure on the specimen, which can be either a slab or a cylinder. The specimens are usually laboratory compacted,

although it is also possible to use field compacted specimens. Before testing, the specimens are temperature conditioned and air-dried or water saturated. The APA wheel-track test is further described in the AASHTO standard TP63-03 (AASHTO, 2006). More information about the HWTD, FPRT and ELWTT wheel-track tests can be found in CEN standard SS-EN 12697-22 (2004).

Williams and Prowell (1999) evaluated the ability of the APA, the FPRT and the HWTD to predict flow rutting performance on WesTrack. Trench studies revealed that most of the permanent deformations appeared in the upper layers. In these layers, high temperature is a critical factor that was used for wheel-track testing. The test temperatures were 60 °C for the APA and the FPRT and 50 °C for the HWTD. It was found that all wheel-track devices showed a reasonable level of correlation with the performance of WesTrack. The correlations were 89.9%, 83.4%, and 90.4% for the APA, FPRT, and HWTD, respectively (Williams and Prowell, 1999).

3.7   Accelerated Loading Testing

Accelerated Loading Testing (ALT), also called Accelerated Pavement Testing (APT) in the US, is a test method used to simulate pavement deterioration on a full-scale test track. ALT can be employed for a number of purposes. The primary applications are evaluation of different pavement structures and materials, validation of laboratory test methods and development of deterioration models (Hugo and Epps Martin, 2004). However, APT is expensive and should therefore be complemented with less costly test methods (Sousa et al., 1991). Different civil engineering methods should be combined to obtain a high degree of knowledge. Figure 3.29 provides an overview of the costs and the knowledge that can be achieved with different methods.
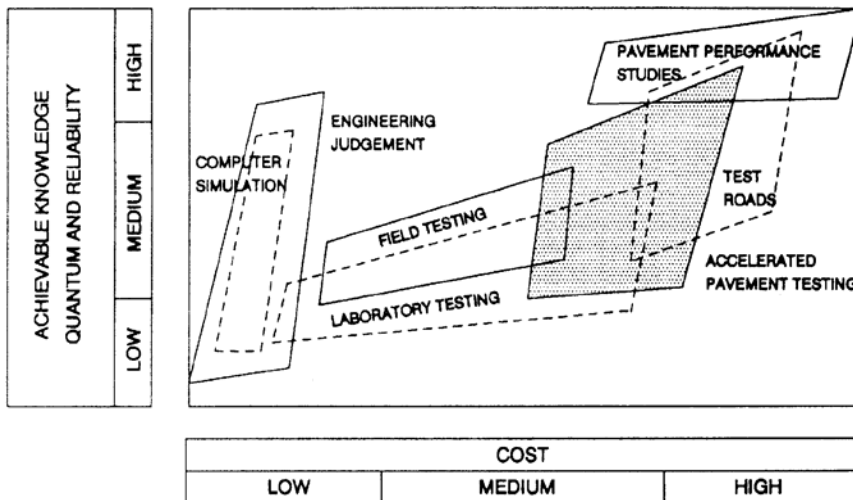
Figure 3.29. Interrelationship between pavement engineering facets that collectively and individually contribute to knowledge (Hugo and Epps Martin 1991) after (Hugo and Epps Martin 2004).

The factors affecting pavement deterioration and APT are traffic properties, material properties and the climate. The traffic loading can be applied statically or dynamically and uni-directionally or bi-directionally by using one single axle or multiple axles. Other traffic properties are the type of suspension system, tire type, contact pressure, speed and lateral wander. The loading can be performed using either conventional trucks or a loading device. If a loading device is used, the test track can be either linear or circular. APT typically involves extensive data collection using strain and stress gauges inside the pavement structure (Hugo and Epps Martin, 2004).

Material properties are determined by means of fundamental laboratory tests. It must, however, be noted that AC pavements experience ageing effects that change their properties during their service life. The most noteworthy change is called "age strengthening". APT is not able to account for this factor, but it must be acknowledged when results are evaluated. Climate factors such as temperature, wind, radiation and water can often be controlled (Hugo and Epps Martin, 2004). All the above factors are determined in order to study the effects under certain conditions. Nevertheless, it is difficult or impossible to imitate the complete deterioration effect caused by the vast variability of influencing factors found in existing pavements. It must therefore be recognized that APT represents a simplified case compared to actual pavement conditions. Accelerated Pavement Testing programs are often partnering projects between authorities, universities, contractors and/or APT device manufacturers.

There are several types of APT facilities around the world. Long test tracks are often subjected to conventional heavy traffic under natural environmental conditions. They typically consist of a large number of sections with a unique AC structure for evaluation purposes. The Heavy Vehicle Simulator (HVS) has also been employed on selected surfaces in some cases. Some of the most notable test tracks of this kind are American: the WesTrack in Mississippi (Epps et al., 2001; Hugo and Epps Martin, 2004**)**, the NCAT test track in Alabama (Powell , 2001; Hugo and Epps Martin, 2004) and the MnRoad research facility in Minnesota (Hugo and Epps Martin, 2004), as shown in Figure 3.30. Trench studies on the MnRoad Mainline sections have also been used to assess the contribution of permanent deformation in each AC layer within the Mechanistic-Empirical Pavement Design Guide model (NCHRP, 2004).

Figure 3.30. The MnRoad research facility (TRB Committee on FS/APT, 2006).

Circular or oval facilities are loaded by specially designed loading devices in their natural environment. Circular facilities are suitable for high-speed simulation. Some examples are the circular LCPC (OECD, 1991) in France seen in Figure 3.31, ETHZ in Switzerland (Dawson et al., 2002), Lira in Romania (Metcalf, 2004; Dawson et al., 2002), Vuis-Cesty in Slovakia (Dawson et al., 2002) and the oval CEDEX test track in Spain (Dawson et al., 2002; Hugo and Epps Martin, 2004).

Figure 3.31. The LCPC circular test track (TRB Committee on FS/APT, 2006).

Corté et al. (1994) employed the LCPC circular test track to evaluate how rutting propensity was affected by the choice of binder, axle configuration and speed, among other things. The binder types used were conventional 50/70 bitumen, SBS-polymer modified bitumen, the Shell Multigrade bitumen and a very thin 10/20 asphalt mix layer on a high-modulus coated material. In the first phase, two super single-wheel axles were employed at the radii of 16.5 m and 19.5 m, while two dual-wheel axles were placed at a distance of 15.5 m and 18.5 m from the center, as shown in Figure 3.32 (Corté et al. 1994).

The results provide valuable data for evaluation of binder performance under specific conditions, as shown in Figure 3.33. It was also possible to rank the different impacts of super single and dual tires at the specific speeds; see Figure 3.34. One of the conclusions drawn was that asphalt mixes with modified and hard bitumen had much higher resistance to permanent deformation than the reference mix. It was also established that super single axles are more aggressive than dual tire axles and that low speed increases rutting (Corté et al. 1994).
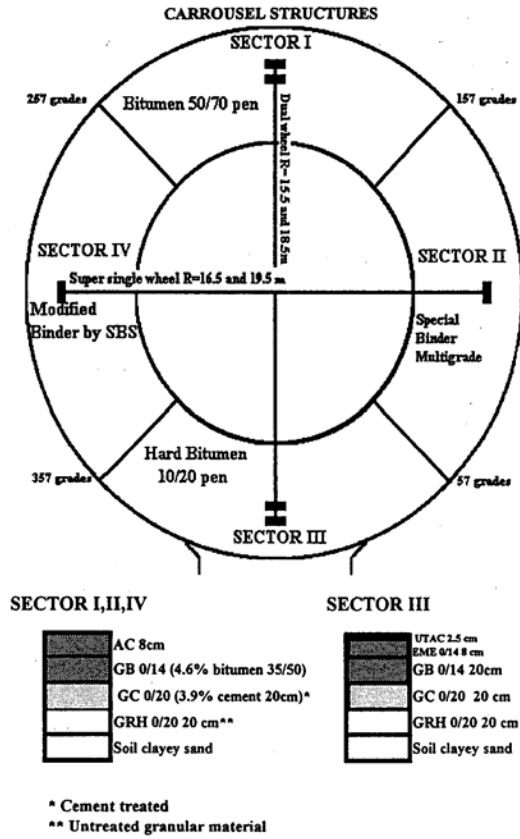
Figure 3.32. Description of pavement sectors (Corté et al. 1994).
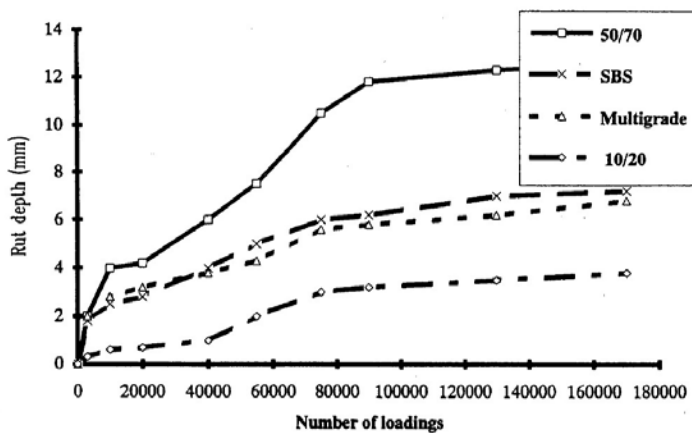
Figure 3.33. Test track results: rut depth evolution on the four sectors (super single wheel, r = 16.5 m, v = 40 km/hr) (Corté et al.1994).

51
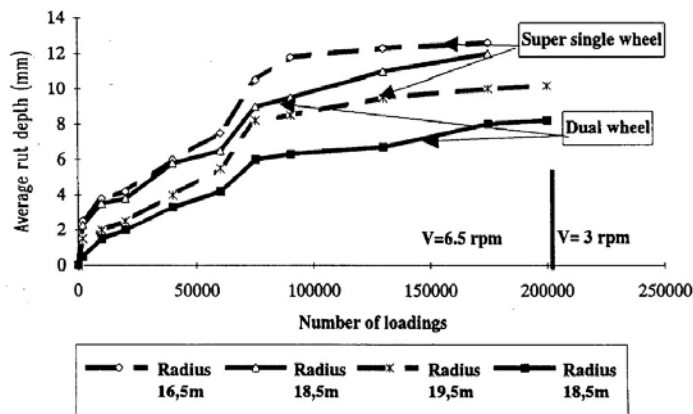
Figure 3.34. Rut depth evolution for Sector I (Note: according to the reference, the radii for the dual wheel axles were 15,5 m and 18,5 m). (Corté et al. 1994).

Other APT programs rely solely on slower linear devices, e.g. the Heavy Vehicle Simulator (HVS), Danish Road Testing Machine (RTM) (Bredahl Nielsen et al., 1999), Accelerated Loading Facility (ALF) or Mobile Load Simulators (MLS) (Hugo and Epps Martin, 2004). They are often fully mobile and can be run on in-service pavements or test tracks in a natural or controlled environment. One example is the HVS-NORDIC Mark IV, shown in Figure 3.35, which has been employed in Sweden, Finland and Poland. The loading wheel can be dual or single, and the loading can be uni-directional or bi-directional. Up to 25,000 loadings can be simulated every 24 hours, including daily maintenance. The half-axle load is 20-110 kN and can be varied dynamically ±20% sinusoidally. The speed is up to 15 km/hr and the maximum lateral shifting is ±0.75 m (Huhtala and Wiman, 1998).

Figure 3.35. The HVS-NORDIC (TRB Committee on FS/APT, 2006).

3.8 Models and theories for prediction of permanent deformation in asphalt materials

Pavement performance modeling is used for designing new and rehabilitated pavements and for assessing pavement residue. High model precision prevents over- and under-dimensioning, thus saving resources and avoiding premature failure. Empirical modeling, which is based on observation, is the most basic form of modeling. However, it does not provide intrinsic knowledge of the deterioration mechanisms. Mechanistic modeling requires extensive research and laboratory testing but should, if it works, produce highly accurate results. Models typically employ a mechanistic framework that is complemented with empirical considerations to correspond to observation. Another distinction can also be made between constitutive models and pavement deterioration models.

3.8.1 Mechanistic-Empirical Pavement Design Guide

The Mechanistic-Empirical Pavement Design Guide (M-E PDG) was developed within the NCHRP projects 1-37A and 1-40D. It succeeds the AASHTO Guide for Design of Pavement Structures from 1993. The major improvement offered by the M-E PDG is the introduction of mechanistic principles. The mechanistic model is supplemented by empiricism in order to reflect observed deterioration from the Long Term Pavement Performance (LTPP) database.

The purpose of the M-E PDG was to provide a better overall tool for prediction and diagnostics of several road distress mechanisms. The concept includes fatigue and low temperature cracking, rutting and increase of roughness (IRI). The analysis can be performed at three accuracy levels: Level 1, Level 2 and Level 3. The level determines the quality and amount of input data and, consequently, the accuracy of the results. Level 1 analysis involves detailed input data that provide exact results, while Level 3 default input data produce low accuracy results. Input data from different levels can be mixed, but the result can never reach a higher level than the lowest input level. The analysis is performed by applying multi-layer elastic theory, except at Level 1, where the non-linearity of unbound materials is considered by means of a finite element procedure. This feature is, however, a research utility rather than a routine pavement design tool. The following description will focus entirely on permanent deformations in asphalt concrete layers.

Observation has confirmed that rutting appears in three distinct stages, as Figure 3.36 illustrates. Volumetric changes in the primary stage typically result in a high initial level of rutting. A constant low rate of rutting can be observed during the second stage, as the volumetric changes decrease while the shear deformation rates increase. The tertiary stage shows a high level of rutting due to increasing shear deformations.

Only the second stage is actually modeled. The primary stage is an extrapolation of the secondary stage, while the tertiary stage is disregarded. This is because the tertiary stage is very difficult to model. The rut depth of the tertiary stage is also generally much greater than what would be accepted in practice. The M-E PDG only models the maximum rut depth, located in the middle of the wheel track, and not the entire transverse profile. No real plastic shear deformations are modeled within the system, which may seem disturbing. However, most of the shear deformations occur in the tertiary stage, which is not dealt with here.
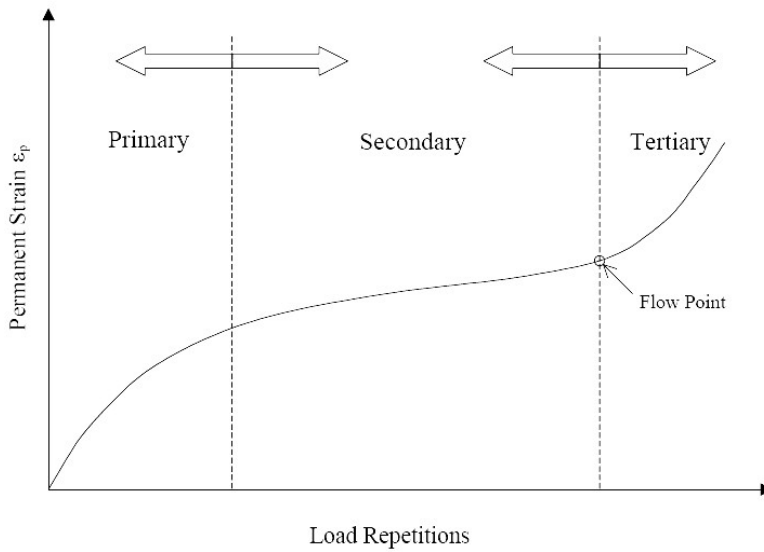
Figure 3.36. Typical repeated load permanent deformation behavior of pavement materials (NCHRP, 2004).

Development
The M-E PDG uses an incremental damage growth approach in which the year is divided into sub-seasons, i.e. into increments. Permanent deformations are calculated at the end of each increment. The model employs the layer-strain concept to summarize the contributions of the layers:

$$RD = \sum_{i=1}^{n_{sublayers}} e_p^i h^i \tag{3.20}$$

where:
RD   Rut depth
$n_{sublayers}$ Number of sub-layers
ε_p^i Plastic strain in middle of sub-layer i
h^i Thickness of sub-layer i

54

The M-E PDG constitutive relationship defines the ratio of plastic to elastic strain as dependent on temperature and number of passages. The equation also includes calibration factors derived from laboratory testing, field observation and trench studies.

$$\frac{\pmb{e}_p}{\pmb{e}_r} = k_1 a_1 \pmb{b}_{r1} T^{a_2 \pmb{b}_{r2}} N^{a_3 \pmb{b}_{r3}}$$ (3.21)

where

$\pmb{e}_p$ Accumulated plastic strain at N repetitions of load
$\pmb{e}_r$ Resilient strain of the asphalt material
k_1 Variable confining pressure factor
a_i Laboratory determined non-linear regression coefficients
β_{ri} Laboratory to field calibration factors
N Number of load repetitions
T Temperature [° F]

The resilient strain is determined by using the multi-layer linear elastic program JULEA, which is integrated with the M-E PDG software. The three-dimensional stress state is defined as:

$$\pmb{e}_r = \frac{1}{|E^*|}\left(\pmb{s}_z - \pmb{ms}_x - \pmb{ms}_y\right)$$ (3.22)

where

$|E^*|$ Dynamic modulus
σ_z Vertical stress
σ_x Lateral stress along x-axle
σ_y Lateral stress along y-axle
μ Poisson's ratio

The laboratory determined non-linear regression coefficients were derived from an analysis of comprehensive confined and unconfined axial repeated load testing data. The original coefficients were later updated due to model enhancements (NCHRP, 2006B; NCHRP, 2004):

$a_1 = 10^{-3.35412}$
$a_2 = 1.5606$
$a_3 = 0.479244$

Rut depth data from the LTPP database can be used to calibrate the model with regional field observation. Field calibration factors are not employed by default in the current version, v0.910, of M-E PDG software. Nevertheless, it is recommended that each regional agency should find a local set of factors, using the assessment guide that NCHRP Project 1-40B will eventually provide.

The permanent deformation model must also assess the contribution of each layer. Trench data from seven MnRoad sections were used to define an empirical variable confining pressure factor. The lack of trench data from the LTPP sections is recognized as a serious limitation that should be addressed. Using MnRoad trench data, the empirical variable confining pressure factor was found to have the following form:

$$k_1 = (C_1 + C_2 * depth) * 0.328196^{depth} \tag{3.23}$$

$$C_1 = -0.1039 * h_{ac}^2 + 2.4868 * h_{ac} - 17.342 \tag{3.24}$$

$$C_2 = 0.0172 * h_{ac}^2 - 1.7331 * h_{ac} + 27.428 \tag{3.25}$$

where

k_1 Variable confining pressure factor
h_{ac} Total thickness of all asphalt layers

Layering
The pavement structure is divided into sub-layers in order to accurately describe the varying properties. The top two sub-layers are half an inch, followed by 1-inch layers to the depth of 4 inches. The next layer is 4 inches, and after that the rest is used as the final asphalt sub-layer.

The dynamic modulus of each sub-layer is dependent on temperature and loading frequency. The frequency, in turn, is dependent on vehicle speed, depth and the stiffness of overlying materials. The calculation involves determining the effective pulse length in the middle of the sub-layer, as shown in Figure 3.37.
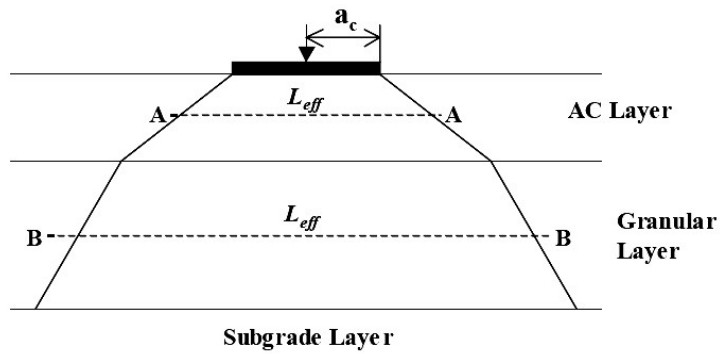
Figure 3.37. Principal drawing of load distribution as a function of depth (NCHRP, 2004).

Each asphalt layer thickness is transformed into an equivalent sub-grade thickness by using Odemark's theories, as is demonstrated in Figure 3.38.
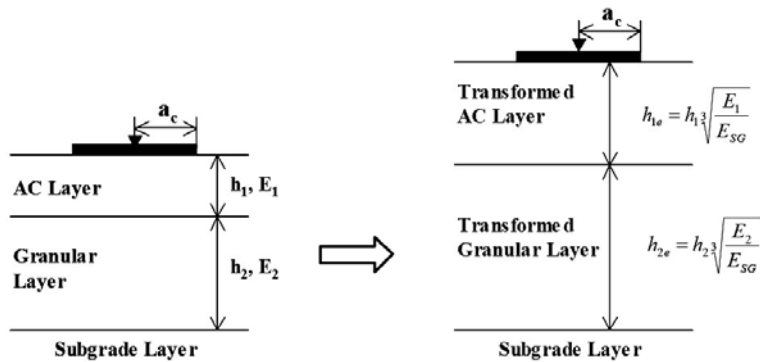
Figure 3.38. Transformation of layers into layers of equivalent stiffness (NCHRP, 2004).

The load distribution angle is assumed to be 45° throughout the fictive construction, as shown in Figure 3.39.
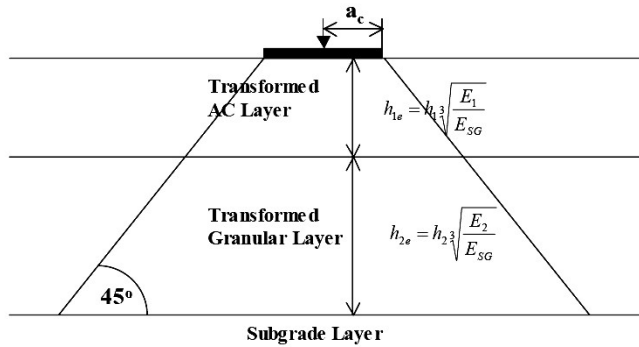
Figure 3.39. Principal drawing of load distribution in the transformed construction (NCHRP, 2004).

The effective pulse length in the middle of each sublayer is calculated on the basis of the tire contact radius and depth. The frequency is then defined as follows:

$$f = \frac{17.6v}{L_{eff}} \qquad (3.26)$$

where

f   Frequency
v   Vehicle speed
L_{eff} Effective length

Frequency and temperature determine the reduced frequency that can be applied on a mastercurve to obtain the dynamic modulus, as explained in Chapter 3.6.1.

Wander
The effect of lateral wander mitigates the distress that the pavement is subjected to. It is assumed to be normally distributed, and the standard deviation of 10 inches is often used as a default value. However, very few studies have been made in this area, which is why it is hard to quantify. Naturally, the crucial point always occurs in the center of distribution. The impact of lateral wander on permanent deformation is non-linear and is therefore directly taken into consideration by calculating pavement response.

Climate

The great impact of the climate on pavement deterioration is recognized in the M-E PDG. Variation in climate conditions leads to variation in material properties, which, in turn, leads to variation in stresses and strains. In order to systematize, the year is divided into seasons and sub-seasons. The normal season is one month or half a month during freeze and thaw. However, there are still great temperature variations within this time frame. This is dealt with by dividing each season into five sub-seasons in which traffic conditions are the same. In other words, the temperatures of the 10th, 30th, 50th, 70th and 90th percentiles are each used to describe 20 % of the traffic, as shown in Figure 3.40.
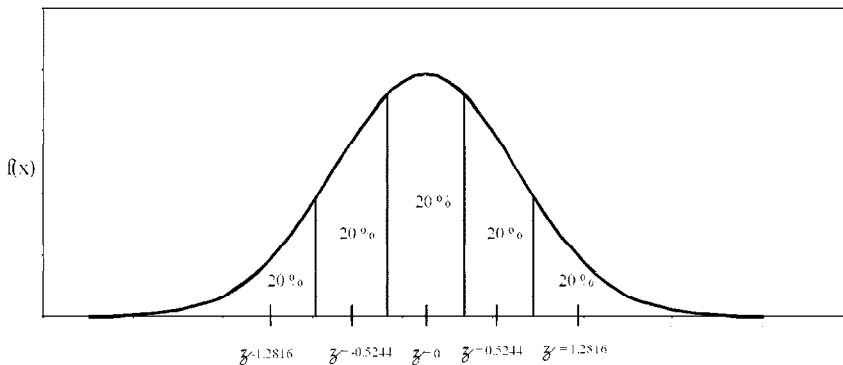
Figure 3.40. Temperature distribution for a given period of analysis (NCHRP, 2004).

Reliability

The model results is calibrated to correspond to the mean rutting observed in pavements. A reliability analysis was included to quantify the rutting deviation of pavements. The expected deviation is assumed to be normally distributed for values greater than the mean value. Standard errors are assessed for each average predicted AC rutting interval by using the LTPP database. The added safety margin is a function of the mean rut depth and the reliability level selected. The default reliability level is 90 %, while 50 % corresponds to the mean value.

3.8.2   Viscoelastic modeling

Viscoelastic modeling is a comprehensive analytical method for deterioration modeling. Stresses and strains can be determined throughout the pavement structure by using proper boundary conditions. This approach accounts for the time-dependency of materials, and moving wheel loads can therefore be considered directly. The strain response of the asphalt pavement consists of four parts: the elastic ε_e, plastic ε_p, viscoelastic ε_{ve} and viscoplastic ε_{vp}, as explained in Figure 3.41.
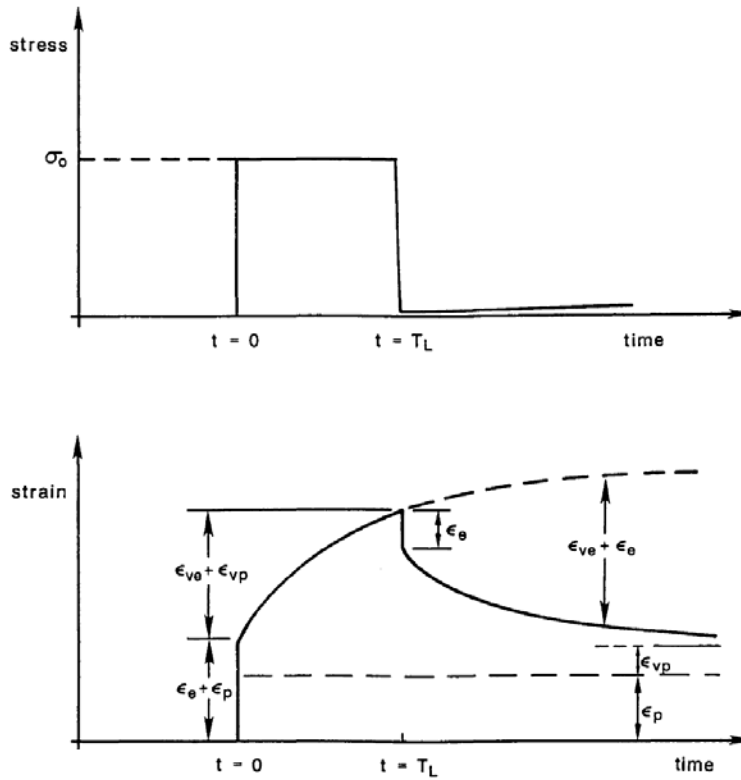
Figure 3.41. Description of components in viscoelastoplastic materials (Lytton et al., 1993B).

The material properties are therefore defined on the basis of generalized compliance relationships or finite numbers of Maxwell, Kelvin-Voigt, Burger and/or Huet-Sayegh elements. The strain responses of these elements are illustrated in Figure 3.42 to Figure 3.45 (Lytton et al., 1993B).
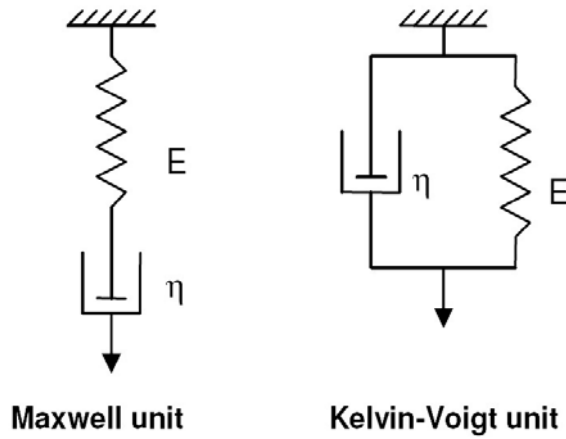
Figure 3.42. Schematic diagram of the Maxwell and the Kelvin-Voight elements for modeling viscoelastic behavior (SAMARIS, 2004).
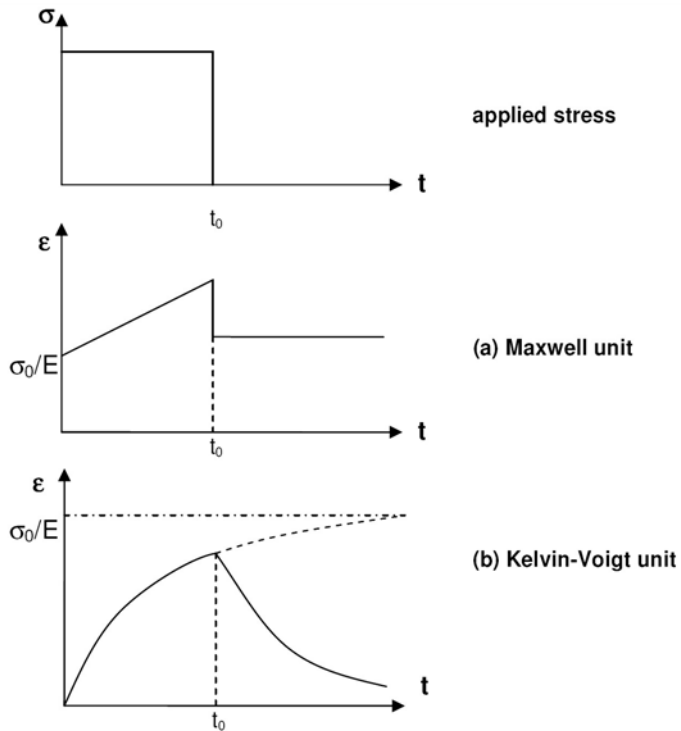
Figure 3.43. Principal reactions of the Maxwell and the Kelvin-Voigt units on stress in the form of a step function by Mang (2000) after SAMARIS (2004).
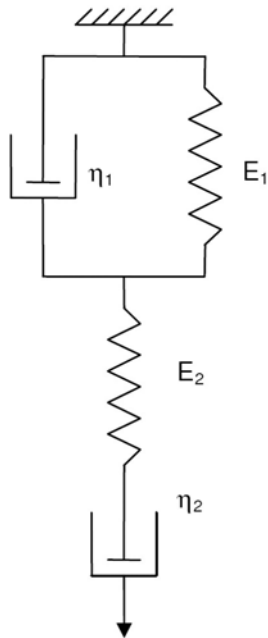
Figure 3.44. Schematic diagram of the Burger element that consists of a Maxwell and a Kelvin-Voigt unit in serial connection (SAMARIS, 2004).
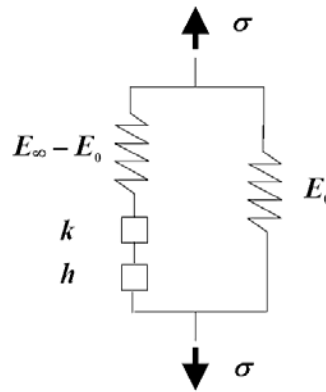
Figure 3.45. Schematic diagram of the Huet-Sayegh element (SAMARIS, 2004).

.

The viscoelastic approach can be either non-linear or linear, i.e. the stiffness can be stress-dependent or not. Non-linearity can be useful, since it accounts for large deformations and changing material properties due to permanent deformations. However, the mathematics of non-linear viscoelasticity is very complex and requires a great deal of computational power. The advantage over the simpler empirical methods is that time-dependency and lateral flow are accounted for. It is therefore theoretically more potent, even though results have not been as good as anticipated (Sousa, 1991).

Continuum Damage Mechanics

Continuum Damage Mechanics (CDM) is a viscoelastic material model that considers a continuous material phase. Physical linear or non-linear viscoelastic strains are transformed into elastic pseudo-strains by using the extended elastic-viscoelastic correspondence principle. This makes it possible to separate viscoelastic and viscoplastic strain response. The distributed damage is modeled by using pseudo-strain and micro-crack growth under the assumption of linear viscoelasticity. Kim and Little (1990) applied the model to asphalt concrete, using data obtained with the uniaxial tensile relaxation test and the constant-strain-rate monotonic test.

In order to assess permanent deformation, a viscoplastic component was subsequently added by using a strain-hardening model (Chehab, 2002). Material parameters were determined with the complex modulus test, the monotonic test and the repetitive creep and recovery test. The viscoelastoplastic model predicted responses accurately, until the microcracks expanded into major macrocracks. The CDM approach with or without viscoplasticity has shown promising results and has been employed by many researchers, e.g. Nilsson (2003) and Lundström (2004).

The Björklund viscoelastic model

A linear viscoelastic approach for assessment of permanent strain in multi-layered AC constructions was presented by Björklund (1984). The model input is the creep function in shear, $J(t)$, and compressibility, $X(t)$, which are obtained by means of laboratory analysis. The viscoelastic equations of equilibrium are transformed into linear elasticity equations. This is accomplished by using mathematical functions and transforms. A number of boundary conditions were assumed. Among these are the following:

- The material must behave linear-viscoelastic. Strains must be low enough, for example.
- Isothermal conditions are prevalent.
- The material compressibility is entirely viscoelastic, as no plastic post compaction is assumed.
- The elastic compressibility can be modeled as a function of Poisson's ratio and the creep function in shear.
- No shear forces exist at the pavement surface.
- No permanent deformation exists in the traffic direction.

This model was verified with simulations using the PAVIS 3 (Pavement Viscoelasticity, 3 layers) software, and the agreement was found to be good (Björklund, 1984). Said (2004) developed the model further by substituting binder viscosity with AC shear modulus multiplied by loading time. This resulted in the following equation:

$$e_p = \frac{\sigma_0 * a * z}{V * G * t}\left[1 - \frac{z}{\sqrt{(z^2 + a^2)}}\right] \tag{3.27}$$

where

σ_0 Tire pressure
a   Radius of contact area
Z   Depth from road surface
V   Vehicle velocity
G   Shear modulus
t   Loading time

The total rut depth was calculated by integration of the layer thickness. The results obtained with the model corresponded well with results from an Extra-Large Wheel Tracking Test (Said, 2004).

VEROAD
VEROAD (Viscoelastic road analysis Delft) is a program for linear viscoelastic multilayer analysis that was evaluated by Nilsson (2001A). Viscoelasticity is considered by employing the correspondence principle. The linear viscoelastic problem in the time-domain is transformed into a linear elastic problem in the frequency-domain. The elastic problem is then solved for each frequency and subsequently the responses are transformed back into the time-domain. The responses from a variable traffic load are added in order to obtain the total permanent deformation (Nilsson, 2001A).

The Burger model can be employed to describe material properties. The four Burger model parameters are constant within the interval 0.1-30 Hz and can be determined using stiffness and phase angle from a number of frequencies. VEROAD is dependent on the fact that some assumptions are applicable. Thus, the theory of linear viscoelasticity must be valid, and no volume change is accounted for. Material layers should be homogenous and horizontally infinite, while the bottom layer is a half-space. A continuous material phase is assumed, as no cracking will occur. Finally, the system must be in equilibrium. A comparison between VEROAD results and full-scale tests has shown very good agreement (Nilsson, 2001A).

3.9   Conclusions

3.9.1   Flow rutting mechanisms

Permanent deformation, or rutting, can be divided into three mechanisms: structural rutting, wear rutting and flow rutting. Only flow rutting will be further discussed. Initially, the asphalt mix is compacted by traffic. Subsequently, plastic flow will result in a lateral displacement that is manifested by ruts accompanied by upheavals on both sides. The latter form of deformation is regarded as the most common flow rutting mechanism. Observations from laboratory testing and full-scale testing have shown that permanent deformation occurs in three distinct stages. Rutting formation is fast in the first stage, but stabilizes in the second, only to accelerate again in the third and final stage.

3.9.2   Effect of material properties

Asphalt mix properties are dependent on constituent properties and their proportions. The two most serious distress mechanisms are permanent deformation and fatigue. The requirements placed on asphalt mix for high resistance against both types of distress are somewhat conflicting, which makes mix design a matter of compromise. To obtain resistance to flow rutting, the mineral aggregate of ordinary Hot Mix Asphalt should have large maximum aggregate size, a continuous gradation curve, high angularity and a rough surface structure. The asphalt binder should provide the mix with sufficient stiffness at high temperatures. Adding polymers to the mix can be beneficial in order to increase overall stiffness and/or decrease temperature susceptibility. Short-term and long-term ageing significantly increases the mix stiffness. This mainly occurs during mixing/laying and during the first few years of pavement service. Binder content and air void content are two key factors that should be controlled to guarantee high resistance to permanent deformation.

3.9.3   Compaction principles

Asphalt concrete specimens for the characterization of a mix can be cored from the pavement or produced in a laboratory. Laboratory compaction is afflicted with difficulties in imitating field conditions in terms of air void content, particle orientation and mechanical properties. One of the advantages is a high precision in terms of temperature, compaction force and material quantity. The most common laboratory compactors can be divided into plate compactors, vibratory compactors and gyratory compactors. There has been some criticism against using the gyratory compactor for specimen reproduction. The principal argument is that the center of the specimen tends to reach a higher density than the eccentric parts. It has been reported by several investigators that gyratory specimens can have significantly different mechanical properties than field cores, even though material and air void content are equal. There are, however, other studies that have suggested that gyratory compaction is at least as good as any other compaction method.

3.9.4   Analysis of the traffic loading effect on flow rutting

The impact of traffic loading is the direct cause of flow rutting. Traffic variables are vehicle speed, axle load, tire pressure, axle configuration and lateral wander. Low vehicle speed, in combination with the viscoelastic behavior of asphalt mixes, increases flow rutting. High axle loads have been found to mainly result in high strain levels at high depth if the contact pressure is constant. High tire pressure combined with constant axle load will instead increase strain near the surface. Tire pressure is therefore a more influential factor than axle loading as far as flow rutting is concerned. The tire-pavement contact stress distributions are non-uniform but are often uniformly modeled, which overestimates the strain. The use of the super-single tire configuration is increasing at the expense of traditional dual tires. However, super-single tires have been found to cause significantly more rutting than dual tires. The occurrence of lateral wander reduces the growth of ruts.

3.9.5   Pavement temperature

The properties of asphalt concrete are highly dependent on temperature. Therefore, performance prediction and design of pavements require an accurate modeling of the pavement temperature profile. The most important factors to consider are conduction, convection, shortwave and longwave radiation, surface icing, infiltration, evaporation and condensation. Local meteorological data are used as model input. Existing temperature models are steadily evolving and are on their way to being implemented in standard pavement design tools.

3.9.6   Laboratory test principles and methods

Laboratory testing is employed for determining material properties, and the test results are typically used for modeling or ranking purposes. The tests can be divided into simulative and fundamental tests. The fundamental test methods differ in terms of geometry, dynamic or static load as well as load shape and amplitude. Some test types determine predominantly viscoelastic properties, while others rather measure the viscoplastic properties. All test methods have advantages and disadvantages, which implies that a combination will provide a higher degree of knowledge. The choice of certain test methods is sometimes prescribed by a deterioration model or methodology.

3.9.7   Accelerated Loading Testing

Accelerated Loading Testing is a test method used to simulate pavement deterioration on a full-scale test track. It enables an evaluation of different pavement structures and materials, a validation of laboratory test methods and a development of deterioration models under realistic conditions. An accelerated loading facility can be run in a controlled or natural environment, and the loading can be applied with conventional traffic or with a loading device. There are three typical kinds of facilities. Long test tracks are subjected to conventional heavy traffic and natural environmental conditions. Circular test tracks are typically loaded with a high-speed loading device without environmental control. Linear test tracks use relatively slow-moving devices that are often mobile. They can be employed in a controlled or non-controlled environment.

3.9.8   Models and theories for prediction of permanent deformation in asphalt materials

Deterioration modeling of asphalt concrete pavements can be either mechanistic, empirical or a combination of the two. Mechanistic modeling assesses the deterioration mechanisms analytically, while empirical modeling is simple and based entirely on observation. Current practical modeling is often based on mechanistic principles and supplemented by empirical additions. Mechanistic approaches on asphalt concrete include modeling of material characteristics. Viscoelastic modeling can be linear or non-linear and accounts for material time-dependency and lateral flow.

4   METHOD

The objectives were reached using a Heavy Vehicle Simulator (HVS) test, specimen production, laboratory testing and modeling of permanent deformation in the asphalt layers according to the Mechanistic-Empirical Pavement Design Guide (M-E PDG) software, as illustrated in Figure 4.1. Model results were evaluated and compared with HVS test results. Field calibration factors were assessed in order to adjust the model to the observations.
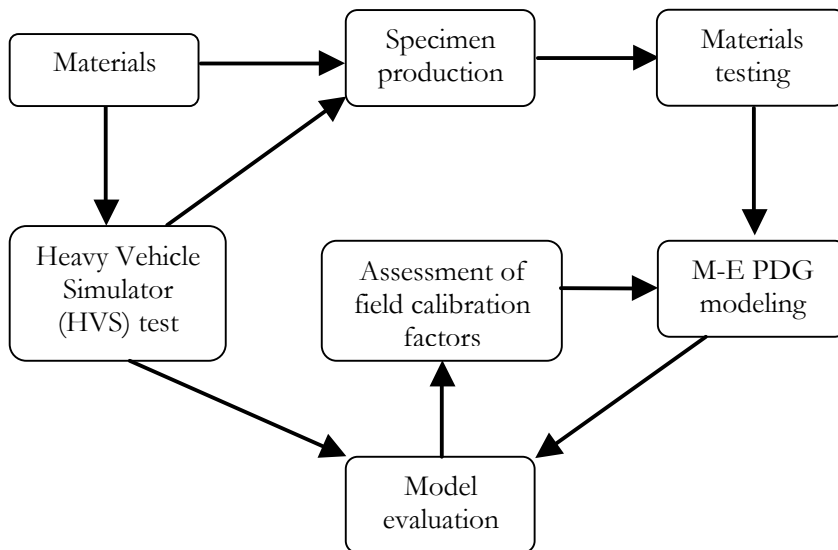
Figure 4.1. Schematic method description.

The Mechanistic-Empirical Pavement Design Guide (M-E PDG) simulates permanent deformation in asphalt concrete pavement, among other things. In order to evaluate the model, its results should be compared with the deterioration of existing pavements. Accelerated loading testing with measurement of permanent deformations can be used to achieve this.

In this case, a Heavy Vehicle Simulator (HVS) was employed in a controlled environment to perform accelerated testing. The HVS loading device simulated the impact of slow-moving super single tire half-axles on two asphalt concrete (AC) sections. More details on the HVS can be found in Chapter 3.7. The two tested sections were a standard AC structure and an enhanced variant, in which the binder layer was polymer modified to increase its resistance to permanent deformation. During the HVS test, permanent deformation data of each layer was collected continuously by using pavement-integrated gauges. This data was used to evaluate the effect of

polymer modification of the binder layer and later for comparison with M-E PDG model results. In addition, data describing the constant climate and loading properties was noted as it was to be used as input data in the model.

In addition to climate and loading properties, the M-E PDG model also requires material input data, e.g. dynamic modulus data derived with the uniaxial test. In this situation, an interesting opportunity arose. Kim et al. (2004) reported that the indirect tensile testing (IDT) using 38 mm high gyratory compacted cylindrical specimens can determine dynamic moduli as well as uniaxial testing using 150 mm high gyratory compacted cylindrical specimens. It should be noted that the test methods have two fundamental differences. First, the IDT induces tensile stress in the specimens while the uniaxial test is purely compressive. Secondly, the IDT loading direction is perpendicular to the compaction direction while those directions are the same in the uniaxial test. Nonetheless, Kim et al. (2004) found an analytical solution correlating the modulus of the IDT and the uniaxial test based on linear viscoelasticity. In order to test these results, the mastercurves from the IDT and uniaxial test were compared. Both specimen types were gyratory compacted out of the asphalt mix that was stored during laying of the HVS test pavement.

Kim et al. (2004) used only 38 mm high gyratory compacted specimens for IDT. Specimens can also be cored directly from most asphalt concrete layers without using artificial compaction methods. Since pavement layers of 150 mm height are rare, it is often not feasible to obtain cored uniaxial specimens. However, cored IDT specimens were obtained from the HVS test sections. In order to study whether cored specimens can be used instead of gyratory compacted specimens, mastercurves derived with specimens from the two origins were compared. The characteristics of the asphalt mixes, especially the conventional and polymer modified binder layer mixes, were also evaluated.

The modeling of permanent deformation in the two HVS test pavements was carried out using the M-E PDG software. All affecting factors surrounding the HVS test were modeled using input data at the highest possible levels of accuracy. For the structures and materials, the input data consisted of dynamic modulus data, conventional binder test data and general mix properties. The results of the uncalibrated model were evaluated and compared with the HVS test results. Both the total asphalt concrete rut depth and the permanent deformation of each asphalt concrete layer were taken into consideration. In order to achieve better total rut depth correlation, field calibration factors were assessed using a trial-and-error process. The model's behavior and the results were further discussed in the light of experiences from other investigations, e.g. Agardh and Busch (2006) and the M-E PDG documentation (NCHRP, 2004).

5   HEAVY VEHICLE SIMULATOR TESTING

The Heavy Vehicle Simulator (HVS) test was carried out at the Swedish National Road & Transport Research Institute (VTI) in Linköping, Sweden. This entire chapter is based on data and documentation from Wiman (2007). An asphalt concrete (AC) pavement with two sections was constructed. The idea was to test an enhanced AC structure and compare it with a standard AC structure constructed according to Swedish norms (ATB Väg, 2005). It was expected that the enhanced structure would show higher resistance to flow rutting than the reference structure.

5.1   Materials

The asphalt materials used were a conventional ABT11 70/100 (ABT) wearing course, a conventional ABb22 70/100 (ABb) binder course, a polymer modified ABb22 70/100 (ABbm) binder course and a conventional AG22 160/220 (AG) asphalt base course. Detailed asphalt mix properties are shown in Table 5.1. All asphalt mix types were produced at Ludden asphalt plant in Norrköping, Sweden. The aggregates were crushed granite/tonalite from the Ludden quarry, Norrköping, and the asphalt binder was Venezuelan/Russian base bitumen fluxed with North Sea bitumen. The type and amount of added polymer in the modified binder mix cannot be revealed for reasons of company secrecy. Nevertheless, the asphalt mixes can be evaluated in respect to mechanical properties.

Table 5.1. Properties of the asphalt mixes according to recipe.

Mix type	ABT	ABb	ABbm	AG
Max. aggregate size [mm]	11	22	22	22
Binder content	6.5 %	5.0 %	5.0 %	4.5 %
Bitumen type	70/100	70/100	Modified 70/100	160/220

5.2   Structure

The standard AC structure consisted of a 35 mm thick ABT wearing layer, an 82 mm ABb binder layer and an 81 mm AG asphalt base layer, as shown in Figure 5.1. The enhanced AC structure was a similar structure that consisted of a 39 mm thick ABT wearing layer, an 84 mm polymer modified ABb binder layer and a 79 mm AG asphalt base layer. All layer thickness data was obtained during and after construction by means of surface measurement and pavement coring. The polymer modification had the purpose of increasing resistance to permanent deformation. The two AC structures were placed on an approximately 200 mm thick aggregate base layer resting on approximately 2500 mm of fine sand with a rigid Portland cement concrete foundation beneath. The entire construction was drained.

Pairs of inductive coils, called EMU coils, where integrated at the top and bottom of each asphalt layer beneath the middle of the wheel track. The displacement between a pair of EMU coils can provide permanent strain data for each layer as described by Wiman (2006). Three pairs of EMU coils were located at different longitudinal positions in each layer of both AC structures. In addition, several other instruments were integrated in the pavement structure: longitudinal and transversal strain gauges below the AC structure, vertical stress gauges in the middle of the unbound base layer and temperature gauges at three depths. However, most data from these instruments was only used for test control purposes. Each AC structure was 8 m long, of which the middle 6 m was instrumented.
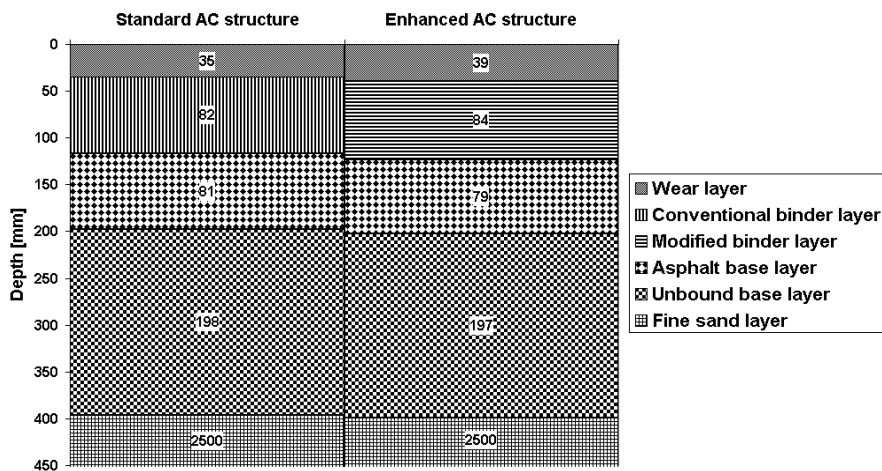
Figure 5.1. The two AC structures subjected to HVS testing.

5.3   Loading and climate

The HVS was configured to simulate the repeated load of heavy vehicles using a super single tire traveling back and forth. The wheel load was 60 ± 0.5 kN, the tire pressure was 900 ± 30 kPa and the speed was 12 ± 0.3 km/h. The HVS wheel loading was applied bi-directional and the lateral wander distribution shown in Figure 5.2 was used. The lateral displacement was automatically shifted between loadings in order to simulate traffic wander behavior. Realistic traffic lateral wander data is often difficult to assess. However, the HVS test results were only to be compared with a model in which the lateral distribution of the HVS test constituted the input data.
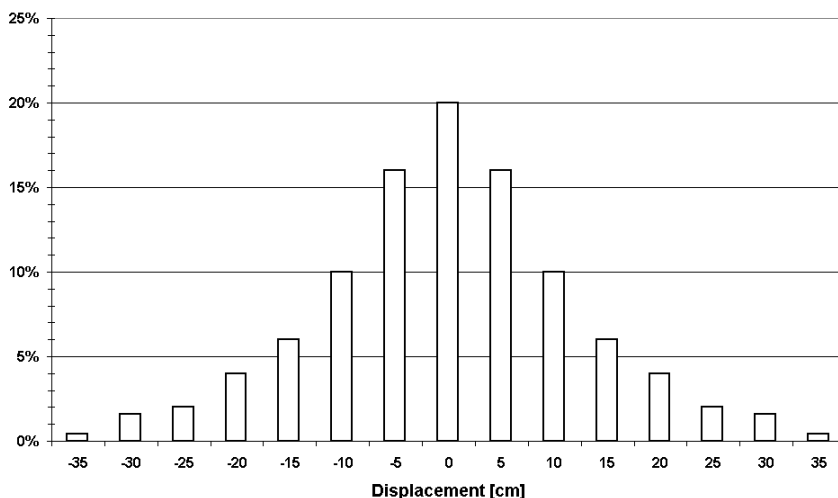
Figure 5.2. The lateral wander distribution during the HVS test.

The HVS test was performed inside a climate-controlled chamber. In order to test the temperature susceptibility of the pavement structures, the loading was conducted at three different pavement temperatures, as shown in Figure 5.3. The temperature levels were +10 °C, +20 °C, and +30 °C with no temperature gradient. Although not entirely comparable to realistic pavement conditions, this can be taken into account during modeling, which makes it possible to compare results.

Before loading, the temperature was stabilized at +10 °C throughout the entire construction. 151,000 passages were simulated, after which the temperature was raised to +20 °C. Another 315,000 passages were then carried out. Finally, the pavement was tempered at +30 °C, after which it was subjected to a further 108,000 passages. At this stage, the HVS test was interrupted due to excessive permanent deformation that caused malfunction of the pavement integrated gauges.

At intervals during the simulation, permanent deformation of each asphalt layer was measured using EMU coils along with surface measurement of the transversal profiles. During HVS loading, stress was measured in the middle of the unbound base layer. Additional data from other response measurements and the falling weight deflectometer was also collected but was not used in the study.
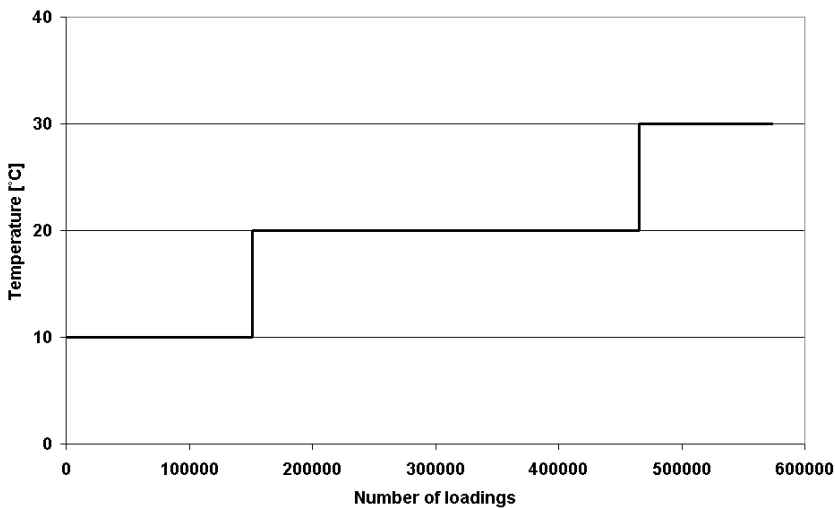
Figure 5.3. Temperature and loading sequence during the HVS test.

Due to the nature of accelerated loading tests, ageing effects cannot be simulated. It is known that long-term ageing causes asphalt concrete to stiffen, especially during the first service years (The Shell Bitumen Handbook, 2003). The possible effect of low AC stiffness would result in HVS test rut depths that are higher than expected on an existing asphalt pavement.

5.4   Results and discussion

The HVS pavement provided different sources of permanent deformation data. The total rut depth was assessed by means of surface measurements. Permanent deformation in each asphalt concrete layer was measured on cored pavement specimens from the wheel track and also by using EMU coils. Mean values of the EMU coils were used throughout the analysis. After 532,360 loadings, the wear layer EMU coils malfunctioned due to excessive flow rutting. Testing was continued up to 573,600 loadings, after which pavement cores were extracted and measured.

5.4.1   Wear layer

Permanent deformation in the wear layer was higher in the standard AC structure than in the enhanced AC structure, as shown in Figure 5.4. The deformation was irregular, which was expected due to the proximity of the loading wheel that causes lateral flow. However, as only mean values were used, the strain data variation was considered acceptable up to 532,360 passages, at which point one of the EMU coils failed.

Number of passages
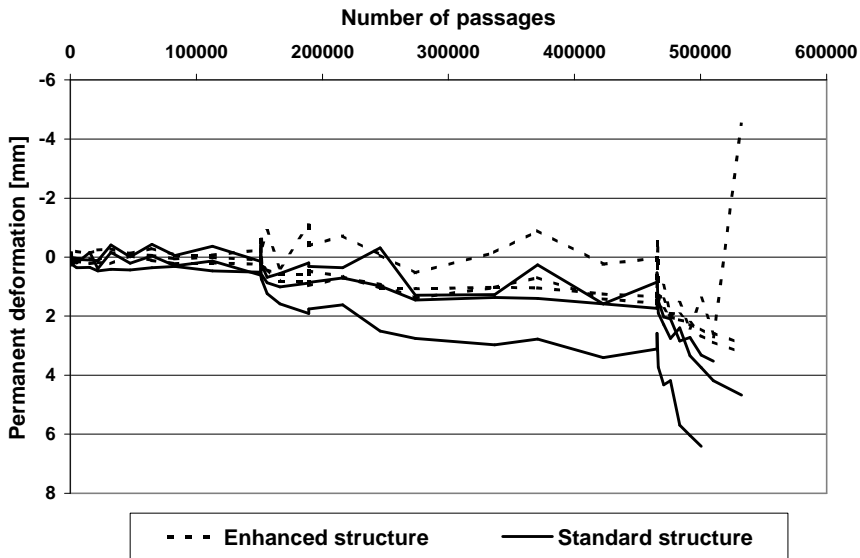
Figure 5.4. Permanent deformation in the wear layers of both AC structures measured by each pair of EMU coils.

5.4.2 Binder layer

EMU coil data from the conventional and modified binder layers showed that the spread was relatively coherent in each group, with one exception, as shown in Figure 5.5. Therefore, the spread was considered acceptable and mean values were used.

Number of passages
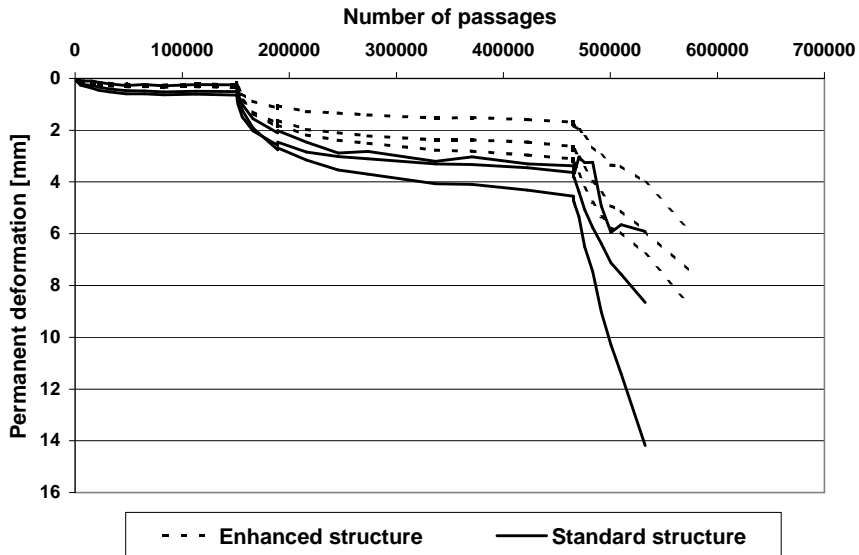
Figure 5.5. Permanent deformation in the conventional and modified binder layers measured by each pair of EMU coils.

5.4.3   Asphalt base layer

Unfortunately, the EMU coils in the asphalt base layer of the standard structure malfunctioned at an early stage. In order to obtain results for analysis and modeling, it was therefore necessary to make an assessment. The polymer modified binder layer was stiffer than the conventional binder layer, as shown in Chapter 7. Therefore, it is logical that the enhanced structure exhibited an improved load distribution capability that resulted in less stress in the unbound base layer beneath the AC structure, according to the vertical soil pressure cell data presented in Figure 5.6. When the moving loading device was applied, the stress was measured with both Geokon and Nottingham soil pressure cells, which differ in size and function. Note that the stress levels increase between 150,000 and 200,000 loadings, which is the effect of the temperature change from +10 °C to +20 °C. The temperature affects the asphalt concrete stiffness and thereby its load distribution capability, which in turn affects the stress level in the unbound materials.
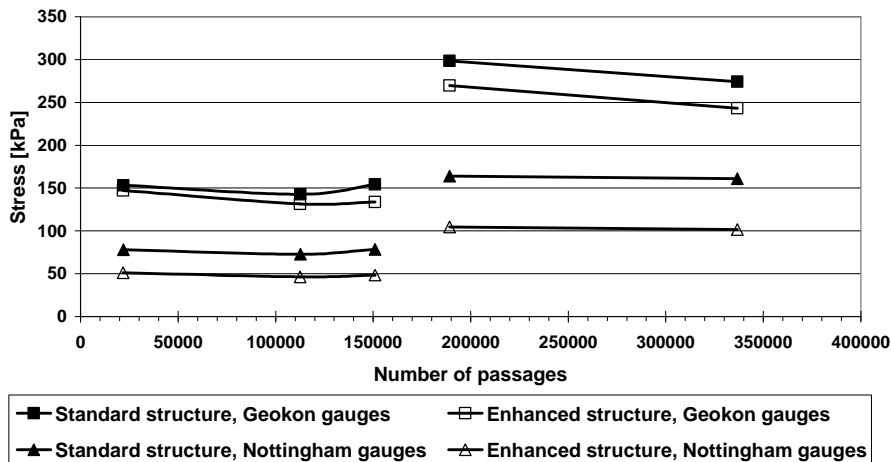
Figure 5.6. Stress measured in the middle of the unbound base layer during HVS loading.

Logically, stiff asphalt concrete that provides good load distribution will result in modest permanent deformation of the underlying layers, e.g. the asphalt base layer. Therefore, it can be argued that the standard structure asphalt base layer should result in permanent deformation that is as high as or higher than the enhanced structure asphalt base layer.

In order to strengthen the hypothesis, a single pavement core was obtained from the wheel track of each AC structure after the HVS test had been completed. The thickness of each layer was measured and compared to the initial layer thickness recorded during laying. This resulted in permanent deformation data from each asphalt concrete layer. In the core from the standard AC structure, the AG layer contribution to total AC rut depth was

24%, as can be seen in Table 5.2. When the asphalt base deformation data of the enhanced structure was combined with wear- and binder layer deformation data from the standard structure, the asphalt base layer contribution was 31%. Therefore, it was determined that the asphalt base deformation data from the enhanced structure could be used as an approximation for asphalt base deformation data for the standard structure. It was recognized that the assumed strain data was probably underestimated.

Table 5.2. The contribution of each layer to the total rut depth of the standard and enhanced AC structures.

		Wear layer	Binder layer	Base layer	Total AC structure
EMU coil data at N=500530 in standard AC structure	Deformation [mm]	4	8	6*	18
	Deformation contribution of total AC rut depth	25%	43%	31%*	100%
Core data at N=573600 in standard AC structure	Deformation [mm]	7	18	8	33
	Deformation contribution of total AC rut depth	21%	55%	24%	100%
EMU coil data at N=500530 in enhanced AC structure	Deformation [mm]	2	5	6	13
	Deformation contribution of total AC rut depth	17%	37%	45%	100%
Core data at N=573600 in enhanced AC structure	Deformation [mm]	4	4	2	10
	Deformation contribution of total AC rut depth	40%	40%	20%	100%
* EMU coil data from the base layer of the standard AC structure was not obtained and was therefore approximated using the corresponding data from the enhanced AC structure.					

Eisenmann and Hilmer (1987) conducted elastic multi-layer simulations to investigate how various conditions of load and tire pressure conditions affects elastic strain at different depths. They found that the elastic strain, which affects permanent deformation, peaks at approximately 50 mm, i.e. the upper part of the binder layer. As expected, a large portion of the permanent deformation in the AC structures of this study appeared to occur in the binder layer.

However, the EMU coil data did not completely match the core data. Therefore, no far-reaching conclusions should be drawn on the contribution of permanent deformation from each layer. The potential measurement error on AC cores is large and variation in data from both coring and EMU measurements should be expected. Ideally, at least three cores should be obtained and measured in order to increase measurement accuracy. Another alternative is to perform a trench study. The data from coring or trenching should be used to validate the EMU coil data.

The variation in the EMU coil data from the asphalt base layer, illustrated in Figure 5.7, was considered acceptably low. Mean values were used later.
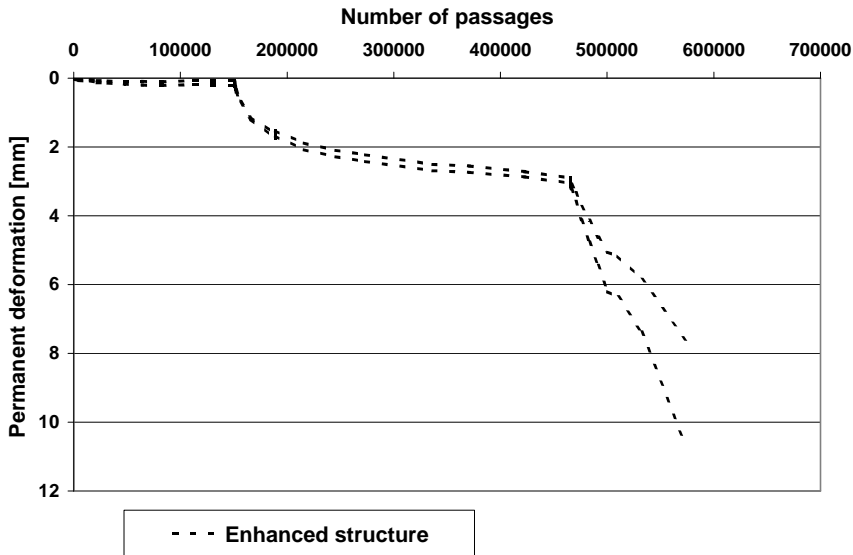
Figure 5.7. Permanent deformation in the base layer of the enhanced AC structure measured by each pair of EMU coils.

5.4.4   All layers

After the HVS test had been completed, the total rut depth was determined by means of surface measurement, as shown in Table 5.3. Further, the core permanent deformation data of all asphalt layers in Table 5.2 was re-used. Using this data, the permanent deformation in the unbound materials was calculated. The asphalt concrete contribution to total rut depth was assessed. It was found that the flow rutting in the enhanced AC structure was only a third of the permanent deformation in the standard AC structure. The addition of polymers is known to reduce permanent deformations, as discussed in Chapter 3.2, but the magnitude was unexpectedly high. The permanent deformation of the unbound layers appeared to be similar under both AC structures.

Table 5.3. Contribution of permanent deformation from the bound and unbound layers to total rut depth in the two structures after 573 600 passages.

	Standard structure	Enhanced structure
Asphalt concrete permanent deformation [mm]	33	10
Unbound materials permanent deformation [mm]	14	16
Total rut depth [mm]	47	26
Asphalt concrete contribution to total rut depth	70%	38%

In order to obtain total flow rutting from a second source, EMU coil data from each layer was summed up and presented in Figure 5.8. These data imply that the total flow rutting of the enhanced AC structure was two thirds of the permanent deformation of the standard AC structure. Consequently, the single pavement cores and the EMU coils showed different total flow rutting. Data from the EMU coils should be considered more reliable due to the single core sample size.

It was observed that the flow rutting of the standard structure accelerated at the end of the simulation. This implies that it could have reached the third AC permanent deformation stage, as described in Chapter 3.1. However, the strain gauges in the AC layers could not confirm the observation as they had failed at the time.
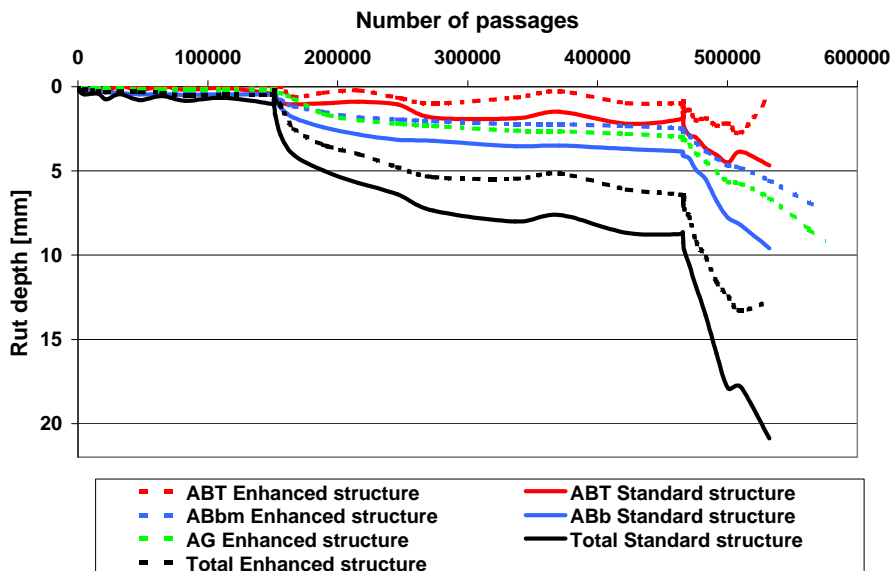
Figure 5.8. Permanent deformation of each asphalt layer in the standard and enhanced AC structures subjected to the HVS test.

5.5 Conclusions

HVS testing showed that polymer modification of the binder layer reduced flow rutting in a conventional 220 mm asphalt concrete structure to approximately two thirds, as measured with EMU coils. The corresponding result from measurement on a single core was approximately one third. Further, the polymer modification also increased the load distribution capability, as shown with soil pressure cells. However, the permanent deformation of the unbound layers was not significantly affected in this investigation.

6 SPECIMENS

Specimens were produced to be used in the three laboratory test set-ups. These were the uniaxial test using gyratory compacted specimens, the indirect tensile test using gyratory compacted specimens and finally the indirect tensile test on specimens cored from the Heavy Vehicle Simulator (HVS) test pavement. It would also have been interesting to perform the uniaxial test on pavement cores but the layer thickness did not allow sufficient specimen height. Due to a lack of material, no AG base mix specimens could be produced with the gyratory compactor.

The Mechanistic-Empirical Pavement Design Guide (M-E PDG) recommends that dynamic modulus data to be obtained using the uniaxial test on two gyratory compacted specimens (NCHRP, 2004). However, some safety margin is appropriate. Therefore, the target number of uniaxial specimens for each test set-up and mix type was three, although two was considered to be acceptable. The same line of argument was applied for both gyratory compacted and cored indirect tensile test specimens.

6.1 Specimen preparation

The asphalt mix used for gyratory compaction was sampled during the construction of the test sections. Therefore, it was short-term aged during mixing and mixture conditioning of HMA. The compactor, an ICT-150 RB with mould and inserts, is shown in Figure 6.1 and Figure 6.2.

Figure 6.1. The ICT-150 RB gyratory compactor at VTI, Linköping.

Figure 6.2. The mould and its components.

Gyratory compacted plugs with the dimensions D150xH180 mm and D150xH80 mm were produced for the uniaxial test and the indirect tensile test, respectively. The gyratory compaction was carried out according to the EN 12697-31 standard (CEN, 2005) with some deviations. More details on gyratory compaction can be found in Chapter 3.3. The target density of each specimen group was equal to the target density of the corresponding HVS test pavement layer.

A 2.00° angle of gyration was used in comparison to the standard settings of EN 12697-31, which is 1.00° (CEN, 2005), or T312-04, which is 1.25° (AASHTO, 2006). This was motivated by the difficulties in reaching the target density in 180 mm high plugs out of the dense ABT wearing mix. Material properties of each mix were to be compared using these specimens. Therefore, it was decided that all gyratory compacted specimens should use the 2.00° angle of gyration. This increased the shearing action of the gyratory compactor, which accelerated the compaction.

After gyratory compaction, the D150xH180 mm plugs were cored and cut to uniaxial test specimens with the dimensions D100xH150 mm as shown in Figure 6.3 and Figure 6.4. An ocular inspection indicated that the bottom of the uniaxial test specimens in some cases had higher air void content than the top. The uneven air void distribution was partly expected, as gyratory compaction is known to produce specimens with lower density in its eccentric parts (Raaberg, 1999; Viman, 1998; Masad et al., 1999). Therefore, the specimens were approved and no further investigation was carried out.

Figure 6.3. A cored and cut uniaxial specimen.

Figure 6.4. The outer shell of the gyratory compacted plug.

After gyratory compaction, the D150xH80 mm plugs were cut into D150xH50 mm indirect tensile test specimens, as shown in Figure 6.5. Since the IDT specimens produced by gyratory compaction where cut but not cored, some displayed small surface cavities. These should weaken the specimen without affecting the air void content. On the other hand, it should be noted that the greatest stresses and strains in the indirect tensile test occur in the middle of the specimen where there are no open cavities.
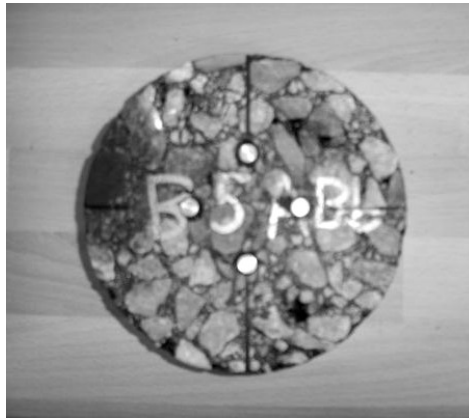
Figure 6.5. An indirect tensile test specimen cored from the pavement and prepared with glued-on brass knobs.

It was suspected that the occurrence of surface cavities might depend on undue shear forces between the inside of the mould and the plug surface. The shear forces may be the result of high friction, which in turn may be the result of insufficient preheating of the mould or the absence of a mould lubricant. The EN 12697-31 (CEN, 2005) standard preheating time for the mould and its inserts was decreased from two hours to half an hour and the prescribed lubricant was disregarded. Further, the filled mould was not stored at the test temperature for half an hour before compaction. However, the possible increase in friction was not considered significant. This point was illustrated by the relative ease with which the plugs were extracted from the mould.

Cores with a diameter of 150 mm were obtained from the HVS test pavement. Both asphalt concrete structures were represented by four undamaged cores. The coring was located between the main wheel track and the AC edge. The layers of each AC plug were cut into indirect tensile test specimens with the dimensions D150xH40 mm. The binder and base layers each consisted of two sub-layers and specimens are not allowed to have joints. Therefore, only the top 40 mm portion of each pavement layer was used for specimen fabrication.

6.2 Specimen properties

The properties of the selected uniaxial specimens (UNI) and indirect tensile test (IDT) specimens are shown in Table 6.1. Gyratory compacted uniaxial test specimens were to be compared with gyratory compacted IDT specimens, which in turn were to be compared to cored IDT specimens. The difference in mean air void content between two compared groups should be minimal. Nilsson (2001B) reported that a reduction in air void content caused an increase in asphalt mix stiffness. In this study, mean air void differences higher than 1.5% were recognized as having an undue impact on stiffness.

The low number of gyrations of the ABbm mix specimens should be noted. Most of the gyratory compaction occurs during the first gyrations, but it is uncertain whether 4-5 revolutions can provide sufficient compaction effort or not. The cause is most likely a too low bitumen viscosity due to an excessive compaction temperature, which was 160 °C compared to 140 °C for a conventional 70/100 asphalt mix. However, the compaction temperature in question was recommended by the asphalt mix producer and the EN 12697-31 standard (CEN, 2005) allows temperature adjustments when using modified mixes. It is unclear whether an excessive temperature and few gyrations produce specimens different from those compacted at lower temperature and with a higher number of gyrations.

Table 6.1. Properties of gyratory compacted specimens.

ID tag	Test type	Mix type	No. of revolutions [max 400]	Air voids in specimen	Air voids mean	Air voids standard deviation
17	UNI	ABT	400	4.2%	4,0%	0.2%
33			364	3.8%		
21	UNI	ABb	400	5.3%	6.0%	0.7%
22			400	6.7%		
23			400	5.8%		
18	UNI	ABbm	17	6.3%	5.8%	0.5%
19			17	5.9%		
20			24	5.3%		
34	IDT	ABT	44	3.9%	4.4%	0.5%
35			52	4.5%		
36			47	4.9%		
27	IDT	ABb	400	5,0%	4.4%	0.6%
41			254	3.8%		
42			400	4.4%		
46	IDT	ABbm	5	8.4%	8.1%	0.4%
50			4	7.9%		

The four AC cores derived from each of the pavement structures supplied an abundant number of IDT specimens. Three specimens from each layer were selected and its properties are shown in Table 6.2.

Table 6.2. Air void properties of the cored specimens.

ID tag	Test type	Mix type	Air voids in specimen	Air voids mean	Air voids standard deviation
B3ABT			3.7%		
B4ABT	IDT	ABT	4.4%	4.3%	0.6%
B7ABT			4.9%		
B5ABb			6.6%		
B6ABb	IDT	ABb	6.4%	6.8%	0.5%
B7ABb			7.4%		
B1ABbm			6.8%		
B3ABbm	IDT	ABbm	6.9%	6.7%	0.2%
B4ABbm			6.5%		
B3AG			8,0%		
B5AG	IDT	AG	7.8%	7.9%	0.1%
B7AG			7.9%		

6.3   Conclusions

As it in some cases was difficult to reach the target density, i.e. pavement core density, it was necessary to increase the angle of gyration to 2.00°. In order to achieve proper mix viscosity, the compaction temperature of polymer modified mixes should be carefully evaluated before actual specimen production.

7 DYNAMIC MODULUS TESTING

Laboratory testing of materials was carried out in order to obtain dynamic modulus data of all asphalt mixes that were used in the Heavy Vehicle Simulator (HVS) test pavement. The Mechanistic-Empirical Pavement Design Guide (M-E PDG) recommends the uniaxial test using 150 mm high gyratory compacted specimens (NCHRP, 2004). However, Kim et al. (2004) reported that indirect tensile testing (IDT) using 38 mm high gyratory compacted cylindrical specimens were able to determine dynamic moduli as well as uniaxial testing using 150 mm high gyratory compacted cylindrical specimens. It should be noted that the test methods have two fundamental differences. First, the IDT induces tensile stress in the specimens while the uniaxial test is purely compressive. Second, the IDT loading direction is perpendicular to the compaction direction while the directions are the same in the uniaxial test. More detailed descriptions of the test methods can be found in Chapter 3.6. Despite the differences, Kim et al. (2004) found an analytical solution based on linear viscoelasticity. In order to test these results, the mastercurves from the IDT and the uniaxial test was compared using gyratory compacted specimens only. In addition, IDT specimens were also cored directly from most asphalt concrete layers. Due to layer thickness limitations, it was not feasible to obtain cored uniaxial specimens.

In this investigation, the asphalt mixes were tested using three test set-ups: the uniaxial test using gyratory compacted specimens, the indirect tensile test using gyratory compacted specimens, and the indirect tensile test on specimen cored from the pavement layers. The dynamic moduli of the uniaxial test and IDT were compared using procedures and equations recommended by Kim et al. (2004) in order to evaluate the effect of using IDT instead of the uniaxial test when testing cored specimens. To assess the possibility of using cored specimens in lieu of gyratory compacted specimens and visa versa, IDT dynamic modulus results derived using gyratory compaction and coring were compared. In addition, the characteristics of the asphalt mixes were also evaluated using dynamic modulus from each test set-up. Other material properties such as phase angle and Poisson's ratio was not included in the analysis as the main task was to provide the M-E PDG with dynamic modulus data.

All dynamic modulus testing was performed using a Universal Testing Machine (UTM) supplied by Industrial Process Control (IPC) Global, Australia. It consists of a loading cell, a temperature chamber, a communication unit and an ordinary desktop computer. The temperature was monitored using multiple thermometers in the temperature chamber and inside a dummy specimen that was located next to the test specimen. This made it possible to determine that the temperature had stabilized before testing.

7.1 Uniaxial testing

The dynamic modulus uniaxial compressive test was performed on gyratory compacted specimens with the dimensions D100xH150 mm. The uniaxial test arrangement is shown in Figure 7.1. The Mechanistic-Empirical Pavement Design Guide recommends dynamic moduli data derived from the uniaxial test with two specimens and three LVDTs (Linear Variable Displacement Transducers) attached (NCHRP, 2004). This corresponds to an estimated limit of accuracy of ±13.1 %. If three specimens and three LVDTs are used for each asphalt mix, the estimated limit of accuracy is ±12.0 % (AASHTO, 2006). It was determined that uniaxial dynamic modulus testing was to be performed using four LVDTs on two or three specimens to obtain sufficient accuracy. Therefore, the estimated limit of accuracy is somewhat better than ±13.1 %.

The four axial LVDTs were evenly distributed around the circumference. Vertically, the LVDTs were mounted in the middle 100 mm of the specimen. A friction-reducing end treatment was applied on the top of the specimen before mounting the end plate.

The test strain should be kept within the linear viscoelastic range in order to obtain representative results and to avoid material damage, as discussed in Chapter 3.6. The target strain level was determined at 50-75 microstrains based on results from earlier studies (Nilsson, 2001A; Witczak et al., 2002). Due to specimen variation, some strain deviations were expected.
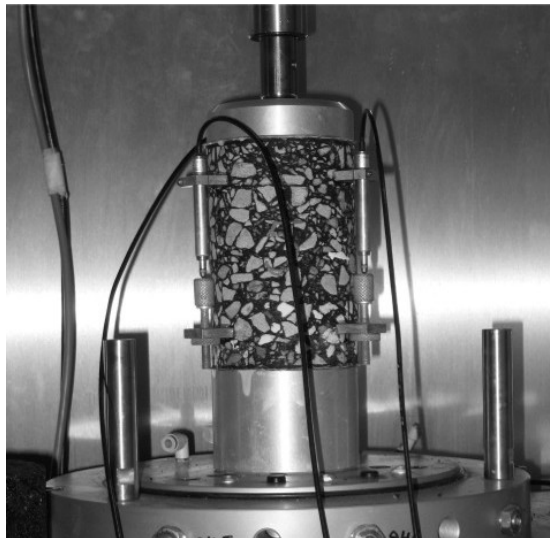
Figure 7.1. The uniaxial test specimen with LVDTs, end plates, and loading cell.

The test specimen was subjected to 100 pre-conditioning loading cycles at 25 Hz that induced approximately 30 microstrains. It was then subjected to compressive haversine loading at six test frequencies: 200 cycles at 25 Hz, 200 cycles at 10 Hz, 100 cycles at 5 Hz, 20 cycles at 1 Hz, 15 cycles at 0.5 Hz, and 10 cycles at 0.1 Hz. After each frequency, the specimen was allowed to rest for 5 minutes to relax the accumulated viscoelastic strain. The procedure was repeated at each temperature. The frequency sweep was repeated at the test temperatures -10 °C, +5 °C, +20 °C, +35 °C, and +55 °C in that order. Another frequency sweep was also carried out at +20 °C to check whether the dynamic moduli had changed during testing. The temperature accuracy was kept within ±0.5 °C and the minimum tempering time was four hours. Therefore, there was ample time for material relaxation.

The AASHTO Provisional Standards (AASHTO, 2006) were later obtained and a comparison was made between the performed uniaxial test and the uniaxial test standard TP62-6 (AASHTO, 2006). It allows a 0.5 % maximum air void difference between specimen and target air void content. However, the air void differences for uniaxial tests were typically 0-1%. The single highest difference for any uniaxial test specimen was 1.5 %.

Further, the TP62-6 (AASHTO, 2006) prescribes that the specimen axis and its ends should be perpendicular. The allowed margin of error is one degree, which the uniaxial specimens of this study could not match. This was illustrated by the fact that the specimen was provided with a friction reducing end treatment on the top only. Otherwise, uniaxial testing would have been impracticable due to lateral displacement. However, it was recognized that the test cannot be purely uniaxial due to the lateral constraint at the bottom.

7.2 Indirect tensile testing

The dynamic modulus indirect tensile test (IDT) was performed on gyratory compacted and cored specimens with the dimensions D150xH50 mm and D150xH40 mm. The indirect tensile test arrangements are shown in Figure 7.2. Before testing, vertical and horizontal pin and core gauges were mounted in the center of the specimen on both sides. Thus, both tensile and compressive deformations were measured.
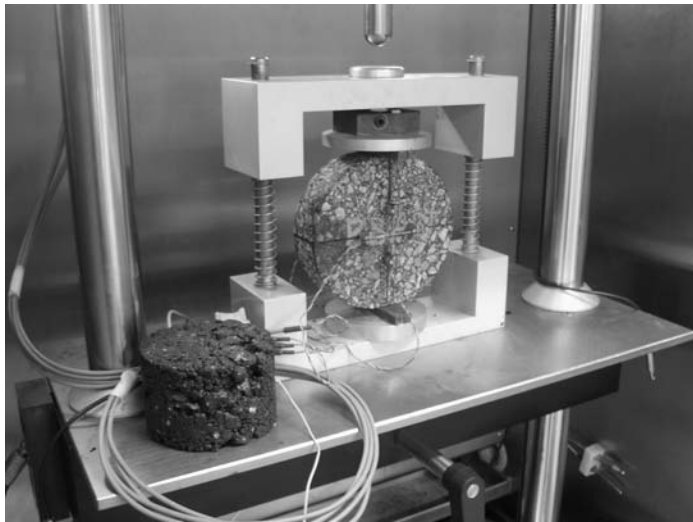
Figure 7.2. The indirect tensile test arrangement with a thermometer inside the dummy specimen.

The test specimen was subjected to 100 pre-conditioning loading cycles at 25 Hz that induced approximately 30 microstrains. It was then subjected to compressive haversine loading at six test frequencies: 200 cycles at 25 Hz, 200 cycles at 10 Hz, 100 cycles at 5 Hz, 20 cycles at 1 Hz, 15 cycles at 0.5 Hz, and 10 cycles at 0.1 Hz. After each frequency, the specimen was allowed to rest to relax the accumulated viscoelastic strain. The frequency sweep was repeated at the test temperatures -10 °C, +5 °C, +20 °C, and +35 °C in that order. No temperatures higher than +35 °C were used because of the risk of material damage and effects on specimen geometry. Occasionally, the test was also prematurely interrupted for this reason. After testing, another frequency sweep was carried out at +20 °C to check whether the dynamic modulus was affected by the testing. The temperature accuracy was kept within ±0.5 °C and the time for temperature adjustments between every frequency sweep was at least four hours. This means that there was ample time for material relaxation.

7.3   Material damage statistics

During the dynamic modulus testing, the viscoelastic strain occasionally exceeded the target interval of 50-75 microstrains. Therefore, statistical analysis was employed to determine whether the specimens were damaged or not. A specimen can be considered damaged if it can be shown that its mechanical properties have been significantly altered during testing. Dynamic modulus data derived from damaged specimens can be questioned.

The available data for statistical analysis was dynamic modulus data obtained at +20 °C during and after testing as described before. It should be noted that only 21 of the total 28 specimens were statistically analyzed due to a lack of control frequency sweep data. This was partly due to some problems with the deformation gauges. Further, some permanent deformation was observed during testing of all IDT GYR specimens. In order not to risk specimen failure and subsequent damage on the pin and core gauges, the control frequency sweep at +20 °C was not carried out.

The issue of determining a suitable statistical analysis method was of some concern. Ideally, the single t-test, the paired t-test or the Wilcoxon rank sum test (Devore and Farnum, 1999) should be applied on dynamic modulus data from at least ten specimens for each mix. A separate analysis should be carried out for each specimen type and frequency. However, each mix was represented by no more than two or three specimens, which undermines any statistical result.

In order to increase sample size, the specimens were analyzed as a group. The ratio of the dynamic modulus during and after testing, defined as the damage ratio (R), was calculated at each frequency and temperature for each specimen. This resulted in a sample size of 123 and the expected mean ratio $E(R) = 1$ as the specimens were assumed undamaged. This hypothesis was tested using the one-sample t-test (Devore and Farnum, 1999). The null and alternative hypotheses to be tested were defined as:

$$H_0 : E(R) = 1$$

$$H_a : E(R) \neq 1$$

The specimen mean damage ratio of dynamic moduli during and after testing ranged from 0.91 to 1.18. The overall mean damage ratio was 1.04 with a standard deviation of 0.09. The null hypothesis H_0: $E(R) = 1$ was tested using the one-sample t-test and rejected at the $\alpha = 0.01$ significance level. Therefore, it was concluded that the dynamic modulus testing had statistically changed the mechanical properties of the specimen group. However, the uniaxial test using two specimens and three LVDTs corresponds to an estimated limit of accuracy of ±13.1 % (AASHTO, 2006). Therefore, the 4% average loss of dynamic modulus was considered acceptable.

To complement the statistical analysis, the mean damage ratio, mean elastic strain and maximum elastic strain were calculated for each specimen. The scatter plots shown in Figure 7.3 and Figure 7.4 indicate that the damage ratio was not positively dependent on either mean elastic strain or maximum strain.
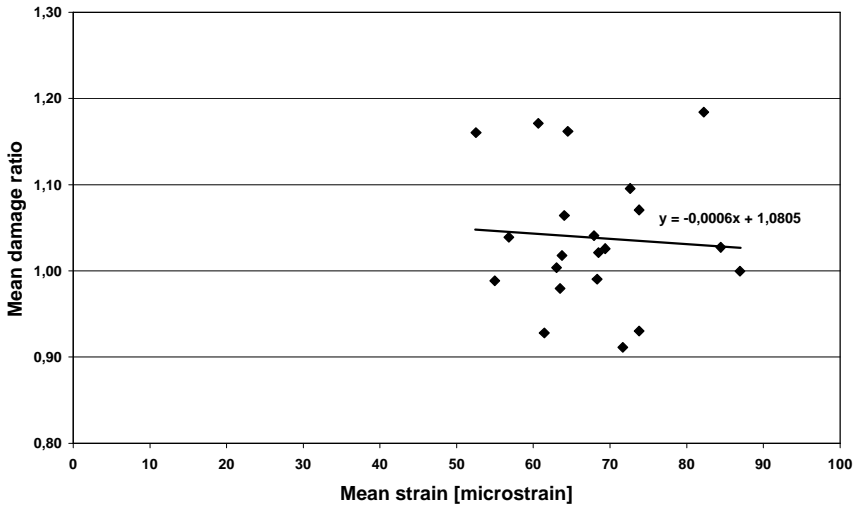
Figure 7.3. A scatter plot showing the relation of mean damage ratio and mean strain for each specimen.
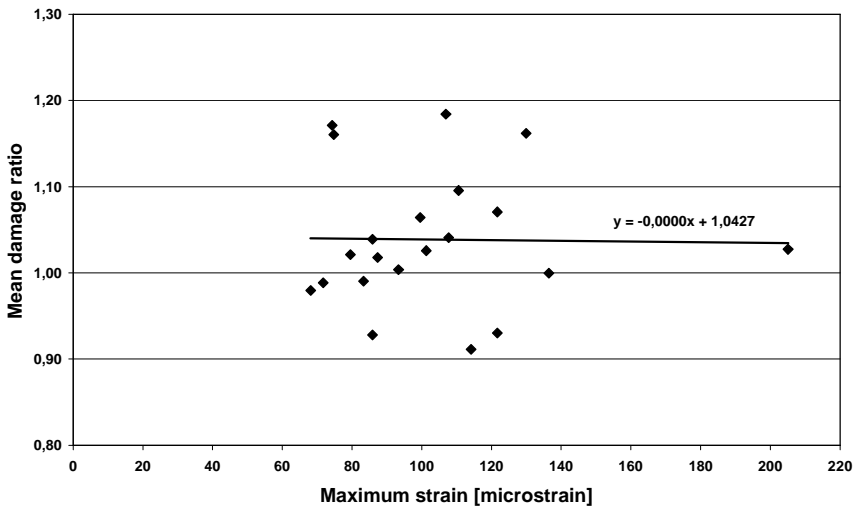
Figure 7.4. A scatter plot showing the relation of mean damage ratio and maximum strain for each specimen.

7.4   Results

The uniaxial and indirect tensile tests produced stresses and strains from which dynamic moduli were calculated according to Equations 3.7-3.9. Each specimen produced data from one load cell and four LVDTs or pin and core gauges, which resulted in a dynamic modulus at each temperature and frequency. The average dynamic moduli in each group of two or three specimens are presented in Table 7.1 to Table 7.4 along with their standard deviations. These were considered acceptably small except for the uniaxial test on gyratory compacted ABb mix specimens that also had a varying air void content. However, the deviating specimen could not be excluded as it had the correct air void content and the other two could not be excluded due to sample size considerations. Therefore, all three specimens were used.

Mastercurves were constructed by using dynamic modulus data and Equations 3.11 to 3.19. The constants of the sinusoidal equation were found by means of the Excel Solver function. Therefore, the sigmoidal extrapolation of test results should not be over-emphasized.

The mastercurves derived from the uniaxial test using gyratory compacted specimens (UNI GYR) were compared to those of the indirect tensile test using gyratory compacted specimens (IDT GYR), which in turn were compared to those of the indirect tensile test on specimens cored from the pavement (IDT COR). This comparison was carried out for each mix separately and enabled both test types and compaction methods to be evaluated. The performance of the mixes in each test set-up was also evaluated.

Table 7.1. Dynamic moduli and their standard deviations from each of the test set-ups using ABT wearing mix specimens.

T [°C]	f [Hz]	ABT IDT COR		ABT IDT GYR		ABT UNI GYR	
		Dynamic modulus IE*$_{av}$I [MPa]	Standard deviation s [MPa]	Dynamic modulus IE*$_{av}$I [MPa]	Standard deviation s [MPa]	Dynamic modulus IE*$_{av}$I [MPa]	Standard deviation s [MPa]
-10	25	17387	1071	17948	1602	26216	1841
-10	10	16136	1091	17268	1407	24955	1951
-10	5	15003	1299	16484	1305	23886	1880
-10	1	13331	1127	14705	1010	21427	1805
-10	0,5	12266	1040	13829	832	20240	1668
-10	0,1	10105	836	11816	508	17523	1395
5	25	9939	1122	11154	327	16853	1153
5	10	9585	839	9889	347	14964	683
5	5	8271	310	8933	347	13682	547
5	1	5953	162	6858	515	10711	301
5	0,5	4909	280	5968	618	9528	197
5	0,1	2955	282	4307	544	6963	54
20	25	4398	178	5209	669	8316	155
20	10	3408	92	4179	802	6823	5
20	5	2741	72	3604	634	5804	48
20	1	1610	94	2321	453	3770	186
20	0,5	1267	62	1909	388	3079	214
20	0,1	745	53	1189	240	1851	230
35	25	1009	111	1841	526	2861	119
35	10	750	98	1266	331	2031	140
35	5	649	94	1022	240	1565	142
35	1	483	66	632	168	850	113
35	0,5	N/A	N/A	544	143	656	97
35	0,1	N/A	N/A	449	112	388	66
55	25	N/A	N/A	N/A	N/A	708	94
55	10	N/A	N/A	N/A	N/A	505	69
55	5	N/A	N/A	N/A	N/A	400	87
55	1	N/A	N/A	N/A	N/A	287	86
55	0,5	N/A	N/A	N/A	N/A	260	90
55	0,1	N/A	N/A	N/A	N/A	227	96

Table 7.2. Dynamic moduli and their standard deviations from each of the test set-ups using ABb binder mix specimens.

T [°C]	f [Hz]	ABb IDT COR		ABb IDT GYR		ABb UNI GYR	
		Dynamic modulus IE*$_{av}$I [MPa]	Standard deviation s [MPa]	Dynamic modulus IE*$_{av}$I [MPa]	Standard deviation s [MPa]	Dynamic modulus IE*$_{av}$I [MPa]	Standard deviation s [MPa]
-10	25	16709	651	19090	1105	27019	5238
-10	10	16181	599	18459	985	25623	5422
-10	5	15567	517	17878	1116	24697	5315
-10	1	13753	367	16292	1159	22289	4864
-10	0,5	12933	331	15574	1130	21267	4742
-10	0,1	10845	166	13791	1174	18838	4234
5	25	10512	431	13795	1315	18779	2869
5	10	9179	257	12575	1268	17047	2561
5	5	8248	183	11625	1270	15791	2380
5	1	6126	185	9449	1172	12847	2057
5	0,5	5267	170	8491	1094	11700	1854
5	0,1	3531	187	6496	884	9260	1401
20	25	4828	605	7895	1009	10458	1007
20	10	3847	175	6583	875	8845	815
20	5	3091	213	5666	854	7698	717
20	1	1864	191	3949	496	5408	569
20	0,5	1525	154	3312	439	4595	522
20	0,1	881	97	2186	218	3036	428
35	25	1401	75	3369	431	4266	557
35	10	1150	177	2456	421	3281	483
35	5	731	44	1954	173	2679	409
35	1	551	N/A	1298	153	1617	287
35	0,5	N/A	N/A	1092	95	1306	259
35	0,1	N/A	N/A	770	33	812	206
55	25	N/A	N/A	N/A	N/A	1286	262
55	10	N/A	N/A	N/A	N/A	928	211
55	5	N/A	N/A	N/A	N/A	734	164
55	1	N/A	N/A	N/A	N/A	461	116
55	0,5	N/A	N/A	N/A	N/A	388	96
55	0,1	N/A	N/A	N/A	N/A	287	68

Table 7.3. Dynamic moduli and their standard deviations from each of the test set-ups using ABbm modified binder mix specimens.

T [°C]	f [Hz]	ABbm IDT COR		ABbm IDT GYR		ABbm UNI GYR	
		Dynamic modulus IE*$_{av}$I [MPa]	Standard deviation s [MPa]	Dynamic modulus IE*$_{av}$I [MPa]	Standard deviation s [MPa]	Dynamic modulus IE*$_{av}$I [MPa]	Standard deviation s [MPa]
-10	25	16933	909	12429	253	28921	1667
-10	10	16269	721	11760	221	27612	1600
-10	5	15729	708	11401	136	26607	1467
-10	1	14077	622	10248	12	24138	1304
-10	0,5	13340	596	9754	9	23074	1253
-10	0,1	11648	467	8556	141	20567	1119
5	25	10774	352	8370	46	20050	1382
5	10	9694	278	7539	2	18277	1292
5	5	8796	303	6921	10	16991	1301
5	1	6846	240	5477	53	14070	1124
5	0,5	6020	220	4898	77	12877	1093
5	0,1	4349	162	3722	67	10191	1011
20	25	5427	272	4608	497	11561	976
20	10	4450	205	3856	317	9696	837
20	5	3966	179	3420	310	8456	751
20	1	2672	74	2404	262	6035	621
20	0,5	2236	52	2065	261	5147	572
20	0,1	1467	9	1437	195	3490	497
35	25	1878	333	1992	202	4647	630
35	10	1686	309	1591	100	3664	554
35	5	1223	128	1461	123	3037	482
35	1	950	160	884	103	1863	345
35	0,5	783	91	843	68	1522	305
35	0,1	590	139	636	96	931	206
55	25	N/A	N/A	N/A	N/A	1454	303
55	10	N/A	N/A	N/A	N/A	1068	250
55	5	N/A	N/A	N/A	N/A	859	218
55	1	N/A	N/A	N/A	N/A	529	145
55	0,5	N/A	N/A	N/A	N/A	440	123
55	0,1	N/A	N/A	N/A	N/A	309	89

Table 7.4. Dynamic moduli and their standard deviations from each of the test set-ups using AG asphalt base mix specimens.

T [°C]	f [Hz]	AG IDT COR	
		Dynamic modulus IE*$_{av}$I [MPa]	Standard deviation s [MPa]
-10	25	14272	486
-10	10	13575	541
-10	5	12791	348
-10	1	10898	288
-10	0,5	10063	271
-10	0,1	7987	210
5	25	8263	142
5	10	7152	117
5	5	6373	180
5	1	4439	179
5	0,5	3709	192
5	0,1	2400	199
20	25	3496	182
20	10	2638	172
20	5	2144	173
20	1	1240	155
20	0,5	1025	145
20	0,1	604	121

7.4.1 Comparison of tests using each asphalt mix separately

ABT

The UNI GYR using ABT mix specimens showed higher dynamic moduli than the IDT GYR at medium and high reduced frequency, as shown in Figure 7.5. The dynamic moduli derived with the IDT COR are somewhat lower than the IDT GYR dynamic moduli at medium reduced frequency.
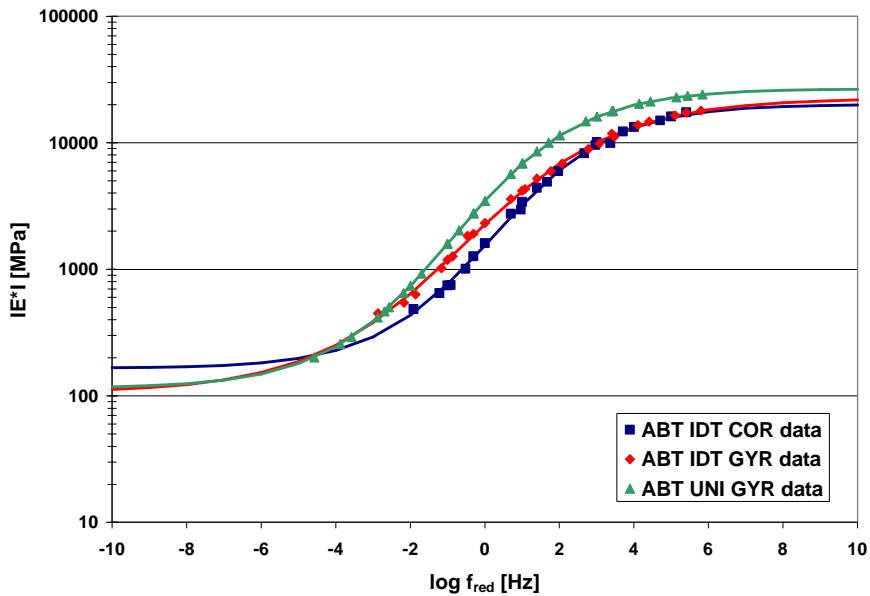
Figure 7.5. Mastercurves of the ABT mix type derived with the uniaxial test using gyratory compacted specimens, IDT using gyratory compacted specimens and IDT using pavement cores.

ABb

Testing using ABb mix specimens once again indicated that the UNI GYR dynamic moduli were higher than for the IDT GYR at medium and high reduced frequency, although similar at low reduced frequency. This is shown in Figure 7.6.

The dynamic moduli of the IDT GYR were higher than the IDT COR at low and medium reduced frequency. However, comparison is difficult as the air void difference between the compared groups was approximately 2%. The air void content can significantly affect stiffness, as shown by Nilsson (2001B). Nevertheless, the dynamic modulus difference decreased at high reduced frequency.
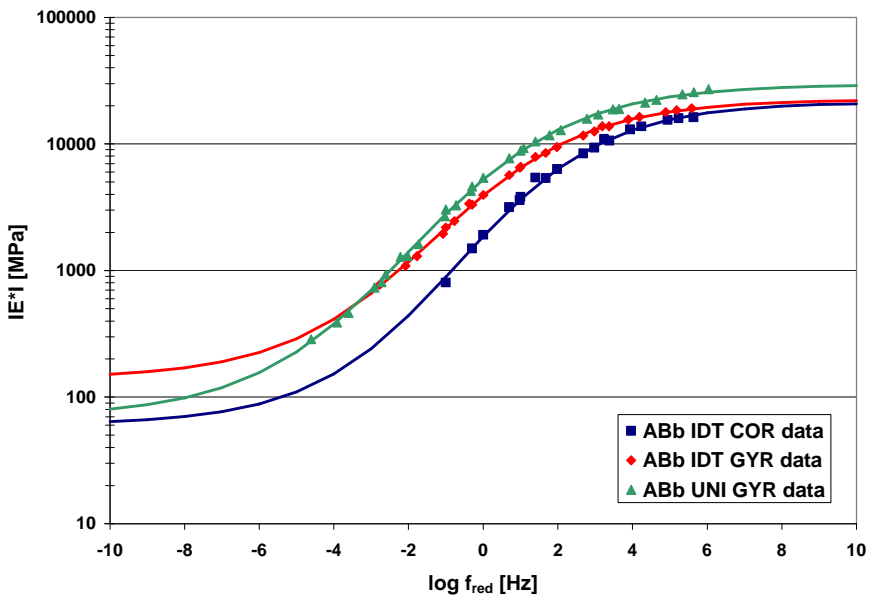
Figure 7.6. Mastercurves of the ABb mix type derived with the uniaxial test using gyratory compacted specimens, IDT using gyratory compacted specimens and IDT using pavement cores.

ABbm

The UNI GYR using polymer modified ABbm mix specimens showed higher dynamic moduli than the IDT GYR at medium and high reduced frequency as shown in Figure 7.7. This can be due to the approximately 2 % lower air void content in the UNI GYR specimens compared to IDT GYR specimens. Nilsson (2001B) also showed that the air void content can have this effect on stiffness. However, the UNI GYR strength decreased drastically at low reduced frequency.

The IDT COR and the IDT GYR showed identical dynamic moduli except at high reduced frequency, where there was a limited difference.
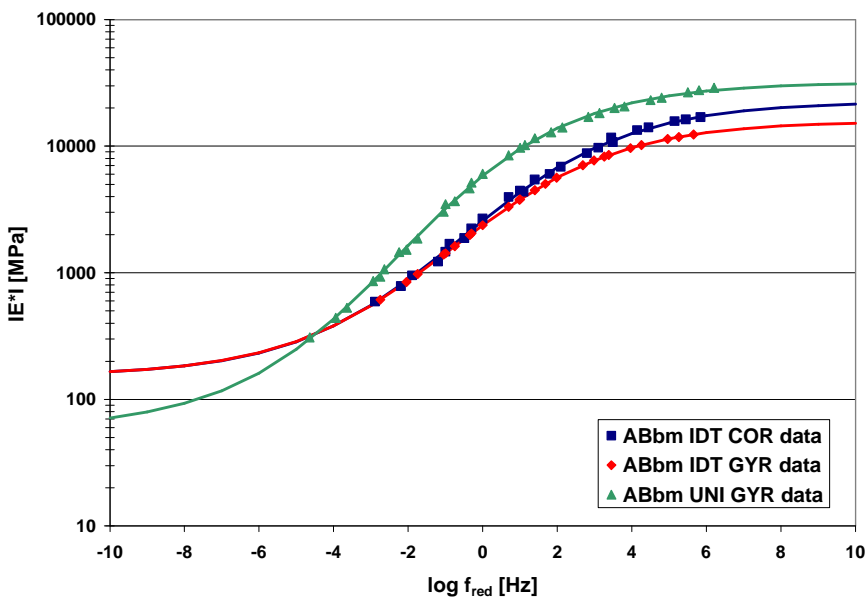
Figure 7.7. Mastercurves of the ABbm mix type derived with the uniaxial test using gyratory compacted specimens, IDT using gyratory compacted specimens and IDT using pavement cores.

7.4.2 Comparison of mix properties

Uniaxial test on gyratory compacted specimens
The results from this test showed that the stiffness of the conventional and modified binder mixes, ABb and ABbm, were practically identical, as shown in Figure 7.8. This was not expected as the bitumen of the modified mix was considerably stiffer than the conventional mix, as shown in Figure 7.8. As expected, the bitumen rich and fine-graded ABT mix is less stiff than the binder mixes, especially at middle and low reduced frequency.
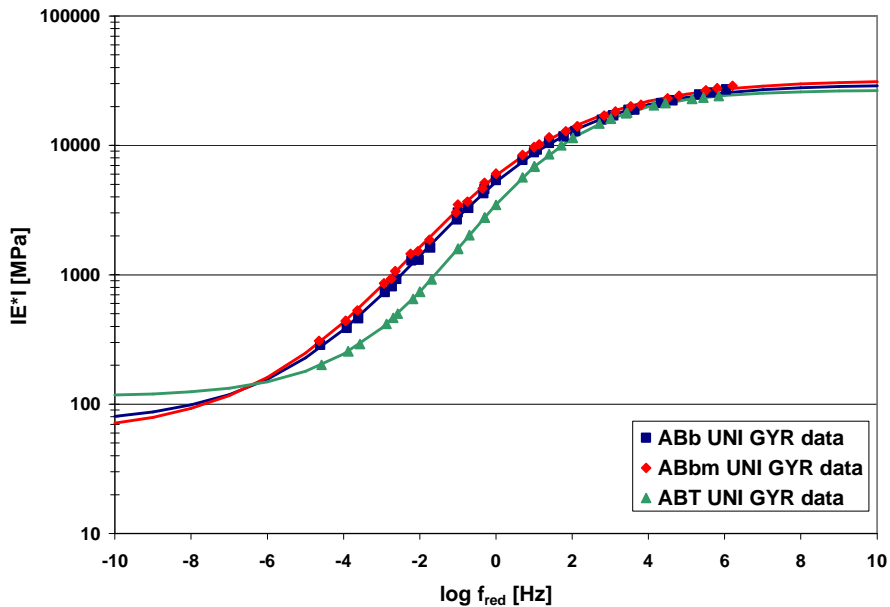
Figure 7.8. Mastercurves of the ABb, the modified ABbm and the ABT mix types derived with the uniaxial test using gyratory compacted specimens.

Indirect tensile test on gyratory compacted specimens

The conventional ABb binder mix showed higher stiffness than the modified ABbm in spite of the higher viscosity of the polymer modified bitumen compared with the conventional mix, as shown in Figure 7.9. However, the mean air void difference due to over-compaction of ABb specimens was 2.4 % and the corresponding value due to under-compaction of the ABbm specimens was 1.3 %, which results in a total air void difference of 3.7 %. This was unacceptable and the absolute stiffness of the specimen groups should therefore not be compared. Nonetheless, even though the ABbm mix was less stiff than the ABb mix, it exhibited a lower susceptibility to changes in temperature and frequency.

Furthermore, even though the air void content of the ABT mix specimens matched the test pavement, its absolute stiffness should not be compared with the other mix types due to compaction problems.
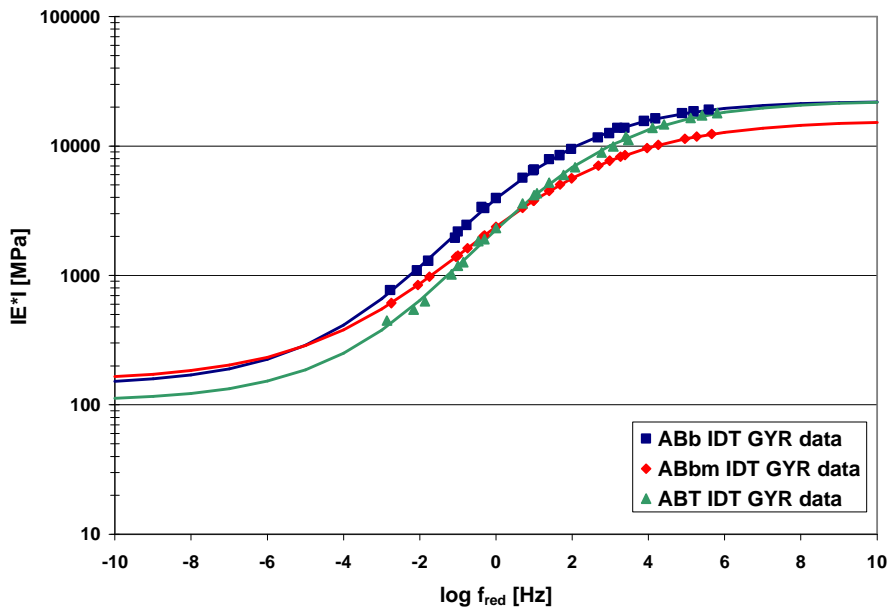
Figure 7.9. Mastercurves of the ABb, the modified ABbm and the ABT mix types derived with the indirect tensile test using gyratory compacted specimens.

Indirect tensile test on cored specimens

It was observed that the polymer modified ABbm had higher dynamic moduli than the unmodified ABb, especially at low reduced frequency, as shown in Figure 7.10. This means that the polymer modified mix is more resistant to permanent deformation. It is also in agreement with the binder properties of the ABb with the ABbm mix types, as shown in Table 8.8. The ABT was surprisingly stiff at low frequency in spite of its fine gradation compared to the coarse ABb mix. The low overall dynamic moduli of the AG mix specimens were also observed.
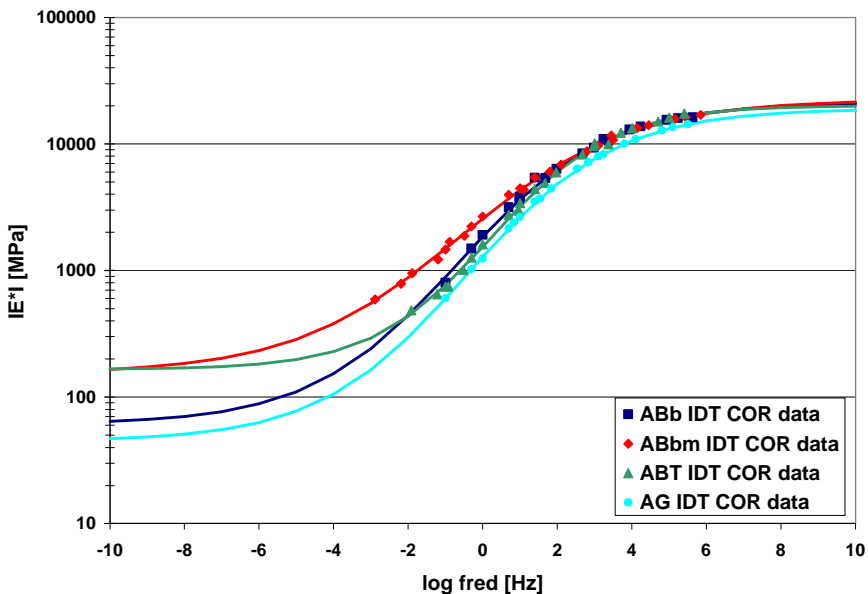
Figure 7.10. Mastercurves of the ABb, the modified ABb, the ABT and the AG mix types derived with the indirect tensile test using pavement cores.

7.4.3 Discussion

Comparison of tests using each asphalt mix separately

At high reduced frequency, the uniaxial test on gyratory compacted specimens generally showed substantially higher moduli than the indirect tensile test on gyratory compacted specimens, as shown in Figure 7.5 to Figure 7.7. However, at low reduced frequency, the difference was small. This indicates that the two test set-ups produce dynamic moduli with different dependency on frequency and temperature. This result was not in compliance with the findings of Kim et al. (2004), who reported that dynamic modulus data can be obtained with the indirect tensile test instead of with the uniaxial test. Their analytical solution employed linear viscoelasticity to transform specimen deformation into comparable dynamic moduli derived

from the uniaxial compressive test and verified it with tests on twelve mixes, of which six are reproduced in Figure 7.11.
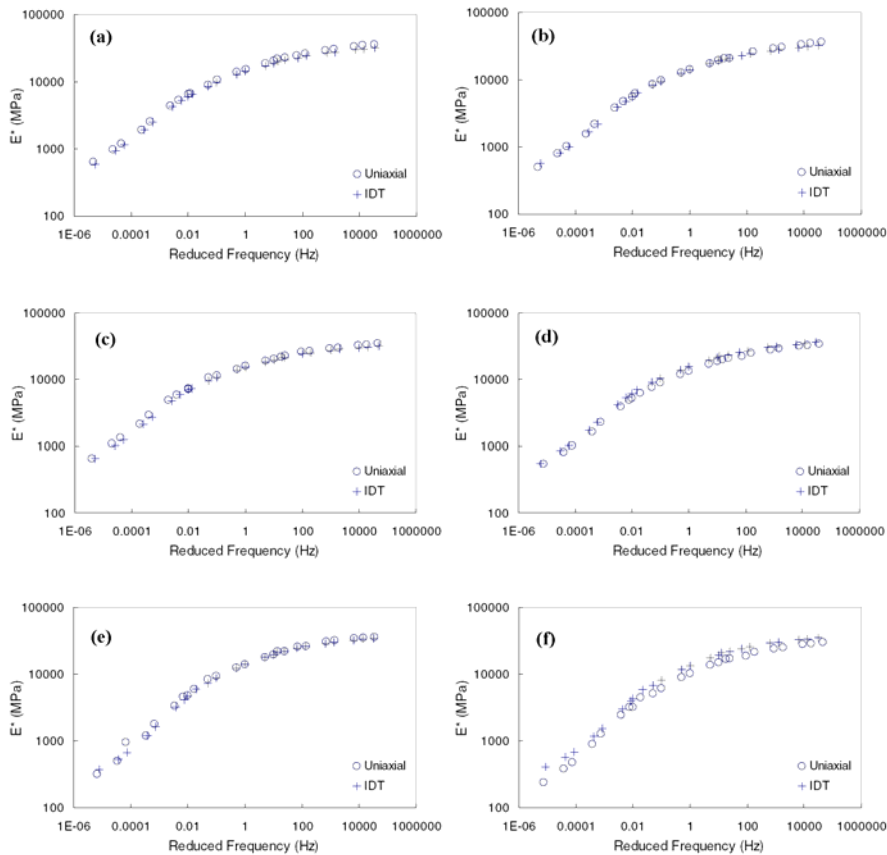
Figure 7.11. Mastercurves by Kim (2004) from the uniaxial test and the indirect tensile test using gyratory compacted specimens of selected mixes: (a) fine 12.5 mm wearing layer mix (b) coarse 12.5 mm wearing layer mix (c) fine 19.0 mm intermediate layer mix (d) coarse 19.0 mm intermediate mix (e) fine 25.0 mm base layer mix (f) coarse 25.0 mm base layer mix.

However, the discrepancy between the indirect tensile test and the uniaxial test in this work can be explained by a number of plausible reasons. One is the observed uneven air void distribution of the uniaxial specimens due to gyratory compaction, as reported in Chapter 6. The deviation of only using lubrication on the top end of the specimens was also likely to affect the results. However, none of these factors were further investigated and the uniaxial test results should therefore not be over-emphasized. This conclusion is reinforced by the unexpected similarity between the mastercurves of the conventional and modified binder mixes, derived with

the uniaxial test on gyratory compacted specimens, despite the known differences in bitumen viscosity.

The indirect tensile test generally produced similar dynamic moduli independently of compaction method, as shown in Figure 7.5 and Figure 7.7. Due to unintentional variations in specimen compaction densities, stiffness was affected, which complicated comparison, as shown in Figure 7.6. Decrease in stiffness due to high air void content was reported by Nilsson, (2001B).

The recommended dynamic modulus test within the M-E PDG concept is the uniaxial test on gyratory compacted specimens that allows pavements not yet constructed to be evaluated. However, the objective in this work was to evaluate the existing HVS test pavement from which asphalt concrete specimens could be obtained. Due to the indications of deficiencies that were reported in this study, dynamic modulus data from uniaxial testing on gyratory compacted specimens proved to be unsuitable. In order to obtain any reliable data, it was assumed that the uniaxial test can be replaced by the indirect tensile test as suggested by Kim et al. (2004). Gyratory compaction can experience difficulties in imitating pavement core properties regarding air void content, particle orientation and mechanical properties (Airey et al., 2006), and cores from the actual pavement are always the most representative specimens. The indirect tensile test on cored specimens was therefore selected to provide the input data for the M-E PDG software.

Comparison of mix properties
The uniaxial test on gyratory compacted specimens produced identical mastercurves using the ABb and ABbm mixes, followed by the ABT mix. The polymer modified bitumen had considerably higher stiffness than the conventional mix. Therefore, it was expected that the ABbm mix would be stiffer than the ABb mix. However, the uneven specimen air void distribution and lack of lubrication weakens the reliability of the uniaxial test results. Further, the ranking derived with the IDT on gyratory compacted specimens was not reliable due to large air void differences. However, the indirect tensile test on cored specimens was reliable and resulted in the following stiffness ranking: ABbm, ABb, ABT, AG. The polymer modified ABbm was especially stiff at high temperature and low frequency. These results also correlate with expected stiffness based on the properties and proportions of bitumen and aggregates.

7.5 Conclusions

Dynamic modulus testing at reasonable strain levels caused an average 4% reduction of dynamic modulus, based on results during and after testing. It should be noted that dynamic modulus testing is considered nondestructive. However, specimens tested at unintentionally high strain levels did not appear more damaged than those in which less strain were induced.

Mastercurves derived with the uniaxial test and the indirect tensile test using gyratory compacted specimens were not similar, contrary to expectation. Foremost, they appeared to have different dependency on time and temperature. However, it is likely that the discrepancy was due to problems with the gyratory compaction and dynamic modulus testing of the uniaxial specimens. Mastercurves derived with the indirect tensile test using gyratory compacted and cored specimens were similar in this investigation. However, in those cases where the air void content differed between groups, no conclusions could be drawn.

Based on the results of the three test types, the IDT on cored specimens were considered the most representative. Mastercurves from this test set-up was used to evaluate the ABT, ABb, polymer modified ABbm and AG mix types. The general mix stiffness ranking, beginning with the stiffest, was ABbm, ABb, ABT, AG. The polymer modified ABbm was especially stiff at high temperature and low frequency, as expected.

8 SIMULATION OF PERMANENT DEFORMATIONS

The growth of permanent deformations was performed using the Mechanistic-Empirical Pavement Design Guide (M-E PDG) v0.910 software. A detailed model description can be found in Chapter 3.8. The conditions of the HVS test constituted the software input, as described in Chapter 5.

The first M-E PDG simulation was carried out using no field calibration factors, which is called the National calibration option in the software. The model results were evaluated and compared with the HVS test results. After that, field calibration factors were assessed using the Regional calibration option. Field calibration factors that adjusted the model to HVS test results were found and discussed.

8.1 Input data

The essential input data for the M-E PDG consists of traffic and climate data as well as structural and material properties. These parameters were derived from the Heavy Vehicle Simulator (HVS) test and laboratory tests of materials and were occasionally assumed. Data from the HVS test was recorded using SI units and converted into U.S. customary units to fit the M-E PDG software. Only Level 1 input data was used, except for the unbound materials and the Poisson's ratio of the asphalt concrete, which were both defined at Level 2. This was because the models were not yet comprehensive enough to benefit from Level 1 input data. However, the software appears to accept the Poisson's ratio at Level 2 using the Level 1 option. In conclusion, all input data was of the highest applicable level.

The HVS test temperature was changed twice during loading breaks as described in Chapter 5.1. The temperature was allowed to stabilize before the loading continued as shown in Figure 8.1. In addition, a technical problem was experienced that delayed the HVS test on one occasion. These scenarios cannot be accurately characterized within the software as it uses a continuous traffic flow and a climate model that needs time to reach from the surface down to the deep asphalt concrete layers.

Consequently, the model climate change had to take place during loading. In order to decrease the impact of the error, the intense and irregular HVS loading sequences were translated into fewer daily loadings over a longer period of simulation. This is possible since the M-E PDG model does not take viscoelastic effects on permanent deformation into account. However, the M-E PDG software includes an ageing model that slightly increases the asphalt concrete stiffness as time passes. The ageing function cannot be turned off, which implies that the model should use the same simulation time as HVS, in order not to cause any difference. This means that either the temperature change error or the ageing error could be taken into

consideration, but not both at the same time. The temperature was considered to be a more important factor than ageing. Therefore, a simulation time of approximately five years and 300 loadings per day was assumed reasonable.
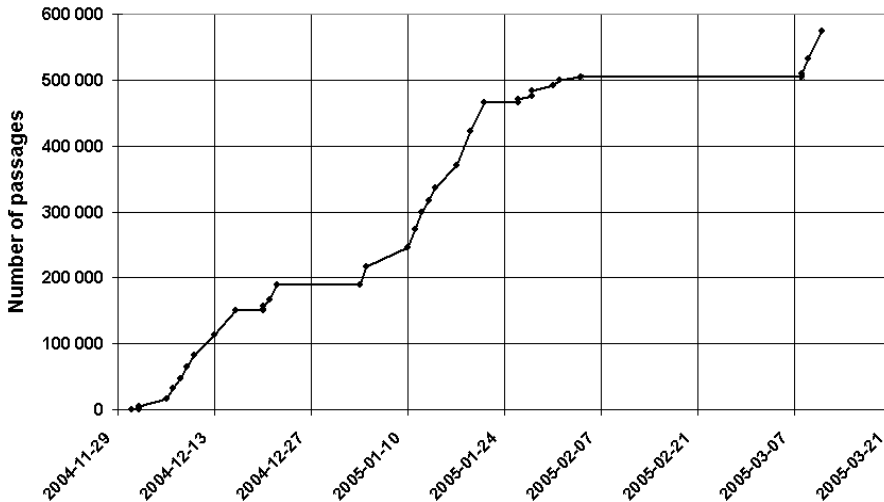
Figure 8.1. The number of passages as a function of time during the HVS testing.

Another mitigation of the HVS test temperature change error was the use of the highest allowable thermal conductivity and the lowest allowable heat capacity for all materials. Adjustment of the material thermal properties did not result in any additional errors as the HVS test climate was controlled.

8.1.1 Traffic

The traffic settings were adjusted to simulate the HVS test conditions as closely as possible. The M-E PDG traffic section supports a special axle configuration for the purpose of simulating accelerated loading testing. However, the feature did not support input of the HVS loading speed, which made the conventional traffic option necessary. It was determined that 300 daily axle loads should be used in order to decrease the temperature change error, as discussed earlier. This was translated into a daily two-way traffic of 300 heavy vehicles with two single axles per vehicle.

The relevant input parameters values were set according to Table 8.1 while input parameters that should not affect the simulation were not taken into consideration. The HVS loading was characterized by single axle heavy vehicles with axle loads twice as high as the 60 kN HVS half-axle load. In order not to model possible edge effects that were not present during the HVS test, the mean wheel location from the lane marking and design lane width were given the maximum allowed values of 72 inches and 15 feet, respectively. The combination effect of the two modeled half-axles, which did

not exist in the HVS test, was also minimized by using the highest permitted average outside axle width, i.e. 20 feet. It should also be noted that the HVS used super single tires and that M-E PDG only use dual tire axles. Setting the dual tire center-to-center distance to zero solved this problem.

Table 8.1 The traffic input data.

Initial two-way AADTT	300
No. of lanes in design direction	1
Percent trucks in design direction	50
Percent trucks in design lane	100
Operational speed [mph]	7.46
Vehicle class distribution	100 % Vehicle class 5 (2 single axles)
Traffic growth factors	No growth
Axle load distribution factors	100% at 27000 lb for single axles
Mean wheel location from the lane marking [in]*	72
Traffic wander standard deviation [in]	4.84
Design lane width [ft]	15
Number of axles/trucks	Vehicle class 5: 2 single axles
Average outside axle width [ft]	20
Dual tire spacing [in]	0
Tire pressure [psi]	131

8.1.2   Climate

The climate was taken into account by producing Integrated Climate Model (ICM) input files to simulate HVS conditions. All climate input data is summarized in Table 8.2. The number of HVS loadings at each test temperature and the model assumption of 300 daily loadings were used to calculate the model number of days at each temperature. Factors such as precipitation, average relative humidity, wind speed, sunshine, and ground water had no impact on the climate controlled HVS test. The only climate assumption was the 50% average relative humidity, which does not affect permanent deformation results in this work.

Table 8.2. The climate input data.

Start date and end date [YYYY-MM-DD]	1997-01-01 to 2002-04-06
Annual water depth [ft]	100
Average relative humidity	50 %
Temperature	50 °F between 1997-01-01 and 1998-05-25 68 °F between 1998-05-26 and 2001-04-10 86 °F between 2001-04-11 and 2002-04-06
Precipitation	0
Wind speed	0
Percent sunshine	0
Hourly ground water depth [ft]	100

8.1.3   Structure and materials

The standard and enhanced structures were defined using the geometry and materials used in the HVS test. All layers from the surface to the bedrock must be defined before simulation. However, the software limits the number of sublayers in each construction. Therefore, it was necessary to simulate a 30-inch bottom fine sand layer instead of the 98-inch layer used in the HVS construction. The layer thickness data for both AC structures is shown in Table 8.3.

Table 8.3. The layer thickness input data.

	Standard AC structure [in]	Enhanced AC structure [in]
ABT wearing layer	1.38	1.54
ABB binder layer	3.23	0.00
ABbm modified binder layer	0.00	3.31
AG asphalt base layer	3.19	3.11
Crushed stone	7.80	7.80
Fine sand: A-1-a	30	30
Massive and continuous bedrock	∞	∞

It was determined that the dynamic modulus data derived from the indirect tensile test on cored pavement specimens should be used as discussed in Chapter 7. The M-E PDG software requires dynamic modulus data from testing at temperatures up to at least 125 °F, which is approximately 52 °C. However, the pavement cores could not be tested at higher temperatures than 35 °C due to excessive permanent deformation. The problem was solved by using idealized mastercurve data derived from the sigmoidal function. The error due to this deviation should not be significant as the time-temperature principle was assumed valid. The same assumption and the same temperature interval were used by Kim et al. (2004) as support for the analytical linear viscoelastic solution that allows dynamic modulus determination using the indirect tensile test. The dynamic modulus data for all asphalt mixes are presented in Table 8.4 to Table 8.7.

Table 8.4. The dynamic modulus [psi] input data of the ABT wearing mix.

Temperature [°F]	Frequency [Hz]					
	0.1	0.5	1	5	10	25
14	1412000	1774000	1917000	2202000	2304000	2421000
41	457000	726000	867000	1230000	1393000	1605000
68	111000	179000	224000	375000	466000	610000
95	44000	57000	65000	97000	117000	154000
131	28000	30000	31000	35000	38000	43000

Table 8.5. The dynamic modulus [psi] input data of the ABb conventional binder mix.

Temperature [°F]	Frequency [Hz]					
	0.1	0.5	1	5	10	25
14	1511000	1835000	1964000	2231000	2331000	2449000
41	523000	784000	914000	1241000	1387000	1578000
68	129000	216000	269000	436000	529000	671000
95	40000	62000	75000	124000	155000	208000
131	17000	21000	24000	33000	39000	49000

Table 8.6. The dynamic modulus [psi] input data of the ABbm modified binder mix.

Temperature [°F]	Frequency [Hz]					
	0.1	0.5	1	5	10	25
14	1598000	1892000	2011000	2264000	2362000	2481000
41	660000	905000	1023000	1316000	1446000	1619000
68	216000	317000	374000	541000	628000	758000
95	84000	116000	135000	195000	229000	286000
131	40000	48000	53000	67000	76000	90000

Table 8.7. The dynamic modulus [psi] input data of the AG asphalt base mix.

Temperature [°F]	Frequency [Hz]					
	0.1	0.5	1	5	10	25
14	1161000	1462000	1586000	1850000	1951000	2072000
41	344000	541000	644000	918000	1046000	1218000
68	87000	148000	186000	311000	382000	495000
95	31000	48000	59000	99000	124000	168000
131	14000	19000	21000	31000	38000	49000

In addition to dynamic modulus data, general mix and bitumen properties was determined by means of conventional laboratory tests on pavement cores carried out by the Swedish National Road and Transport Research Institute (VTI) and bitumen testing by Skanska. The results are presented in Table 8.8. All asphalt mixes were characterized with the highest allowable thermal conductivity and the lowest allowable heat capacity in order to decrease the error of temperature shifts during loading, as discussed earlier. The commonly used Poisson's ratio of 0.35 was assumed.

Table 8.8. The bitumen and general asphalt mix input data.

	ABT	ABb	ABbm	AG
Bitumen softening point at 13000 P [°F]	117	117	144	101
Bitumen absolute viscosity at 140 °F [P]	1750	1750	14000	601
Bitumen kinematic viscosity at 275 °F [cS]	377	377	860	202
Bitumen specific gravity at 77 °F	1.02	1.02	1.02	1.02
Bitumen penetration at 77 °F [dmm]	85	85	60	190
Bitumen Brookfield viscosity [cP]	N/A	N/A	N/A	N/A
Mix reference temperature [°F]	68	68	68	68
Mix effective binder content [%]	6.5	5.0	5.0	4.5
Mix air voids [%]	4.34	6.77	6.75	7.88
Mix total unit weight [pcf]	146	147	145	147
Mix thermal conductivity [BTU/hr-ft-°F]	1	1	1	1
Mix heat capacity [BTU/lb-°F]	0.1	0.1	0.1	0.1
Mix Poisson's ratio	0.35	0.35	0.35	0.35

The properties of the unbound materials in Table 8.9 were assessed using the PMS Objekt (2005) summer/autumn moduli for crushed stone, coarse soil, and bedrock. The coefficient of lateral pressure was given the standard estimation 0.66.

Table 8.9. The unbound materials input data.

	Poisson's Ratio	K_0	E [Mpsi]
Crushed stone	0.35	0.66	65000
A-6	0.35	0.66	14500
Massive and continuous bedrock	0.35	-	750 000

8.2   Results

8.2.1   Simulation using no field calibration factors

The M-E PDG software simulation was carried out using no field calibration factors, i.e. $\beta r_1 = \beta r_2 = \beta_{r3} = 1$, which is called the National calibration option. The shapes of the model and HVS test rut depth graphs were similar and the model rut depth was approximately 2/3 of the HVS rut depth, as shown in Figure 8.2. The model correlation of each layer was also evaluated. The model showed good correlation regarding the wear layer and the binder layer. The model's results for the asphalt base layer were compared with the measured permanent deformation of the asphalt base. It should be noted that the HVS test measurements were probably underestimated, as discussed in Chapter 5.4.3. The model's results for the asphalt base layer were much lower than the conservative HVS assessment, which implies that the model seriously underestimated the permanent deformation of the asphalt base layer.

Figure 8.2 Permanent deformation in each layer of the HVS test standard AC structure and the M-E PDG model using the National calibration option.

The correlation between total rut depth from the model and HVS test results from the enhanced AC structure was good, as can be seen from Figure 8.3. However, the total rut depth was overestimated during the first phase at +10 °C and underestimated during the +20 °C and +30 °C phases. The evaluation focused on the second and third phases as the first probably consists mainly of post-compaction, which is not directly addressed in the M-E PDG methodology. During the second and third phases, the model value is approximately 4/5 of the HVS test value.

Evaluation of each layer showed that the model and HVS test results in the wear layer and binder layer correlated well. However, the model seriously underestimated the permanent deformation of the asphalt base layer.

Model results from the binder layers of the standard and enhanced AC structures in Figure 8.2 and Figure 8.3 were also compared. The permanent deformation in the standard structure was almost two times larger than in the modified binder layer of the enhanced structure. A certain difference was expected as the modified binder mix had significantly higher dynamic modulus than the conventional mix, especially at low frequency and high temperature.

Figure 8.3. Permanent deformation in each layer of the HVS test enhanced AC structure and the M-E PDG model using the National calibration option.

8.2.2   Simulation using field calibration factors

In order to adjust the model total rut depth to fit HVS test results, the Regional calibration option was used. Field calibration factors were assessed using a trial-and-error procedure based on graph evaluation. The influence of the calibration factors is explained in the M-E PDG constitutive relationship:

$$\frac{\boldsymbol{e}_p}{\boldsymbol{e}_r} = k_1 a_1 \boldsymbol{b}_{r1} T^{a_2 \boldsymbol{b}_{r2}} N^{a_3 \boldsymbol{b}_{r3}}$$

The first step was to assess the temperature calibration factor, β_{r2}. The distinct impact of temperature changes on permanent deformation in the HVS test provided valuable information about the temperature susceptibility. β_{r2} was adjusted until the inclination of the model and HVS test graphs matched at the temperature change points. The factor for the number of loadings, β_{r3}, was then estimated by converging the principal appearances of the graphs. Finally, the general calibration factor, β_{r1}, was assessed by fitting the curves together. The procedure was repeated until the total model rut depth graphically corresponded to the total rut depth of the HVS test. The resulting field calibration factors are shown in Table 8.10.

The assessed field calibration factors of the standard and the enhanced AC structures showed similar tendencies. The temperature susceptibility of the model was increased substantially. This was balanced by a decrease in the impact of the number of loadings and the general calibration factor.

Table 8.10. Assessment of field calibration factors.

	Standard structure	Enhanced structure
b_{r1}	0.30	0.50
b_{r2}	1.50	1.45
b_{r3}	0.70	0.60

The development of permanent deformation using new calibration factors is presented graphically in Figure 8.4 and Figure 8.5. It was noted that the total permanent deformation was overestimated at 10 °C. This can possibly be attributed to post-compaction that is difficult to model due to its low magnitude. Once again, the model seriously underestimated the permanent deformation in the asphalt base layer.
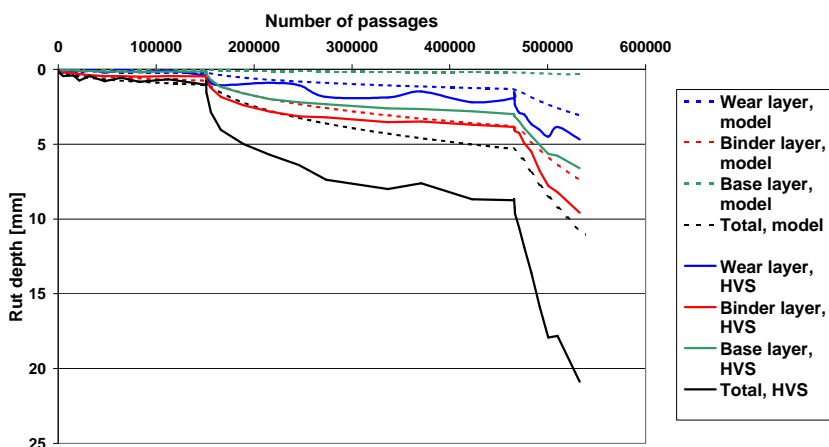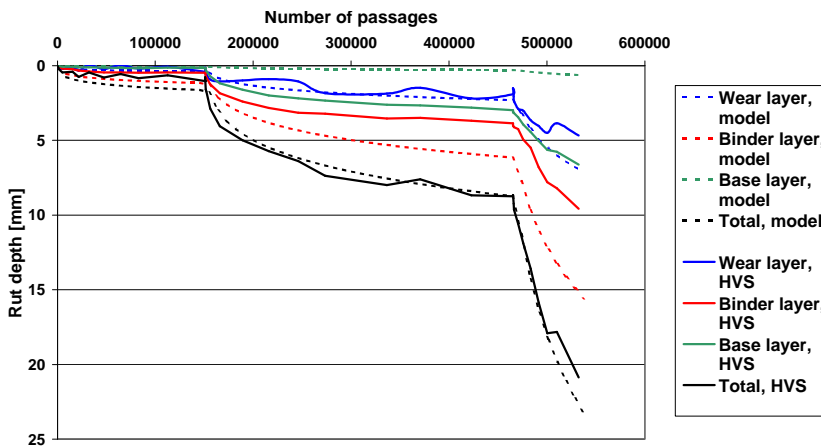

Figure 8.4. Permanent deformation in each layer of the HVS test standard AC structure and the M-E PDG model using the Regional calibration option.
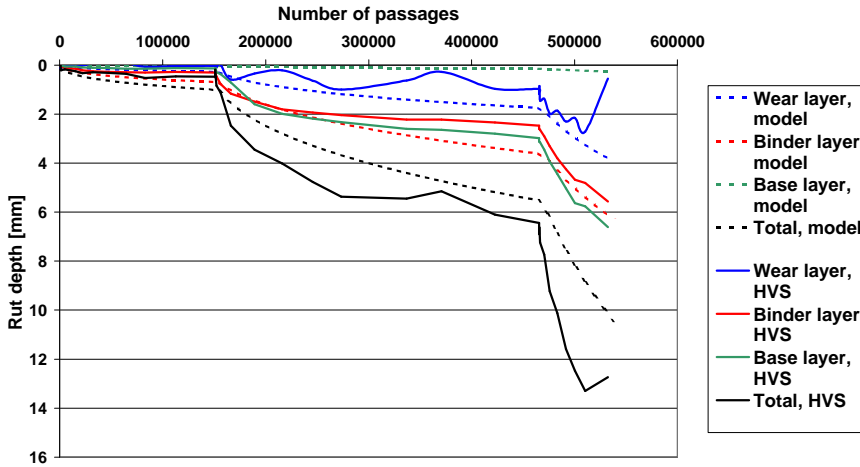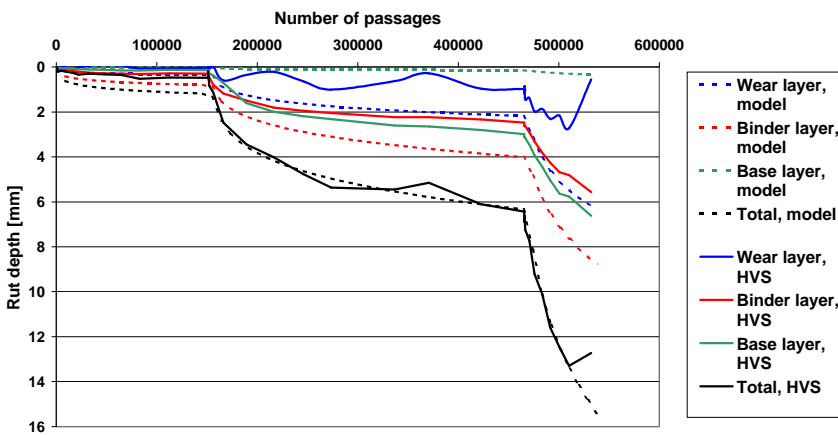

Figure 8.5. Permanent deformation in each layer of the HVS test enhanced AC structure and the M-E PDG model using the Regional calibration option.

8.2.3   Discussion

The analysis showed that the M-E PDG model can be used for prediction of permanent deformations in the AC layers of a flexible pavement. Simulation without calibration factors resulted in an underestimation of the rutting in the HVS test sections.

A significant variation can be expected when comparing observed and predicted rut depths. This is illustrated in Figure 8.6, which shows the predicted and measured rut depths of the sections that the M-E PDG flow rutting model was based on (NCHRP, 2004). Agardh and Busch (2006) employed an early, simplified version of the M-E PDG constitutive equation and adjusted the model to fit rut depths from accelerated loading testing on five full-scale asphalt pavements. Model adjustment provided a set of parameters for each section. The parameters showed a variation of more than a factor of 10 between the different test sections (Agardh and Busch, 2006).

The model to observation variation can be seen as a measure of the mechanistic and empirical proportions of the model. In order to reduce the variation, the mechanistic part of the model should be further developed. This would increase model accuracy and decrease the need for empirical considerations.
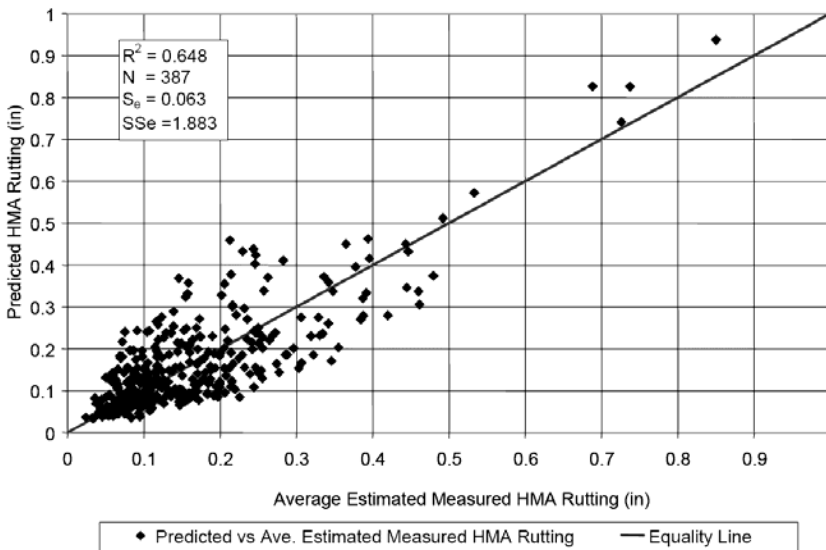
Figure 8.6. Nationally calibrated predicted versus estimated measured asphalt rutting (NCHRP, 2004).

However, in order to adjust the total rut depth of the current model to the regionally observed rut depths, the assessment and use of regional field calibration factors is recommended (NCHRP, 2004). The variation within

each region is expected to be reasonable due to regionally typical construction types, materials and climate. Guidelines for field calibration assessment are being developed within the NCHRP project 1-40B.

In this study, the M-E PDG model clearly underestimated the permanent deformation of the AG asphalt base layer. However, the model was calibrated using a trench study on seven MnRoad sections and their average permanent deformation as a function of depth. In order to incorporate the observations from the MnRoad trench studies into the model, the M-E PDG constitutive equation was adjusted with the empirical depth dependent "confining pressure" factor k_1:

$$k_1 = (C_1 + C_2 * depth) * 0.328196^{depth}$$

$$C_1 = -0.1039 * h_{ac}^2 + 2.4868 * h_{ac} - 17.342$$
$$C_2 = 0.0172 * h_{ac}^2 - 1.7331 * h_{ac} + 27.428$$

where

k_1 Variable confining pressure factor
h_{ac} Total thickness of all asphalt layers

After the incorporation of the k_1 factor, the contribution of each MnRoad asphalt concrete layer was accurately described by the model, as shown in Figure 8.7.
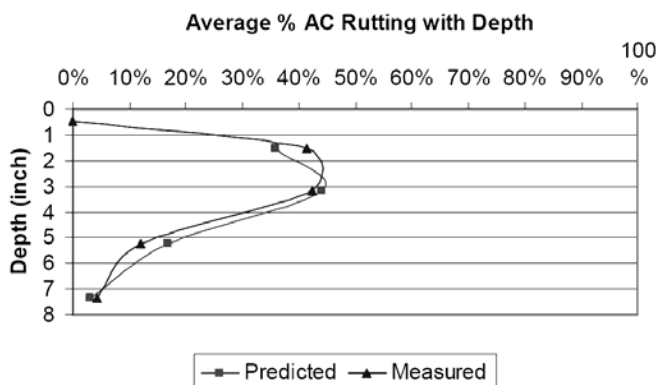
Figure 8.7. Average Percentage Asphalt Rut Depth in the MnRoad trench study (NCHRP, 2004).

A comprehensive mechanistic analysis needs only small adjustments with empirical factors to match observations In this case, the depth variation of k_1 is quite large as can be seen in Figure 8.8. It should be noted that the average

value of k_1 is 1. The result of calibration of AC layer contribution is that the model's permanent deformation in the binder layer increases at the expense of the wear layer and especially the asphalt base layer. In this study, the model's permanent deformation of the asphalt base layers located at 130-220 mm depth seriously underestimated that of the HVS test structures. Hypothetically, if trench data from the two HVS sections in this study had been used to assess k_1, it would have been more constant with depth.

It can also be noted that the current k_1 graph appearance resembles the elastic strain graph found by Eisenmann and Hilmer (1987) using elastic multi-layer simulations, as shown in Figure 3.10 and Figure 3.11. However, this consideration is already included in the mechanistic part of the M-E PDG concept and should therefore not be taken into account again in the empirical part.
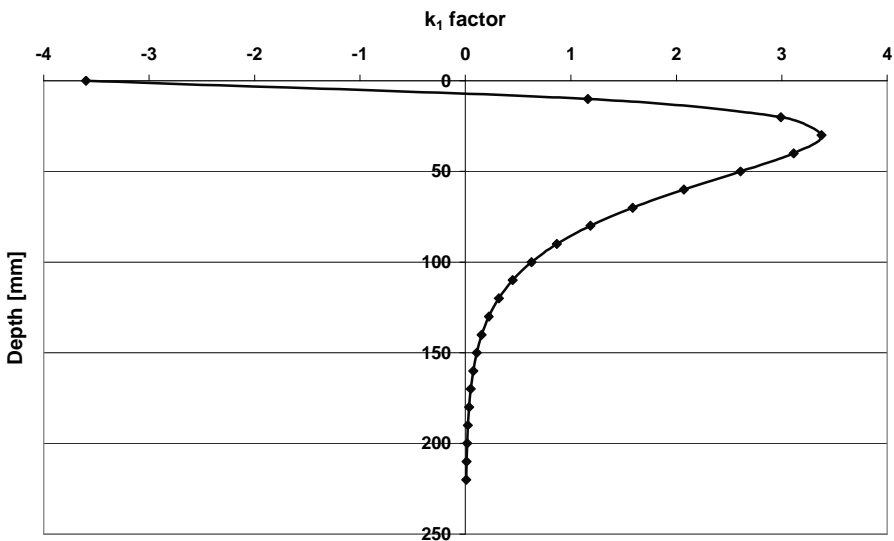
Figure 8.8. The k_1 factor as a function of depth in a 220 mm thick asphalt concrete structure.

As the contribution of each layer to total rut depth was not correctly assessed by the model, the variable confining pressure factor k_1 should be reassessed. This should be based on further trench data derived from an extensive range and number of pavement sections. The need for further trench studies was also recognized and emphasized by the M-E PDG developers NCHRP (2004) as well as in an independent concept review by NCHRP (2006A).

8.3   Conclusions

Simulation using the uncalibrated model underestimated the flow rutting for both asphalt concrete structures. However, the field calibrated model was able to describe the development of total AC rut depth well in this investigation. The field calibration factors that were found increased the temperature susceptibility of the model and decreased dependency on the number of loadings.

The contribution of each layer to total rut depth was not correctly assessed by the field calibrated M-E PDG model. Most importantly, the permanent deformation of the AG asphalt base layer was seriously underestimated. One reason for this may be that the current model is based on a trench study that includes only seven pavement sections at MnRoad.

CONCLUSIONS

9 CONCLUSIONS

The work was carried out in four distinct stages. These were analysis of Heavy Vehicle Simulator (HVS) test results, specimen fabrication, laboratory testing, and modeling of permanent deformation in the asphalt layers using the Mechanistic-Empirical Pavement Design Guide (M-E PDG) v0.910 software.

HVS testing

HVS testing showed that polymer modification of the binder layer reduced flow rutting in a conventional 220 mm asphalt concrete structure to approximately two thirds, as measured with EMU coils. The corresponding result from measurement on a single core was approximately one third. Further, the polymer modification also increased the load distribution capability, as shown with soil pressure cells. However, the permanent deformation of the unbound layers was not significantly affected in this investigation.

Specimen fabrication

Specimens to be used in the uniaxial test and the indirect tensile test were gyratory compacted, cored, and cut to the dimensions D100xH150 mm and D150xH50 mm, respectively. As it was difficult in some cases to reach the target density, i.e. pavement core density, it was necessary to increase the angle of gyration to 2.00°. In order to achieve proper mix viscosity, the compaction temperature of polymer modified mixes should be carefully evaluated before actual specimen production.

Materials testing

Dynamic modulus testing at reasonable strain levels caused an average 4% reduction of dynamic modulus, based on results during and after testing. It should be noted that dynamic modulus testing is considered nondestructive. However, specimens tested at unintentionally high strain levels did not appear more damaged than those in which less strain was induced.

Mastercurves derived from the uniaxial test and the indirect tensile test using gyratory compacted specimens were not similar, contrary to expectation. Most importantly, their dependency on time and temperature appeared to be different. However, it is likely that the discrepancy was due to problems with the gyratory compaction and dynamic modulus testing of the uniaxial specimens. Mastercurves derived from the indirect tensile test using gyratory compacted and cored specimens were similar in this investigation. However, in those cases where the air void content differed between groups, no conclusions could be drawn.

Based on the results of the three test types, the IDT test on cored specimens was considered the most representative in this study. Mastercurves from this test set-up were used to evaluate the ABT, ABb, polymer modified ABbm and AG mix types. The general mix stiffness ranking, beginning with the stiffest, was ABbm, ABb, ABT, AG. The polymer modified ABbm was, as expected, especially stiff at high temperature and low frequency.

Simulation of permanent deformations

The M-E PDG is an advanced concept for prediction and diagnostics that, among other pavement distress factors, addresses permanent deformation in asphalt layers. Its clear division of mechanistic and empirical principles provides a sound basis for future model improvements. The model works with three accuracy levels.

Simulation using the uncalibrated model underestimated the flow rutting for both asphalt concrete structures. However, the field calibrated model was able to describe the development of total AC rut depth well in this investigation. The field calibration factors that were found increased the temperature susceptibility of the model and decreased the dependency on the number of loadings.

The contribution of each layer to total rut depth was not correctly assessed by the field calibrated M-E PDG model. Most importantly, the permanent deformation of the AG asphalt base layer was seriously underestimated. One reason for this may be that the current model is based on a trench study that includes only seven road sections at MnRoad.

Recommendations

In order to make the HVS testing more realistic, the controlled temperature could be switched more often with both increases and decreases, and a temperature gradient could be used.

In order to obtain accurate results with the M-E PDG concept, regional field calibration factors should be assessed. For this purpose, extensive Long Term Pavement Performance data should be available for the region. The data should include data describing the traffic, climate, structure and materials, and surface measurements. Guidelines for field calibration assessment are being developed within the NCHRP project 1-40B.

The contribution of permanent deformation in each AC layer to the total rut depth is based on a trench study that includes only seven pavement sections of MnRoad. The asphalt concrete layers in this study showed a different behavior compared to those sections. The model therefore needs to be improved by NCHRP. In order to collect the necessary data, a large scale trench study on existing pavements in a Long-Term Pavement Performance (LTPP) database should be performed in each region or country.

REFERENCES

AASHTO, 2006- "AASHTO Provisional Standards, 2006 Edition". American Association of State Highway and Transportation Officials, Washington D.C., 2006.

Agardh and Busch, 2006- Agardh, S. and Busch, C. "Incremental-Recursive Rut Depth Prediction Models". Transportation Research Board, National Research Council, Washington D.C., 2006.

Airey et al., 2006- Airey, G..D., Collop, A.C., Zoorob, S.E., Hunter, A.E. "Comparison of Field and Laboratory Compacted Asphalt Mixtures". 10th International conference on asphalt pavements, ISAP, Quebec, 2006.

AMADEUS, 2000- AMADEUS. "Advanced Models for Analytical Design of European Pavement Structures", Final report RO-97-SC.2137, European Commission, 2000.

Asphalt Institute, 1989- Asphalt Institute. "Large Aggregate Asphalt Mixes". Technical bulletin TB-5, ASPHALT Magazine, Asphalt Institute, Lexington, 1989.

ATB Väg, 2005- Allmän teknisk beskrivning för vägkonstruktion (ATB Väg). VV Publ 2005:112. Vägverket, Borlänge, 2005.

Björklund, 1984- Björklund, A. "Creep induced behaviour of resurfaced pavements: Some studies with the aid of beams subjected to a temperature wave and loaded under plane strain conditions". VTI report 271A. Swedish National Road & Traffic Research Institute (VTI), 1984.

Blab, 1999- Blab, R. "Introducing Improved Loading Assumptions into Analytical Pavement Models Based on Measured Contact Stresses of Tires". The International Conference on Accelerated Pavement Testing, Paper No: CS5-3, Reno, 1999.

Bonnot, 1986- Bonnot, J. "Asphalt Aggregate Mixtures". Transportation Research Record 1096, TRB, National Research Council, Washington D.C., 1986.

Bredahl Nielsen et al., 1999- Bredahl Nielsen, C., Ullidtz, P., Zhang, W., Baltzer, S., Macdonald, R.A. "Accelerated Pavement Testing". Report 98, Danish Road Institute, Roskilde, 1999.

Brown and Foo, 1994- Brown, E.R., Foo, K.Y. "Comparison of unconfined- and confined-creep tests for hot mix asphalt". Journal of Materials in Civil Engineering Vol. 6, No. 2, 1994.

Brown et al., 2001- Brown, E.R., Kandhal, P.S. and Zhang, J. "Performance Testing for Hot Mix Asphalt". NCAT report No. 01-05. National Center for Asphalt Technology, Auburn, 2001.

Brûlé, 1996- Brûlé, B. "Polymer-Modifed Asphalt Cements Used in the Road Construction Industry: Basic Principles". Transportation Research Record 1535, TRB, National Research Council, Washington D.C., 1996.

Buchanan and Brown, 2001- Buchanan, M.S. and Brown E.R. "Effect of Superpave Gyratory Compactor Type on Compacted Hot Mix Asphalt (HMA) Density". Transportation Research Record 1761, TRB, National Research Council, Washington D.C., 2001.

Button et al., 1994- Button, J.W., Little, D.N., Jagadam, V., Pendleton, O.J. "Correlation of selected laboratory compaction methods with field compaction". Transportation Research Record 1454, TRB, National Research Council, Washington D.C., 1994.

Chadbourn et al., 2000- Chadbourn, B.A., Skok, E.L.Jr., Newcomb, D.E., Crow, B.L., Spindler, S. "The Effect of Voids in Mineral Aggregate (VMA) on Hot-Mix Asphalt Pavements". Minnesota Department of Transportation, St. Paul, 2000.

Chehab, 2002- Chehab, G., "Characterization of Asphalt Concrete in Tension Using a Viscoelastoplastic Model". Ph.D. Dissertation, North Carolina State University, Raleigh, 2002.

Chowdhury et al., 2001- Chowdhury, A., Grau, J.D.C., Button, J.W., Little, D.N. "Effect of aggregate gradation on permanent deformation of Superpave HMA". Transportation Research Board, National Research Council, Washington D.C., 2001.

Christensen, 1978- Christensen, I.F. "Vågbildning i Asfaltbeläggningar". SBEF report 20, Svenska Byggnadsentreprenörsföreningen, Stockholm, 1978.

Corté et al., 1994- Corté, J-F., Brosseaud, Y., Simoncelli, J-P. and Caroff, G. "Investigation of Rutting of Asphalt Surface Layers: Influence of Binder and Axle Loading Configuration". Transportation Research Record 1436, TRB, National Research Council, Washington D.C., 1994.

Davis, 1988- Davis, R. L. Large Stone Mixes: A Historical Insight. Report IS 103/88, National Asphalt Pavement Association, 1988.

Dawson et al., 2002- Dawson, A., Hildebrand, G., Hofbauer, T., Mateos, A., Wiman, L. "Improvements in Pavement Research with Accelerated Load Testing". COST 347, Work Package 1: Inventory. European Co-operation in the Field of Scientific and Technical Research, 2002.

Deacon et al., 2002- Deacon, J.A., Harvey J.T., Guada I., Popescu L. and Monismith C.L. "Analytically Based Approach to Rutting Prediction". Transportation Research Record 1806, TRB, National Research Council, Washington D.C., 2002.

Devore and Farnum, 1999- Devore, J.L. and Farnum, N.R. "Applied Statistics for Engineers and Scientists". Duxbury Press ITP, 1999.

EAPA, 1995- EAPA. "Heavy duty pavements: The arguments for asphalt". European Asphalt Pavement Association, Breukelen, 1995.

EAPA, 1998- EAPA. "Heavy duty surfaces: The arguments for SMA". European Asphalt Pavement Association, Breukelen, 1998.

Eisenmann and Hilmer, 1987- Eisenmann, J. and Hilmer, A. "Influence of Wheel Load and Inflation Pressure on the Rutting Effect at Asphalt-Pavements - Experiments and Theoretical Investigations", Sixth International Conference on the Structural Design of Asphalt Pavements, Vol. I, Ann Arbor, 1987.

Epps et al., 2001- Epps, A.L, Ahmed, T., Little, D.C., Hugo, F., "Performance Prediction with the MMLS3 at WesTrack", FHWA/TX-01/2134-1, Texas Department of Transportation, Austin, 2001.

FAS Metod 454, 1998- FAS Metod 454-98. The Swedish Asphalt Pavement Association, 1998.

FAS Metod 468, 2000- FAS Metod 468-00. The Swedish Asphalt Pavement Association, 2000.

Gudimettla and Cooley, 2003- Gudimettla, J.M. and Cooley L.A. Jr. "Workability of Hot Mix Asphalt". Transportation Research Board, National Research Council, Washington D.C., 2003.

Guler et al., 2000- Guler, M., Bahia, H.U., Bosscher, P.J. "Development of a Device for Measuring Shear Resistance of HMA in the Gyratory Compactor". Transportation Research Board, National Research Council, Washington D.C., 2000.

Hermansson, 2004- Hermansson, Å. "Mathematical model for paved surface summer and winter temperature: comparison of calculated and measured temperatures". Cold Regions Science and Technology. Vol. 40, pp. 1-17, 2004.

Hinrichsen, 2001- Hinrichsen, J. "A comparison of four brands of Superpave gyratory compactors". Transportation Research Board, National Research Council, Washington D.C., 2001.

Hugo and Epps Martin, 2004- Hugo, F. and Epps Martin, A.L. "Significant Findings from Full-Scale Accelerated Pavement Testing". NCHRP Synthesis 325. Transportation Research Board, National Research Council, Washington D.C., 2004.

Huhtala and Wiman, 1998- Huhtala, M. and Wiman L.G. "Accelerated pavement testing - HVS Nordic". TPPT Symposium Proceedings, p133-147, The Finnish road structures research programme, Espoo, 1998.

Junker, 1987- Junker, J.P. "Entwicklungen zur Bestimmung mechanischer Materialkennwerte an bituminösen Baustoffen, insbesondere an Asphalt". EMPA Bericht Nr. 215, 1987.

Kaloush and Witczak, 2002- Kaloush, K.E. and Witczak, M.W. "Tertiary Flow Charachteristics of Asphalt Mixtures". Journal of the Association of Asphalt Paving Technilogists, Vol. 71, Colorado Springs, 2002.

Kandhal et al., 1998- Kandhal, P.S., Foo K.Y., Mallick, R.B. "A Critical Review of VMA Requirements in Superpave". NCAT report No. 98-1, National Center for Asphalt Technology, Auburn University, Alabama, 1998.

Kandhal and Cooley, 2001- Kandhal, P. S. and Cooley, L.A.Jr. "The Restricted Zone in the Superpave Aggregate Gradation Specification". NCHRP report 464. Transportation Research Board, National Research Council, Washington D.C., 2001.

Kim and Little, 1990- Kim, Y.R. and Little, D.N. "One-Dimensional Constitutive Modeling of Asphalt Concrete". ASCE Journal of Engineering Mechanics, Vol. 116, No. 4, pp. 751-772, 1990.

Kim et al., 2004- Kim, Y.R., Seo, Y., King, M., Momen, M. "Dynamic modulus testing of asphalt concrete in indirect tension mode". Transportation Research Board, National Research Council, Washington D.C., 2004.

Liang et al., 2006- Liang, R.Y., Rabab'ah, S., Al-Akhras, K. "Validation of Enhanced Integrated Climatic Model Prediction over Different Drainable Base Materials". Transportation Research Board, National Research Council, Washington D.C., 2006.

Lundström, 2004- Lundström, R. "On Rheological Testing and Modelling of Asphalt Mixtures with Emphasis on Fatigue Characterisation". Ph.D. Dissertation, Division of Highway Engineering, Royal Institute of Technology, Stockholm, 2004.

Luo and Prozzi, 2005- Luo, R. and Prozzi, J.A. "Evaluation of the Joint Effect of Wheel Load and Tire Pressure on Pavement Performance". Report SWUTC/05/167245-1. Texas Transportation Institute, Texas A&M University System, College Station, Texas, 2005.

Lytton et al., 1993A- Lytton, R.L., Pufahl, D.E., Michalak, C.H., Liang, H.S. and Dempsey, B.J. "An Integrated Model of the Climatic Effects on Pavements". FHWA-RD-90-033. McLean, 1993.

Lytton et al., 1993B- Lytton R.L., Uzan, J., Femando, E.G., Roque, R., Hiltunen, D., Stoffels, S.M. "Development and Validation of Performance Prediction Models and Specifications for Asphalt Binders and Paving Mixes". SHRP-A-357, National Research Council, Washington D.C., 1993.

Mallick, 1999- Mallick, R.B. "Use of Superpave Gyratory Compactor to Characterize Hot Mix Asphalt". Transportation Research Board, National Research Council, Washington D.C., 1999.

Martinez et al., 1991- Martinez, D., Bayomy, F. and Fouad, M. "Selection of maximum therethical specific gravity for asphalt mixture design". Transportation Research Record 1300, TRB, National Research Council, Washington D.C., 1991.

Masad et al., 1999- Masad, E.A., Muhunthan, B., Shashidhar, N., and Harman, T. "Quantifying Laboratory Compaction Effects on the Internal Structure of Asphalt Concrete". Transportation Research Board, National Research Council, Washington D.C., 1999.

Metcalf, 2004- Metcalf, J., "Full Scale Accelerated Pavement Testing. A North American and European perspective". 2nd International Conference on Accelerated Pavement Testing, Minneapolis, 2004.

NCHRP, 2004- "Guide for the Mechanistic-Empirical Design of New and Rehabilitated Pavement Structures". NCHRP report 1-37A. Transportation Research Board, National Research Council, Washington D.C., 2004.

NCHRP, 2006A- NCHRP. "Research Results Digest 307: Independent Review of the Mechanistic Empirical Pavement Design Guide and Software", NCHRP, 2006.

NCHRP, 2006B- NCHRP. "Research Results Digest 308: Changes to the Mechanistic-Empirical Pavement Design Guide Software Through Version 0.900, July 2006", NCHRP, 2006.

Newcomb et al., 2001- Newcomb, D.E., Buncher, M., Huddleston, I.J. "Concepts of Perpetual Pavements". Transportation Research Circular 503, Transportation Research Board, National Research Council, Washington, 2001.

Nilsson, 2001A- Nilsson, R. "Viscoelastic Pavement Analysis using VEROAD". Ph.D. Dissertation, Division of Highway Engineering, Royal Institute of Technology, Stockholm, 2001.

Nilsson, 2001B- Nilsson, B.R. "Fatigue of Asphalt Mixtures- Continuum Damage Mechanics applied to Data from Laboratory Tests". Licentiate's Thesis, Department of Technology and Society, Lund University, Lund, 2001.

Nilsson, 2003- Nilsson, B.R.. "Fatigue of asphalt mixtures: Theory of Viscoelasticity and Continuum Damage Mechanics applied to Uniaxial Fatigue Data from Laboratory Tests". Ph.D. Dissertation. Bulletin Highway Engineering 15, Department of Technology and Society, Lund University, Lund, 2003.

OECD, 1991- OECD. "OECD Full-scale Pavement Test", Organisation for Economic Co-operation and Development, Paris, 1991.

Perret et al., 2004- Perret, J., Dumont, A.G., Turtschy, J.C. "Assessment of resistance to rutting of high modulus asphalt mixes using full-scale accelerated loading tests". 3rd Eurasphalt & Eurobitume Congress, Vienna, 2004.

Peterson et al., 2004- Peterson, R.L., Mahboub, K.C., Anderson, R.M., Masad E., Tashman, L. "Comparing Superpave Gyratory Compactor Data to Field Cores". Journal of Materials in Civil Engineering, Vol. 16, No. 1, pp. 78-83, 2004.

PMS Objekt , 2005- "PMS Objekt version 4". Publikation 2005:42, Vägverket, 2005.

Powell , 2001- Powell B. "As-Built Properties of Experimental Sections on the 2000 NCAT Pavement Test Track". NCAT report 01-02, National Center for Asphalt Technology, Auburn University, Auburn, 2001.

Raaberg, 1999- Raaberg, J. "Investigation of Gyratory Compaction used for Asphalt Mix Design". Report 95, Road Directorate, Danish Road Institute, Roskilde, 1999.

Said et al., 2000- Said S.F., Jacobson T., Hornwall F., Wahlström J. "Evaluation of permanent deformation in asphalt mixes". 2:nd Eurasphalt & Eurobitumen Congress, Eurasphalt & Eurobitume, Barcelona, 2000.

Said, 2004- Said, S.F. "Prediction of flow rutting". International Symposium on Long Lasting Asphalt Pavements, ISAP, Auburn, 2004.

Said, 2005- Said, S.F. "Ageing Effect on Mechanical Characteristics of Asphalt Mixes". Transportation Research Board, National Research Council, Washington D.C., 2005.

Said et al., 2006- Said, S.F., Hermansson, Å., Hakim, H. "Beläggningslagers temperaturer". VTI notat 3-2006, Statens Väg- och Transportforsknings-institut, Linköping, 2006.

SAMARIS, 2004- Sustainable and Advanced MAterials for Road InfraStructure (SAMARIS). Models for permanent deformation for asphalt bound materials in flexible pavements. SAM-05-DE11, Competitive and Sustainable Growth (GROWTH) Programme, 2004.

Sebaaly, 2003- Sebaaly, P.E. "Determination of Pavement Damage From Super-single and Singled-out Dual Truck Tires". NCHRP report 1-36. Transportation Research Board, National Research Council, Washington D.C., 2003.

Siddharthan et al., 2002- Siddharthan, R.V., Krishnamenon, N., El-Mously M., Sebaaly, P.E. "Investigation of Tire Contact Stress Distributions on Pavement Response". Journal of transportation engineering, Vol. 128, No. 2, 2002.

Sousa et al., 1991- Sousa, J. B., Craus, J., Monismith, C.L. "Summary report on permanent deformation in asphalt concrete". SHRP-A/IR-91-104, National Research Council, Washington D.C., 1991.

SS-EN 12697-22 (2004)- SS-EN 12697-22. "Wheel tracking". Swedish Standards Institute (SIS) European Committee for Standardization (CEN), 2004.

SS-EN 12697-25 (2005)- SS-EN 12697-25. "Cyclic compression test". Swedish Standards Institute (SIS) European Committee for Standardization (CEN), 2005.

SS-EN 12697-31 (2005)- SS-EN 12697-31. "Specimen preparation by gyratory compactor". Swedish Standards Institute (SIS) European Committee for Standardization (CEN), 2005.

Tayebali et al., 1994- Tayebali, A.A., Tsai, B., Monismith, C.L. "Stiffness of Asphalt-Aggregate Mixes". SHRP-A-388, Strategic Highway Research Program, National Research Council. Washington DC., 1994.

The Shell Bitumen Handbook, 2003- The Shell Bitumen Handbook, 5th edition. Shell UK Oil Products Limited, 2003.

TRB Committee on FS/APT, 2006- Transportation Research Board Committee on Full Scale/Accelerated Pavement Testing (AFD40). "APT facilities around the world". http://www.k-state.edu/pavements/trb/A2B09 . Accessed 2007-04-30.

Uge and van de Loo, 1974- Uge, P., and van de Loo, P. "Permanent Deformation of Asphalt Mixes". Koninklijke/Shell-Laboratorium, Amsterdam, 1974.

Verstraeten, 1995- Verstraeten, J. "Asphalt materials with a high resistance to flow rutting". Permanent International Association of Road Congresses, PIARC, Paris, 1995.

Viman, 1998- Viman, L. "Gyratorisk packning: inledande försök". VTI notat 70-1998, Statens Väg- och Transportforskningsinstitut, Linköping, 1998.

White et al., 1999- White, T.D., Hua, J., Galal, K. "Analysis of accelerated pavement tests". Proceedings of the First International Conference on Accelerated Pavement Testing, Reno, 1999.

White et al., 2002- White, T.D., Haddock, J.E, Hand, A.J.T, Fang, H. "Contributions of Pavement Structural Layers to Rutting of Hot Mix Asphalt Pavements". NCHRP report 468. Transportation Research Board, National Research Council, Washington D.C., 2002.

Williams and Prowell, 1999- Williams, R.C., Prowell, B.D. "Comparison of laboratory wheel-tracking test results with WesTrack performance". Transportation Research Record 1681, TRB, National Research Council, Washington D.C., 1999.

Williams, 2003- Williams, S.G. "The Effects of HMA Mix Characteristics on Rutting Susceptibility. Transportation Research Board, National Research Council, Washington D.C., 2003.

Wiman, 2006- Wiman, L.G. "Accelerated load testing of pavements: HVS Nordic tests at VTI Sweden 2003-2004". VTI rapport 544A, The Swedish National Road & Transport Research Institute (VTI), Linköping, 2006.

Wiman, 2007- Wiman, L.G. "Accelererad fullskaleprovning av vägkonstruktioner - HVS-tester utförda vid VTI 2004-2005" (Working paper). VTI report 576, The Swedish National Road & Transport Research Institute (VTI), Linköping 2007.

Witczak et al., 2002- Witczak, M.W., Kaloush, K., Pellinen, T., El-Basyouny, M., von Quintus, H. "Simple Performance Test for Superpave Mix Design". NCHRP report 465. Transportation Research Board, National Research Council, Washington D.C., 2002.

Zaghloul et al., 2006- Zaghloul, S., Ayed, A., Abd El Halim, A., Vitillo, N., Sauber, R. "Investigations of Environmental and Traffic Impacts on MEPDG Predictions".

Zhang et al., 2004- Zhang, J., Cooley, L. A. Jr., Hurley, G., Parker, F. "Effect of Superpave defined restricted zone on hot mix asphalt performance". Transportation Research Board, National Research Council, Washington D.C., 2004.

Zhou et al., 2004- Zhou, F., Scullion, T. and Sun, L. "Verification and Modeling of Three-Stage Permanent Deformation Behavior of Asphalt Mixes". Journal of Transportation Engineering, Vol. 130, No. 4, pp. 486-494, 2004.

APPENDIX 1

Table 1. The dimensions of the specimens

Specimen	H_1 [mm]	H_2 [mm]	H_3 [mm]	H_4 [mm]	$H_{average}$ [mm]	D_1 [mm]	D_2 [mm]	$D_{average}$ [mm]
B3ABT	40,18	40,37	40,61	39,97	40,28	151,97	152,01	151,99
B4ABT	40,08	40,34	40,76	40,59	40,44	152,09	151,77	151,93
B7ABT	40,84	39,91	40,35	40,83	40,48	152,25	152,37	152,31
B5ABb	40,96	40,41	40,83	40,77	40,74	152,04	152,09	152,07
B6ABb	40,97	40,68	40,96	40,33	40,74	152,08	152,10	152,09
B7ABb	40,60	39,94	39,97	40,44	40,24	152,09	152,17	152,13
B1ABbm	40,03	40,40	41,30	40,76	40,62	151,95	151,93	151,94
B3ABbm	40,77	39,82	40,07	41,30	40,49	151,68	152,04	151,86
B4ABbm	40,73	39,97	40,55	41,00	40,56	152,03	152,41	152,22
B3AG	39,99	39,92	40,05	40,26	40,06	151,99	152,14	152,07
B5AG	40,17	40,55	40,50	39,94	40,29	151,96	152,39	152,18
B7AG	39,61	40,23	40,37	40,36	40,14	151,17	151,85	151,51
17	151,05	150,84	149,80	150,45	150,54	99,76	99,90	99,83
18	150,39	150,00	150,08	150,33	150,20	99,70	99,64	99,67
19	151,63	150,71	151,60	152,19	151,53	99,74	99,83	99,79
20	151,54	151,90	151,03	150,80	151,32	99,91	99,84	99,88
21	149,12	148,19	147,58	148,68	148,39	99,94	99,80	99,87
22	149,70	149,25	149,40	149,48	149,46	99,85	99,81	99,83
23	150,57	149,57	149,39	150,42	149,99	99,95	99,98	99,97
27	51,17	50,68	51,01	50,35	50,80	150,25	150,13	150,19
33	152,80	151,88	150,70	151,76	151,79	99,66	99,76	99,71
34	49,09	48,64	49,39	49,35	49,12	150,15	150,20	150,18
35	48,71	48,03	48,73	48,57	48,51	150,45	150,94	150,70
36	48,39	48,35	48,12	48,15	48,25	150,21	151,22	150,72
41	49,44	49,37	49,08	49,16	49,26	150,23	150,39	150,31
42	49,44	49,41	48,73	49,06	49,16	150,49	151,20	150,85
46	48,22	48,22	48,38	48,20	48,26	150,12	150,22	150,17
50	48,35	48,49	48,61	48,76	48,55	150,28	149,90	150,09

APPENDIX 2

Table 1. Dynamic modulus data derived during and after testing, and their ratio.

	T [°C]	f [Hz]	ABB UNI GYR [MPa]			ABB IDT GYR [MPa]			ABB IDT COR [MPa]		
			23	22	21	42	41	27	B7	B6	B5
During testing	20	25	11540	9548	10286	9025	7579	7081	5422	4849	4212
	20	10	9720	8107	8707	7544	6372	5832	3810	3693	4038
	20	5	8475	7062	7558	6554	5594	4851	3168	2850	3254
	20	1	6044	4945	5236	4496	3825	3527	1910	1653	2027
	20	0,5	5185	4192	4409	3787	3224	2923	1489	1393	1694
	20	0,1	3530	2793	2786	2422	2145	1991	802	852	989
After testing	20	25	10899	9570	9863	9004	7350	6579	N/A	4990	N/A
	20	10	9316	8107	8365	7580	6169	5601	N/A	4043	N/A
	20	5	8233	7063	7311	6625	5579	4935	N/A	3149	N/A
	20	1	5881	4988	5145	4621	3709	3380	N/A	N/A	N/A
	20	0,5	5047	4234	4356	3879	3193	2889	N/A	N/A	N/A
	20	0,1	3335	2742	2767	2570	2106	1976	N/A	N/A	N/A
Ratio	20	25	1,06	1,00	1,04	1,00	1,03	1,08	N/A	0,97	N/A
	20	10	1,04	1,00	1,04	1,00	1,03	1,04	N/A	0,91	N/A
	20	5	1,03	1,00	1,03	0,99	1,00	0,98	N/A	0,91	N/A
	20	1	1,03	0,99	1,02	0,97	1,03	1,04	N/A	N/A	N/A
	20	0,5	1,03	0,99	1,01	0,98	1,01	1,01	N/A	N/A	N/A
	20	0,1	1,06	1,02	1,01	0,94	1,02	1,01	N/A	N/A	N/A

Table 2. Dynamic modulus data derived during and after testing, and their ratio.

	T [°C]	f [Hz]	ABBm UNI GYR [MPa]			ABBm IDT GYR [MPa]			ABBm IDT COR [MPa]		
			20	19	18	-	50	46	B4	B3	B1
During testing	20	25	12653	11256	10775	-	4960	4256	5460	5139	5681
	20	10	10638	9412	9039	-	4080	3632	4486	4229	4634
	20	5	9299	8211	7858	-	3639	3200	3961	3790	4148
	20	1	6735	5818	5552	-	2589	2218	2699	2588	2727
	20	0,5	5788	4966	4688	-	2249	1880	2258	2177	2273
	20	0,1	4043	3346	3081	-	1575	1299	1477	1460	1464
After testing	20	25	11835	10252	9685	-	N/A	4318	5615	4379	4688
	20	10	10033	8692	8201	-	N/A	3682	4581	3708	4172
	20	5	8880	7677	7160	-	N/A	3205	3950	3240	3559
	20	1	6556	5521	5076	-	N/A	2203	2688	2194	2308
	20	0,5	5668	4742	4312	-	N/A	1888	2273	1870	1914
	20	0,1	4008	3237	2853	-	N/A	1340	1510	1288	1251
Ratio	20	25	1,07	1,10	1,11	-	N/A	0,99	0,97	1,17	1,21
	20	10	1,06	1,08	1,10	-	N/A	0,99	0,98	1,14	1,11
	20	5	1,05	1,07	1,10	-	N/A	1,00	1,00	1,17	1,17
	20	1	1,03	1,05	1,09	-	N/A	1,01	1,00	1,18	1,18
	20	0,5	1,02	1,05	1,09	-	N/A	1,00	0,99	1,16	1,19
	20	0,1	1,01	1,03	1,08	-	N/A	0,97	0,98	1,13	1,17

Table 3. Dynamic modulus data derived during and after testing, and their ratio.

	T [°C]	f [Hz]	ABT UNI GYR [MPa]			ABT IDT GYR [MPa]			ABT IDT COR [MPa]		
			-	33	17	36	35	34	B7	B4	B3
During testing	20	25	-	8426	8206	4564	N/A	5164	4283	4307	4603
	20	10	-	6827	6819	3371	N/A	4193	3368	3344	3513
	20	5	-	5771	5838	3013	N/A	3526	2796	2767	2660
	20	1	-	3638	3901	1882	N/A	2295	1632	1692	1507
	20	0,5	-	2927	3230	1530	N/A	1891	1274	1326	1201
	20	0,1	-	1688	2014	953	N/A	1181	764	786	685
After testing	20	25	-	9001	8232	N/A	5899	N/A	4147	4142	4101
	20	10	-	7594	6780	N/A	4974	N/A	3467	3143	3160
	20	5	-	6489	5817	N/A	4273	N/A	2910	2483	2200
	20	1	-	4048	3806	N/A	2786	N/A	1761	1468	1230
	20	0,5	-	3226	3148	N/A	2305	N/A	1421	1231	955
	20	0,1	-	1802	1917	N/A	1433	N/A	979	805	582
Ratio	20	25	-	0,94	1,00	N/A	N/A	N/A	1,03	1,04	1,12
	20	10	-	0,90	1,01	N/A	N/A	N/A	0,97	1,06	1,11
	20	5	-	0,89	1,00	N/A	N/A	N/A	0,96	1,11	1,21
	20	1	-	0,90	1,02	N/A	N/A	N/A	0,93	1,15	1,23
	20	0,5	-	0,91	1,03	N/A	N/A	N/A	0,90	1,08	1,26
	20	0,1	-	0,94	1,05	N/A	N/A	N/A	0,78	0,98	1,18

Table 4. Dynamic modulus data derived during and after testing, and their ratio.

	T [°C]	f [Hz]	AG IDT COR [MPa] B7	AG IDT COR [MPa] B5	AG IDT COR [MPa] B3
During testing	20	25	3438	3700	3349
	20	10	2532	2836	2546
	20	5	1945	2263	2222
	20	1	1062	1339	1320
	20	0,5	859	1128	1086
	20	0,1	526	543	744
After testing	20	25	3264	3436	N/A
	20	10	2509	2734	N/A
	20	5	1883	1920	N/A
	20	1	1088	1086	N/A
	20	0,5	861	835	N/A
	20	0,1	552	497	N/A
Ratio	20	25	1,05	1,08	N/A
	20	10	1,01	1,04	N/A
	20	5	1,03	1,18	N/A
	20	1	0,98	1,23	N/A
	20	0,5	1,00	1,35	N/A
	20	0,1	0,95	1,09	N/A

Table 5. Descriptive statistics for each specimen.

Test set-up	Specimen	Damage ratios						Specimen mean ratio	Specimen standard deviation	Specimen mean µstrain	Specimen max µstrain
ABB IDT PAV	B5	N/A	N/A	N/A	N/A	N/A	N/A	N/A	N/A	82	107
	B6	0,97	0,91	0,91	N/A	N/A	N/A	0,93	0,04	74	122
	B7	N/A	N/A	N/A	N/A	N/A	N/A	N/A	N/A	61	86
ABB IDT GYR	27	1,08	1,04	0,98	1,04	1,01	1,01	1,03	0,03	84	205
	41	1,03	1,03	1,00	1,03	1,01	1,02	1,02	0,01	68	80
	42	1,00	1,00	0,99	0,97	0,98	0,94	0,98	0,02	63	68
ABB UNI GYR	21	1,04	1,04	1,03	1,02	1,01	1,01	1,03	0,02	69	101
	22	1,00	1,00	1,00	0,99	0,99	1,02	1,00	0,01	87	137
	23	1,06	1,04	1,03	1,03	1,03	1,06	1,04	0,02	68	108
ABBm IDT PAV	B1	1,21	1,11	1,17	1,18	1,19	1,17	1,17	0,03	61	74
	B3	1,17	1,14	1,17	1,18	1,16	1,13	1,16	0,02	53	75
	B4	0,97	0,98	1,00	1,00	0,99	0,98	0,99	0,01	55	72
ABBm IDT GYR	46	0,99	0,99	1,00	1,01	1,00	0,97	0,99	0,01	68	83
	50	N/A	N/A	N/A	N/A	N/A	N/A	N/A	N/A	71	88
ABBm UNI GYR	18	1,11	1,10	1,10	1,09	1,09	1,08	1,10	0,01	73	111
	19	1,10	1,08	1,07	1,05	1,05	1,03	1,06	0,02	64	100
	20	1,07	1,06	1,05	1,03	1,02	1,01	1,04	0,02	57	86
ABT IDT PAV	B3	1,12	1,11	1,21	1,23	1,26	1,18	1,18	0,06	82	107
	B4	1,04	1,06	1,11	1,15	1,08	0,98	1,07	0,06	74	122
	B7	1,03	0,97	0,96	0,93	0,90	0,78	0,93	0,09	61	86
ABT IDT GYR	34	N/A	N/A	N/A	N/A	N/A	N/A	N/A	N/A	81	107
	35	N/A	N/A	N/A	N/A	N/A	N/A	N/A	N/A	73	97
	36	N/A	N/A	N/A	N/A	N/A	N/A	N/A	N/A	81	100
ABT UNI GYR	17	1,00	1,01	1,00	1,02	1,03	1,05	1,02	0,02	64	87
	33	0,94	0,90	0,89	0,90	0,91	0,94	0,91	0,02	72	114
AG IDT PAV	B3	N/A	N/A	N/A	N/A	N/A	N/A	N/A	N/A	62	108
	B5	1,08	1,04	1,18	1,23	1,35	1,09	1,16	0,12	65	130
	B7	1,05	1,01	1,03	0,98	1,00	0,95	1,00	0,04	63	93

One-sample t-test
The analysis is based on data from Table 5.

Hypothesis:

$$H_0 : E(R) = 1$$
$$H_a : E(R) \neq 1$$

Mean damage	1.04
Standard deviation	0.09
Sample size	123
t	5.32
P (double-sided distribution)	0.00

H_0 is rejected at the significance level α=0.01